MOLECULAR MECHANISMS INVOLVED IN THE GENERATION OF INHIBITORY POSTSYNAPTIC STRUCTURES

Dissertation

for the award of the degree
"Doctor rerum naturalium"
of the Georg-August-Universität Göttingen
within the doctoral program
Cellular and Molecular Physiology of the Brain
of the Georg-August University School of Science (GAUSS)

submitted by

Sven Wagner

from Zeulenroda, Germany

Göttingen, 2021

Thesis Committee

Prof. Dr. Nils Brose
Department of Molecular Neurobiology, Max Planck Institute of Experimental Medicine

Prof. Dr. Blanche Schwappach
Dean of the Medical Faculty at the University Medical Center Hamburg-Eppendorf (UKE)
formerly Department of Molecular Biology, University Medical Center Göttingen (UMG)

Dr. Camin Dean
Synaptic dysfunction, German Center for Neurodegenerative Diseases (DZNE)

Members of the Examination Board

Referee: Prof. Dr. Nils Brose
Department of Molecular Neurobiology, Max Planck Institute of Experimental Medicine

Second Referee: Prof. Dr. Thomas Dresbach
Department of Anatomy and Embryology, Göttingen University Medical Center

Further Members of the Examination Board

Prof. Dr. Blanche Schwappach
Dean of the Medical Faculty at the University Medical Center Hamburg-Eppendorf (UKE)
formerly Department of Molecular Biology, University Medical Center Göttingen (UMG)

Dr. Camin Dean
Synaptic dysfunction, German Center for Neurodegenerative Diseases (DZNE)

Prof. Dr. Swen Hülsmann
Department of Neurophysiology, Göttingen University Medical Center

Prof. Dr. Jochen Staiger
Department of Neuroanatomy, Göttingen University Medical Center

Date of oral examination: 25 June 2021

Affidavit

Herewith I declare, that I prepared the PhD Thesis “Molecular Mechanisms Involved in the Generation of Inhibitory postsynaptic structures” on my own and with no other sources and aids than quoted.

Göttingen, 30.04.2021

In memory of my father Horst Wagner

Aim of the Study

Synapses are complex, two-part subcellular compartments that mediate signal transmission between neurons. They consist, on the one hand, of a presynaptic transmitter release site in the transmitting neuron and, on the other hand, of a postsynaptic density in the receiving neuron. Both sides of a synapse represent highly specialized plasma membrane compartments characterized by a defined protein composition, in which transmembrane adhesion and scaffolding proteins control the entry and exit of regulatory and signaling proteins. This results in highly complex presynaptic and postsynaptic protein networks that regulate transmitter release and transmitter receptivity, respectively. GABAergic synapses represent a major synapse type in the mammalian brain. Here, the postsynaptic protein network described above consists of the adhesion protein neuroligin 2 (NL2), the scaffolding protein gephyrin, the guanine nucleotide exchange factor (GEF) collybistin (CB), and γ-aminobutyric (GABA) type A receptors ($GABA_ARs$). The interaction of these proteins during the formation of GABAergic postsynapses is essential and sufficient for the establishment of proper GABAergic synaptic transmission in a major subset of GABAergic synapses (Poulopoulos et al 2009). The interaction of presynaptically localized neurexins with postsynaptically localized NL2 is thought to initiate the formation of the synapse. This interaction is followed by the binding of NL2 to and the activation of CB, which subsequently interacts with the plasma membrane via its pleckstrin homology (PH) domain. Furthermore, CB activation leads to the recruitment of gephyrin, which forms a network of oligomers. The NL2/CB/gephyrin complex recruits $GABA_ARs$ to the developing synapse and leads to the establishment of a functional postsynapse (Krueger et al 2012, Papadopoulos & Soykan 2011, Poulopoulos et al 2009). The entry and exit of $GABA_ARs$ and perhaps other regulatory proteins is controlled by the postsynaptic scaffold. These dynamics are required in processes such as synapse rearrangement or synapse plasticity. As is readily apparent in NL2 and also CB knockout (KO) mice, the NL2/CB/gephyrin/$GABA_AR$ cascade does not suffice to establish all GABAergic synapses. Previous studies demonstrated loss of gephyrin and $GABA_ARs$ in some but not all GABAergic synapses of NL2 and CB KOs (Papadopoulos et al 2007, Poulopoulos et al 2009). In contrast, deletion of gephyrin leads to loss of $GABA_ARs$ at almost all GABAergic synapses (Kneussel et al 1999). The goal of the present work has been to identify other proteins involved in the formation of GABAergic postsynapses instead of NL2 or CB.

In order to search for novel proteins that can act as regulators of the gephyrin-dependent formation of inhibitory synapses, I acquired a set of full-length size-selected and unamplified cDNA expression libraries [30.000 colony forming units (CFU) in total; size-fractionated in 2-3, 3-4 and 4-5 kb pools containing 10.000 CFU each] from developing rat brain (postnatal day 11), which were kindly provided by Dr. Ann-Marie Craig (Vancouver, Canada). These cDNA expression libraries in pcDNA3 had previously been used to identify NL-related synaptogenic proteins (Linhoff et al 2009). For the screening assay, I used a previously described HEK 293 cell line (Flp-In T-Rex-GFP-gephyrin HEK 293) that inducibly expresses GFP-gephyrin upon addition of tetracycline (TET) to the culture medium (Papadopoulos et al 2017). The assay was based on the fact that wild-type and GFP-tagged gephyrin expressed in COS-7 or HEK-293 cells (Kins et al 2000) forms intracellular aggregates, which are dispersed so that gephyrin is redistributed into numerous membrane-associated microclusters if a constitutively active splice variant of CB lacking the SH3 domain (CB_{SH3-}), or if intrinsically inactive CB variants containing the N-terminal SH3 domain (CB_{SH3+}) along with CB activators such as NL2, TC10 or the α2 subunit of $GABA_ARs$ are co-expressed (Mayer et al 2013, Poulopoulos et al 2009, Saiepour et al 2010). The readout of the screen was the transition from intracellular gephyrin aggregates to microclusters. The dysfunction of GABAergic synapses is causally involved in several neurological and psychiatric diseases, including epilepsy and schizophrenia (Cao et al 2020, Sun et al 2011). The identification of proteins involved in the assembly of GABAergic postsynapses is therefore not only of major importance for basic neuroscience but may also have medical implications.

Table of contents

1 Introduction

The human brain is the central processing unit for internal and external stimuli and regulates all corresponding behaviour. Approximately 1 billion neurons are interconnected by more than 1 trillion synapses in the human brain (Kandel & Squire 2000, Noctor et al 2007). Their incomparable interplay enables them to carry out their diverse tasks and functions, thus ensuring the survival of the individual. The number of neuronal connections among each other varies greatly between cells. For example, some neurons can only form a single synapse, whereas others are able to form 100.000. However, the brain does not only consist of neurons, but also of glial cells, which are present in 10 times the number of neurons and support them in their functionality and vitality (Allen & Barres 2009, Doetsch 2003, Ullian et al 2001). These specialized contact points between neurons, the synapses, form the basis for the brain's ability to process stimuli, trigger reactions and adapt to circumstances. The synapses show great flexibility in adapting to the current situation, both quickly and over a longer period of time. All this is done to ensure a fast, reliable and effective transmission of the electrical impulses with which the neural network communicates. Since these structures, which are only a few micrometers in size, are the building blocks of our brain, understanding how they work also contributes to understanding the higher functions of the brain. Based on this knowledge, however, it is also possible to investigate and understand psychiatric diseases and brain malfunctions.

1.1 Principles of synaptic transmission

Electrical signals are used for communication between neurons. Due to the ion distribution, which is mainly maintained by the Na^+/K^+-ATPase, and the permeability of the plasma membrane for the different ions, a negative membrane potential of about -60 mV to -70 mV is formed. Through transient depolarizations of the membrane, the action potentials, the electrical signals are conducted over long stretches of the axon membrane towards the synapse and transmitted there to the next neuron.

Two different types of signal transmission can be found within the human brain, which take place at different synapses. One is the electrical synapse, in which direct contact between two neurons is established via gap junctions, where the electrical signal is transmitted directly via ion channels (Goodenough & Paul 2009). Therefore, the synaptic structures do not contain synaptic vesicles filled with neurotransmitters. Furthermore, transmission can take place in both directions (Furshpan & Potter 1959). These properties serve to synchronize groups of neurons, which takes place in areas of the hippocampus, among others (Oh et al 1999, Palacios-Prado et al 2014).

In contrast to the electrical synapses, the chemical synapses, which have been studied much more intensively, convert the incoming electrical signal into a chemical signal before converting it back into an electrical signal, which makes it possible to better modulate the signal. The electrical signal is conducted over long distances by depolarization along the axon membrane to the synapse, where voltage-dependent calcium channels (VDCC) are opened, leading to calcium influx into the presynaptic terminal (Kandel 2012). As a consequence, a sequence of multiple molecular events is triggered that finally lead to a fusion of neurotransmitter-filled vesicles with the presynaptic plasma membrane. The released neurotransmitter diffuses within a few milliseconds through the 20 nm thick synaptic cleft and binds to receptors located in the postsynaptic membrane (Kandel 2012). By taking up the neurotransmitters, by glial cells or the presynaptic terminal, from the synaptic cleft, transmission is terminated.

The neurotransmitters released in this way can bind to two major classes of receptors. The ionotropic receptors are ion channels which, by binding the ligand, undergo a change in conformation and thus open a pore. Through these channels the selective flow of ions along the concentration and charge gradient takes place, which results in a change of the membrane potential. The creation of a new action potential works according to the all or nothing principle (Kandel 2012). Only if a certain threshold value is exceeded after the spatio-temporal integration of all synaptic inputs to a neuron, the action potential is created at the axon hillhock and passed on along the axon. Therefore, the activity of the individual neuron in a neural network is determined by the synaptic inputs on the dendrites and the soma.

The second class of postsynaptic neurotransmitter receptors are the metabotropic, G-protein coupled receptors (Kandel 2012). After binding of the ligand on the extracellular side, they undergo a conformational change on the intracellular side and thus trigger a signalling cascade that has long-lasting consequences on cell function. Compared to ionotropic receptors, metabotropic receptors do not generate new action potentials. However, they modulate intracellular signal transduction on a longer time scale and thus indirectly influence synaptic transmission (Kandel 2012).

1.2 Comparison of inhibitory and excitatory synapses

Chemical synapses can be divided into inhibitory, excitatory and neuromodulatory synapses. Initial electron microscopic investigations already showed a morphological difference between these synapse types (Figure 1), classified at the time as type I and type II synapses. Type I synapses are mainly found on dendrites and dendritic projections called spines and are characterized by a thickening, especially at the postsynaptic membrane. In contrast, type II synapses are usually located in axosomatic areas and show no asymmetrical thickening of the membranes (Gray 1959). After further investigations it was shown that the synapses described as type I by Gray are excitatory and type II are inhibitory synapses.

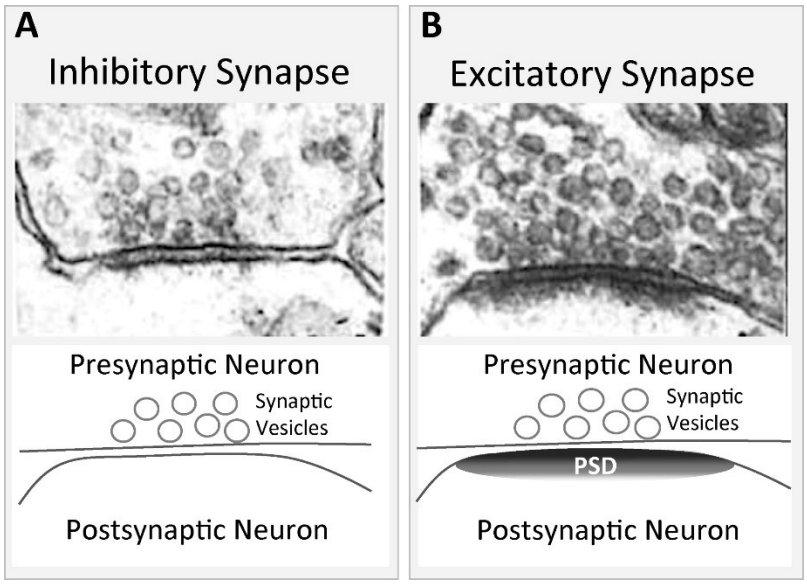

***Figure 1**: Electron microscopic images of symmetric inhibitory and asymmetric excitatory cortical synapses*
Electron microscopic image of an inhibitory (A) and excitatory (B) synapse (top) with schematic drawings (below), showing the symmetrical and asymmetrical arrangement of pre- and postsynaptic specializations. Post-synaptic density, PSD. Source: (Colonnier 1968, Kuzirian & Paradis 2011)

As indicated by the conserved organizational principles of the two synapse types, there also seems to be little difference at the molecular level (Boyken et al 2013). Both postsynapse types contain

neurotransmitter receptors and cell adhesion proteins at the cell membrane to establish a close and well-organized contact between pre- and postsynaptic neuron. Furthermore, in both postsynapses, elements of the cytoskeleton are connected to the transmembrane proteins via a protein network. Only on this basis can a fast, effective and error-free transmission of the signal from neuron to neuron take place (Emes & Grant 2012).

The postsynaptic density (PSD), an electron dense area under the postsynaptic membrane of excitatory synapses, is among the most striking characteristics of neuronal synapses. Numerous protocols have been developed to biochemically purify this structure and thus identify associated proteins (Carlin et al 1980, Davis & Bloom 1973, Fiszer & Robertis 1967). In this way it was shown that less than 10% of the approximately 1500 identified proteins are ion channels and receptors (Bayes et al 2011). These studies indicate the great importance of intracellular scaffolding and signalling components for postsynaptic function (Grant 2013).

A biochemical characterization of inhibitory synapses is much more difficult due to the absence of a defined PSD and the comparatively low number of inhibitory synapses in the brain (Kuzirian & Paradis 2011). This has caused a substantial lack of detailed understanding of the molecular architecture of and the dynamic processes at inhibitory synapses as compared to excitatory synapses. Nevertheless, over the past decades, multiple protein components and molecular mechanisms involved in the development and function of inhibitory post-synapses have been discovered. Aberrations of these and a consequent alteration of the excitation-inhibition balance (E-I balance) in the brain can cause malfunction of neuronal circuits and thus lead to different neurological and psychiatric disorders, such as autism spectrum disorders, schizophrenia or epilepsy (Ramamoorthi & Lin 2011). The E-I balance can be perturbed by both, faulty inhibitory and excitatory neurotransmission, and at any time during development (Ramamoorthi & Lin 2011). In numerous patients, mutations in various components of inhibitory synapses have been identified, with often severe clinical symptoms. All this together demonstrates the extremely strong influence of inhibitory synapses on neural network and brain function.

1.3 Function of inhibitory synapses in neuronal networks

In neuronal networks, inhibitory and excitatory synapses interact to optimally adapt activity. In the case of excitatory synapses, the binding of the neurotransmitter glutamate to postsynaptically localized ionotropic receptors leads to a Na^+ influx and thus to depolarization of the postsynaptic cell (Kuzirian & Paradis 2011). Glutamatergic neurons form the major part of the neurons in the mammalian cerebral cortex. The activity of most such pyramidal neurons is influenced by the diverse class of inhibitory interneurons. Two different types of synaptic inhibition can be distinguished, both based on the binding of a neurotransmitter to postsynaptically localized ionotropic receptors, which lead to a Cl^- influx into the postsynaptic compartment and thus to hyperpolarization. In the brainstem and spinal cord area, glycine acts as the major inhibitory neurotransmitter, whereas GABA plays this role in the forebrain. The glycine and GABA systems differ in the inhibition kinetics of the postsynaptic response. GABA-mediated inhibition in the cerebellum shows a much faster decrease of the postsynaptic potential than glycinergic inhibition (Dumoulin et al 2001). Exactly the opposite situation is true for motor neurons (Jonas et al 1998).

The importance of inhibitory influence was shown in with regard to the field potential oscillation in the hippocampus, where a population of inhibitory interneurons have contact sites with hippocampal pyramidal neurons and thus ultimately give the existing field potential oscillation its characteristic shape

(Bartos et al 2007). Furthermore, it was shown that during early development of neuronal networks, when many neurons have high intracellular Cl^--levels, a depolarization of the membrane potential occurs upon opening of glycine or GABA receptor channels, which increases the intracellular calcium concentration and supports network maturation by a calcium-mediated-intracellular signalling cascade (Cellot & Cherubini 2013). In mature neurons, the expression of specific Cl^--transporters reduces the intracellular Cl^--levels, so that after opening glycine or GABA receptor channels an influx of Cl^- caues hyperpolarisation of the cell. To ensure a functioning neural network, a balance between excitation and inhibition must always be maintained. This happens already during the maturation of neural networks, when the neurons differentiate and migrate to their intended location in the brain to form their connections, which finally enables a fine tuning of network activities and thus complex brain processes (Ramamoorthi & Lin 2011).

1.4 The inhibitory synapse in detail

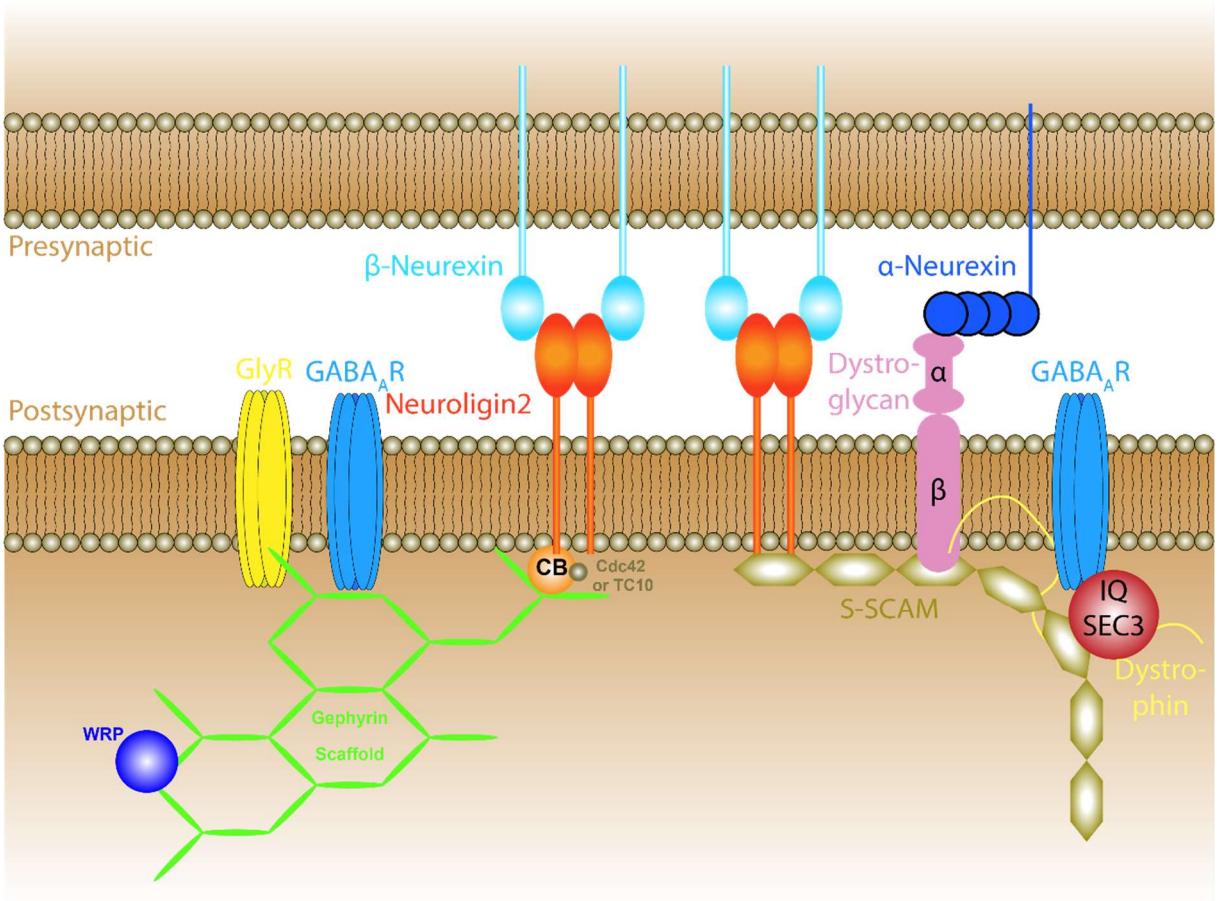

Figure 2 Intracellular components of inhibitory synapses.
Schematic representation of a selection of important intracellular proteins known to affect inhibitory postsynapse structure and function. The presynaptic membrane is shown in the upper half and the postsynaptic membrane is shown in the lower half of the figure. Abbreviations: $GABA_AR$, γ-aminobutyric acid type A receptor; GlyR, glycine receptor; CB, collybistin; IQSEC3, IQ Motif AndSec7 Domain 3; S-SCAM, synaptic cell adhesion molecule; WRP, Wiskott-Aldrich syndrome protein (WASP) family veprolin-homologous protein associated Rac GTPase activating protein.

The lack of a profound understanding of the establishment and development of inhibitory postsynapses, as compared to excitatory postsynapses, has prompted intensified research in this field over the past decades, which has led to the identification of multiple novel synapse components and molecular processes. Neurotransmitter receptors and adhesion molecules on the postsynaptic side are positioned in apposition to the active zone of the presynaptic side. This allows a short diffusion of the neurotransmitters and thus a fast and efficient transmission of the synaptic signal. To achieve optimal positioning of these postsynaptic components, they interact with the scaffold of gephyrin or synaptic scaffolding molecule (S-SCAM) formed under the synaptic plasma membrane, which in turn interact with the cytoskeleton. Multiple other proteins that play a central role in intracellular signaling and synaptic plasticity are enriched in the inhibitory postsynapse. The GEF CB is one of the best characterized proteins of the inhibitory postsynaptic apparatus. It is essential for the synaptic localization of gephyrin and $GABA_A$Rs in many areas of the mammalian brain (Papadopoulos et al 2008, Papadopoulos et al 2007).

1.4.1 Glycine receptors

The glycinergic synapses are involved in circuits of reciprocal and recurrent inhibition in the spinal cord. Poisoning by strychnine, which is a highly specific blocker of glycine receptors (GlyRs), causes muscle stiffness and convulsions due to motor neuron hyperexcitation and activation of antagonistic muscles. The high specificity of the toxin made it suitable as a tool for a more precise breakdown of glycinergic synapses and their transmission. Thus, GlyRs could be successfully isolated using strychnine in an affinity purification process, which led to the cloning of the corresponding cDNAs (Pfeiffer et al 1982).

GlyRs are strongly expressed in the spinal cord, but are also abundant in other regions of the central nervous system (CNS), such as the brain stem, retina and auditory pathways. Significantly smaller levels are found in the cerebellum and the hippocampus (Fujita et al 1991).

GlyRs belong to the pentameric ligand-gated ion channel (LGIC) family, more specifically to the anion-selective ionotropic receptors, whose class also includes nicotinic acetylcholine, serotonin type 3, $GABA_A$R and GABA receptor type C ($GABA_C$R). : Each functional channel is composed of different combinations of α- and β-subunits, which have been initially calculated to coexist in a stoichiometric ratio 3α2β (Lynch 2004). Later, it could be shown that a heteropentamer is composed of two α and three β subunits (Grudzinska et al 2005). There are four possible alpha subunits, with only one β-subunit known. All subunits have five transmembrane domains in common. To induce the opening of the Cl^--channel pore, glycine binds to a pocket that forms at the interface between α- and β-subunits (Lynch 2004). Binding of GlyRs to the scaffold protein gephyrin is mediated by the β subunit located on the cytoplasmic side of the postsynaptic membrane, which forms an elongated loop (Meyer et al 1995a). This binding is so strong that when GlyR is purified via strychnine columns, the gephyrin remains bound to the receptor (Langosch et al 1992, Meyer et al 1995b).

1.4.2 GABA

The binding of GABA to the GABAR mediates inhibition in signal transduction, thus GABA has an important role as a neurotransmitter. The production of GABA, as well as the maintenance of the GABA supply, is the function of the GABA shunt (see **Figure 3**). Due to the strong and specific action of

GABAergic neurons in many brain regions, GABA is present in a 1000-fold higher concentration compared to other neurotransmitters, such as monoamines (Martin & Rimvall 1993). Glucose usually serves as a precursor for GABA, but alternatively the body can use pyruvate or other amino acids as

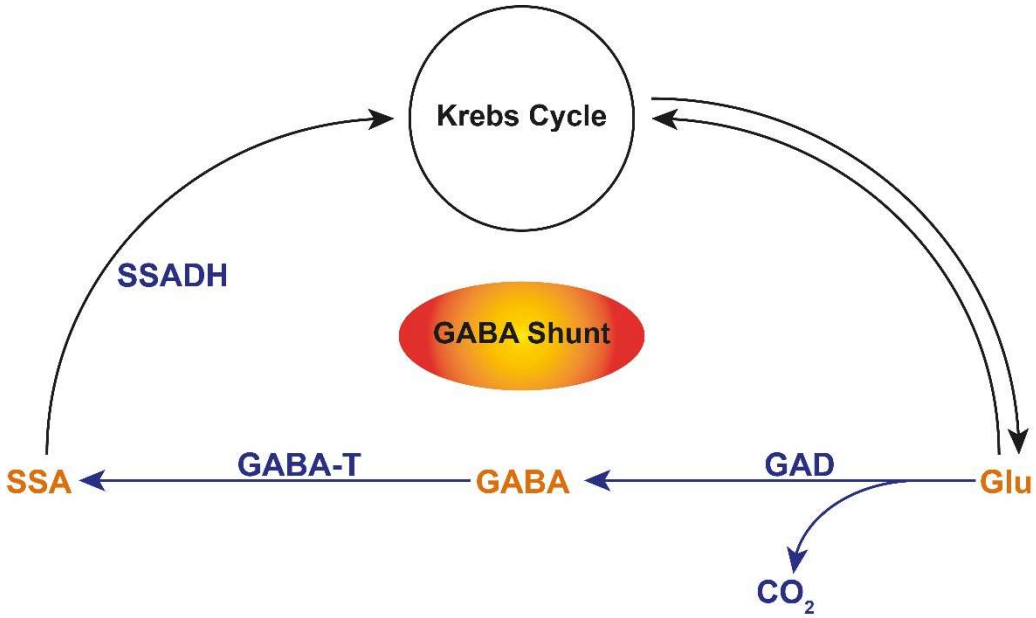

Figure 3 Schematic overview of the maintenance of the GABA supply through interaction of GABA shunt and Krebs cycle.
Under glutamic acid decarboxylase (GAD) activity, GABA is formed by decarboxylation of glutamate (SSA). GABA is metabolized by GABA-T to amber semialdehyde. SSA is converted to glutamine by succinic semialdehyde dehydrogenase (SSADH) and fed into the Krebs cycle. This supplies glutamate for renewed GABA synthesis.

precursors. In a first step, the transamination of α-ketoglutamate to L-glutamic acid takes place by GABA-α-oxoglutarate transaminase (GABA-T). Glutamic acid decarboxylase (GAD) decarboxylates the previously formed glutamic acid to GABA. Interestingly, GAD is only expressed in cells in which GABA functions as a neurotransmitter (Bown & Shelp 1997). GABA, which is later released into the synaptic cleft, binds to the postsynaptically localized GABAR, triggering a depolarization of the postsynaptic membrane. GABA subsequently detaches from the receptors and is subsequently reabsorbed by the presynaptic cell or by the surrounding glial cells. The speed of this process depends mainly on the temperature and the ion concentration. The transporters necessary for the uptake of GABA can transport the neurotransmitter in both directions. For this process, the movement of extracellular sodium along the concentration gradient is necessary and therefore occurs under the dependence of Cl ions. This reuptake of the neurotransmitter through the presynaptic site allows it to be reused. In glial cells, GABA is metabolized by GABA-T to amber semialdehyde in the absence of GAD (Owens & Kriegstein 2002). By conversion by succinic semialdehyde dehydrogenase (SSADH), it is converted to succinic acid so that it can be reused as GABA by entering the Krebs cycle. In the Krebs cycle, the succinic acid is converted into glutamine and reintroduced to the neurons in this form. Glutamine is converted by glutaminase to glutamate in the neurons so that it can be fed back to the GABA shunt (Owens & Kriegstein 2002, Shelp et al 1999).

1.4.3 GABAR

GABA, which was the first neurotransmitter identified to mediate synaptic inhibition, is released from about 17% of the synapses of the mammalian brain (Krnjevic & Schwartz 1966). Due to the variety of subtypes and possible subtype combinations, a high heterogeneity in GABA-mediated inhibition is achieved. Like the GlyRs described above, $GABA_AR$ and $GABA_CR$ also belong to the ligand-gated chloride channels of the LGIC family, whereas the GABA receptors type B ($GABA_BR$) is a G-protein coupled receptor. Due to their sensitivity to substances such as barbiturates, benzodiazepines and alcohol, they have become the focus of numerous studies (DeFeudis 1983). $GABA_AR$ can consist of α_{1-6}, β_{1-3}, γ_{1-3}, δ, ε and η, whereas $GABA_CR$ consists of ρ_{1-3} subunits. In the mammalian CNS, the α_1, β_2, γ_2 combination is the most abundant, which is composed of two α1, two β2 and one γ2 subunit (Burt & Kamatchi 1991, Lobo & Harris 2008).

1.4.3.1 $GABA_AR$

$GABA_AR$ mediate fast inhibitory neurotransmission and belong to the family of Cys-loop ligand-gated ion channels. Other members of this family are acetylcholine receptors, GlyRs and 5HT3 receptors. They all are heteropentamers and share some structural features, such as the large extracellular amino terminus, four transmembrane domains (TMD) and a large intracellular loop between the third and fourth TMD as can be seen in Figure 4 (Jacob et al 2008)

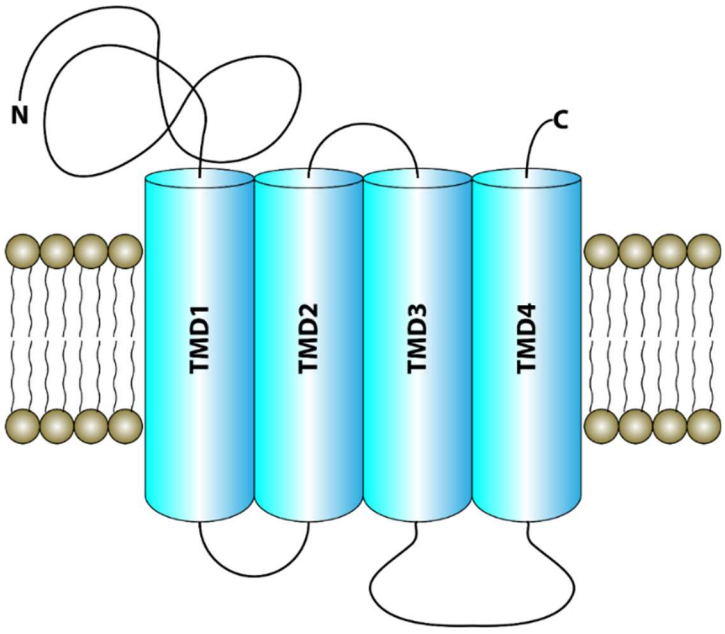

Figure 4 Schematic structure of a $GABA_A$ receptor subunit
The $GABA_AR$ subunits have 4 hydrophobic transmembrane domains (TMD). Between the third and fourth TMD is a large intracellular cis-loop, which contains binding sites for proteins and target sites for post-translational modifications.

Heteropentamers are formed around a functional channel, the composition of which depends on the region and cell type in which the channel is located. For example, this can be observed in the

interneuron innervation of the hippocampus. In the GABAergic innervation of the somata of parvalbumin positive (PV+) basket cells, α1 is found as a subunit, while α2 is present at GABAergic contacts of CCK positive basket cells on the somata of pyramidal neurons (Fritschy & Mohler 1995, Nyiri et al 2001). An example of region-specific subunit expression is α6, which is found exclusively in the cerebellum. The α5 subunit, on the other hand, is mainly expressed in the hippocampus. The composition of the heteropentamers is thought to accommodate the characteristics of inhibition to the needs of the circuitry. Possible adjustable parameters are channel gating, kinetics and pharmacological characteristics (Luddens & Wisden 1991). In general, however, $GABA_AR$s are found in the brain as well as in the spinal cord. A higher level is present in the hippocampus and the cortex cerebri. The GABA molecules can bind to the extracellular part of the receptor. This is usually located in the postsynaptic membrane. In addition to the GABA molecules, psychoactive drugs such as benzodiazepines can also bind to these sites and thus trigger or modify the opening of the receptor pore and the influx of chloride ions. This influx leads to a hyperpolarization of the membrane and thus to an inhibition of the formation of new action potentials (Burt & Kamatchi 1991, Lobo & Harris 2008, Mihic et al 1997).

The most abundant and ubiquitous synaptic $GABA_AR$ subunit is γ2. Loss of the γ2 subunit in KO mice leads to perinatal lethality. In addition, reduction of benzodiazepine binding sites has been described (Gunther et al 1995). Loss of the β3 subunit also leads to perinatal lethality, whereas a small population of mice survives, exhibiting greatly attenuated phenotypic deficits (Homanics et al 1997).

In contrast to $GABA_AR$ and $GABA_CR$, $GABA_BR$ belong to the metabotropic, G-protein coupled receptor family, are mainly located extrasynaptically or presynaptically and mediate only slow inhibition (Luscher et al 2011).

1.4.4 Cell adhesion molecules

Adhesion molecules play an important role in the formation, maturation and stabilisation of pre- and postsynaptic structures. Only through the correct functioning of these processes can optimal and error-free transmission across the synaptic cleft be guaranteed. Adhesion molecules are localised on both the pre- and postsynaptic side and can thus form strong transsynaptic interactions (Fiszer & Robertis 1967).

1.4.4.1 Neurexins and neuroligins

Neurexins and NLs are probably the best studied synapse-specific adhesion molecules. The presynaptically localised neurexins form transsynaptic interactions with the postsynaptically localised NLs to drive pre- and postsynaptic specialisation (Krueger et al 2012). There are three neurexin-encoding genes, which are expressed by two different promoters. Subsequent diverse splicing results in a variety of different neurexin proteins, which has led to the idea that they participate in a synapse-specific recognition code (Sudhof 2008). PSD95/disk-large/zona-occludens-1 domains (PDZ) can bind to the intracellular domain. Thus, it has been postulated that by interacting proteins that contain a PDZ domain and promote neurotransmitter release, such as calcium/calmodulin-dependent serine protein kinase (CASK) and Munc18-interacting protein (Mint), the synaptogenic effect of neurexins is unfolded (Krueger et al 2012). However, later studies showed that neurexins interact also with other proteins via their extracellular domains and thus induce presynaptic differentiation (Gokce & Sudhof 2013).

NLs have 4 different isoforms (NL1-4) in rodents and 5 in humans. They are localised in the postsynaptic membrane and possess an extracellular catalytically inactive acetylcholinesterase (AChE) homology domain, through which dimerization and interaction with neurexins is mediated. They also have a transmembrane domain and a variable intracellular domain that interacts with various postsynaptic density proteins (Sudhof 2008). All NLs are able to bind to PDZ domain-containing proteins (Poulopoulos et al 2009). Although the different isoforms share these structural features, they are located at different synapses. For example, NL1 is found almost exclusively in excitatory synapses (Song et al 1999), whereas NL3 and NL4 are found in both excitatory and inhibitory synapses (Budreck & Scheiffele 2007, Graf et al 2004, Hoon et al 2011). However, the mechanism underlying this differential distribution is unknown (Baudouin et al 2012, Graf et al 2004). An extended functional spectrum of the NLs results from the different dimerization possibilities of the various isoforms.

NL2 is exclusively expressed at inhibitory postsynapses (Varoqueaux et al 2004). NL2 can initiate presynaptic differentiation when expressed in non-neuronal cells and co-cultured with neurons. This induction of differentiation is based on the previously described interaction of NL with neurexins (Scheiffele et al 2000). Conversely, neurexins can lead to clustering of NL2 and gephyrin (Graf et al 2004). Overexpression of NL2 in neurons leads to an increased number of inhibitory synapses on dendritic shafts, as well as an increase in inhibitory postsynaptic currents (IPSCs) in an active dependency manner (Chubykin et al 2007). When NL2 is overexpressed throughout the brain of mice, these exhibit altered behaviour, such as impaired social interactions (Hines et al 2008). The global knock-out (KO) of NL2 in mice is associated with a reduction in IPSC amplitude in the neocortex, as well as a specific reduction in GABAergic transmission in the hippocampus (Chubykin et al 2007). Immunolabeling studies also showed a loss of gephyrin and $GABA_AR$ γ2 in perisomatic regions of the stratum pyramidale, whereas the dendritic spines in the stratum radiatum remained unaffected (Poulopoulos et al 2009). Later studies also showed increased network activity in granule cells in the dentate gyrus of the hippocampus in NL2 KO mice (Jedlicka et al 2011). Another interesting observation is that the loss of NL2 in the somatosensory cortex affects the synapses of different inhibitory interneuron subtypes on excitatory neurons. IPSCs that were excited by stimulation of somatostatin positive neurons were not altered by the loss of NL2. In contrast, IPSCs evoked by PV+ neurons were decreased (Gibson et al 2009b). Due to increased NL4 immunoreactivity in the retina of NL2-deficient mice, it is speculated that the loss of NL2 may be partially compensated by NL4 (Hoon et al 2011).

It can thus be summarised that the central function in the neurexin-NL interaction lies in the synaptic coupling and organisation of inhibitory and excitatory synaptic specialisations (Missler et al 2012). Loss of NL1-3 (Varoqueaux et al 2006) or all α-neurexins (Missler 2003) perturbs synaptic transmission, leading to perinatal death, with synaptogenesis remaining unaltered. Consistent with their essential function in organising and specialising synapses, mutations in the genes encoding NL2-4 have been detected in patients with a wide range of cognitive disorders. For example, a dysfunction of NL2 was identified in a patient with schizophrenia (Sun et al 2011). Numerous mutations of NL3 and NL4 occur in ASD patients (Sudhof 2008). Specifically, a NL4 mutation was reported in a patient with mental retardation (Laumonnier et al 2004). All these reported examples point to an important and central role of the NLs in safeguarding and organising synaptic function.

Besides the transsynaptic interaction of neurexins with NL, the former are also able to bind and interact with other postsynaptic proteins. Interestingly, it has also been described that neurexins can even be localised postsynaptically, and thus inhibit the function of NL1 and NL2 in cis (Lee et al 2013, Taniguchi et al 2007). While at inhibitory synapses only an interaction with NL, $GABA_AR$ and dystroglycan has been described so far (Sudhof 2008), several additional interaction partners of neurexins at the excitatory postsynapses are known (Krueger et al 2012, Linhoff et al 2009).

1.4.4.2 Dystroglycan

Dystroglycan is a ubiquitously expressed transmembrane protein that forms a dimer of α- and β-dystroglycan (Sugita et al 2001). In the majority of tissues, the extracellular domains of the dimer bind to extracellular matrix proteins. In synapses, they interact with neurexins (Sugita et al 2001). Contact with the actin cytoskeleton is formed via interaction with dystrophin via the intracellular domain.

Previous studies showed that dystroglycan is involved in about one third of all inhibitory synapses of mature cultured hippocampal neurons (Levi et al 2002), but loss of dystroglycan does not affect gephyrin and $GABA_AR$ cluster formation (Levi et al 2002). Furthermore, dystroglycan is important for clustering of dystrophin at synapses, which partly colocalises with $GABA_ARs$ (Levi et al 2002). Accordingly, loss of dystrophin clustering results in mislocalisation of $GABA_AR$, whereas gephyrin localisation remains unaffected (Knuesel et al 1999). Taken together, these studies indicate that the dystrophin-associated glycoprotein complex (DGC) contributes to the maturation of a subset of GABAergic synapses, but acts independently of $GABA_AR$ clustering by gephyrin.

1.4.4.3 Slitrk3 and tyrosine phosphatase

Slitrk3 is a membrane protein that has 5 paralogs. The protein family is characterised by homology to Trk family proteins in their intracellular part and by extracellular leucine-rich repeat domains. Slitrk3 is exclusively localised at inhibitory synapses, where inhibitory presynaptic differentiation is initiated by an interaction with protein tyrosine phosphatase (PTP) (Takahashi et al 2012, Yim et al 2013). Slitrk3 deficient mice show a reduction in the density of inhibitory synapses and in inhibitory transmission, and additionally exhibit epileptic seizures (Takahashi et al 2012).

Furthermore, a NL2-Slitrk3 interaction also seems to play an important role in synaptic development. Selective perturbation of this interaction leads to impaired synaptic development with disruption in hippocampal network activity and increased seizure susceptibility (Li et al 2017).

1.4.4.4 IgSF9b and IgSF9

Immunoglobulin superfamily 9 (IgSF9) proteins are homophilic cell adhesion proteins that play a role in neurite growth, axon guidance and synapse maturation as their function (Mishra et al 2014, Woo et al 2013).

immunoglobulin superfamily member 9b (IgSF9b) is the first protein of this family to be described and is associated with depressive disorder (Shyn et al 2011, Woo et al 2013). It is expressed at later developmental stages than NL2 and is involved in the development of inhibitory synapses on inhibitory interneurons. Consistent with the described function, IgSF9b KO mice exhibit reduced synaptic gephyrin clustering associated with diminished inhibitory synaptic transmission (Woo et al 2013). IgSF9b is localized in a subsynaptic domain that is connected to NL2 via the scaffold protein S-SCAM and thus to the $GABA_AR$/gephyrin/NL2 domain (Mishra et al 2014). It was hypothesized that these two domains control the function of inhibitory synapses in a synergistic manner.

It had long been believed that the second member of the family, IgSF9, is involved in the development of excitatory synapses. However, recent studies showed that IgSF9 KO mice show no changes in excitatory synapses, but inhibitory synapse density and inhibitory transmission are reduced

(Mishra et al 2014). In summary, neither family member is able to initiate synapse formation *de novo*, so that their role is rather to regulate the maturation of synapses.

1.4.4.5 Interplay between different cell adhesion systems

Today, numerous synaptic cell adhesion molecules are known, such as NL2, NL4, dystroglycan, which have also been briefly described here in terms of their function and structure. So far, a multitude of modes of action have been deciphered, which can be different, partly overlapping or even cooperative. It has been shown, for instance, that NL2 and IgSF9b are located in the same inhibitory synapses, but in different subsynaptic domains (Woo et al 2013). Loss of either NL2 or Slitrk3 leads to a loss of inhibitory synapses in the stratum pyramidale of the CA1 region of the hippocampus, suggesting that both may be essential for synapse formation in this area (Takahashi & Craig 2013).

On the other hand, negative regulators have also been identified. As an example, MAM domain-containing GPI anchor proteins (MDGAs), members of the Ig superfamily of cell adhesion proteins, interact in cis with NL2 and thus prevent the binding of neurexin to NL2. This results in a reduction in the number of inhibitory synapses as well as inhibitory synaptic transmission (Lee et al 2013). Not only for MDGAs, but also for many other synaptic adhesion molecules, the relevance for normal brain function becomes clear through the various associated psychiatric disorders (Bucan et al 2009, Li et al 2011).

1.5 The scaffold

To ensure efficient and error-free chemical transmission at synapses, it is necessary that the receptors on the postsynaptic side are positioned as closely as possible to the active zone transmitter release site on the presynaptic side. Since the cell membrane is a dynamic construct, it is necessary to trap the receptors in the perfect location. This task is performed by intracellular postsynaptic scaffold proteins, which thus play an essential role in synaptic transmission.

1.5.1 Gephyrin

The most prominent scaffolding protein of inhibitory postsynapses is gephyrin (Luscher et al 2011). Besides its high affinity binding to GlyR, by which gephyrin was identified, it is also able to interact with the α1-3 and β2-3 subunits of $GABA_AR$, but here with much lower affinity (Kirsch et al 1991, Kowalczyk et al 2013, Maric et al 2011, Saiepour et al 2010, Tretter et al 2008, Tretter et al 2011). Gephyrin is able to interact simultaneously with cytoskeletal proteins, specifically kinesin superfamily protein 5 (KIF5) and mammalian enabled /vasodilator stimulated phosphoprotein (Mena/Vasp), as well as with synaptic cell adhesion proteins such as NL2, in addition to receptors (Luscher et al 2011). This ensures that gephyrin acts as a bridge between neurotransmitter receptors and the subsynaptic cytoskeleton. In this way, positioning of the receptors in a favourable position relative to the active zone of the presynapses

can be ensured. Gephyrin undergoes regulation by proteins such as CB [(Kins et al 2000); see also 1.6.1] and heat-shock protein 70 [(Hsc70), (Machado et al 2011)].

The importance of gephyrin in inhibitory transmission has been demonstrated by gephyrin KO mice, which show a reduction in α2- and γ2-subunit-containing $GABA_AR$ at inhibitory synapses, and secondly by RNAi mediated knock down of gephyrin expression, which gave comparable results (Essrich et al 1998, Feng et al 1998, Kneussel et al 1999, Levi et al 2004). An interesting observation is that loss of various $GABA_AR$ subunits, such as the γ2 subunit, also leads to a loss of gephyrin at synaptic sites, indicating an interdependence between gephyrin and $GABA_AR$ clustering (Essrich et al 1998).

Various deletions and point mutations of the human gene GPHN encoding gephyrin, as well as irregular splicing of gephyrin mRNA, have been detected in patients diagnosed with epilepsy (Forstera et al 2010, Lionel et al 2013), autism spectrum disorders (Lionel et al 2013, Prasad et al 2012), schizophrenia (Lionel et al 2013), and hyperekplexia (Rees et al 2003).

In non-neuronal cells, gephyrin is essential for molybdenum cofactor (Moco) biosynthesis (Feng et al 1998). Thus, patients with homozygous genetic defects in GPHN show pathologies associated with Moco degradation (Lionel et al 2013). In vertebrates, gephyrin is highly conserved. However, tissue-specific splicing results in proteins with different subcellular localization (Nawrotzki et al 2012). Further functional diversity is achieved by different posttranslational modifications (Tyagarajan & Fritschy 2014).

A gephyrin monomer, as shown in **Figure 5** , consists of a G domain homologous the bacterial MogA protein, a central linker domain, and an E domain (Luscher et al 2011). MogA and MoeA are involved in Moco biosynthesis in bacteria, which explains one of the functions of gephyrin. Essential properties for clustering are the ability of dimerization of the G domain and trimerisation of the E domain (Saiyed et al 2007). This observation led to a model hexagonal gephyrin structures as a scaffold.

Gephyrin

Figure 5 Domains of monomeric gephyrin
N-terminal G-domain with the ability of dimerization, homologous to the bacterial MogA; Central linker domain; C-terminal E-domain with the ability of trimerisation.

Later structural analysis using atomic force microscopy and X-ray scattering showed that dimerization of the E-domain is inhibited in holo-gephyrin, calling the hexagonal model into question (Sander et al 2013). Further, this study showed that gephyrin exists in different compact and extended states. With the use of different single-molecule-based imaging techniques, a better understanding of the three-dimensional organization of gephyrin at inhibitory postsynapses was achieved (Specht et al 2013). These studies confirmed previous observations that gephyrin forms a two-dimensional lattice with constant spacing. Furthermore, different packing densities of gephyrin in different synapses were also described (Specht et al 2013). This could explain differences in conformation observed in the experiments of Sander et al. (2013).

1.5.2 S-SCAM

Gephyrin is arguably the most important scaffolding protein at inhibitory synapses. However, based on studies showing that the deletion of gephyrin does not lead to a complete loss of $GABA_ARs$ or inhibitory neurotransmission in hippocampal neurons, there must be other scaffold proteins that can partially take

over the function of gephyrin (Levi et al 2004). Another important scaffold protein is S-SCAM (also called membrane-associated guanylate kinase inverted-2 or atrophin interacting protein-1), a 141 kD protein localised at both inhibitory and excitatory synapses (Hirao et al 1998, Sumita et al 2007). S-SCAM has 5 or 6 PDZ domains, one guanylate kinase-like domain, and two WW domains and is similar in structure to PSD-95, the main scaffolding protein at excitatory synapses (Hirao et al 1998). The function and interaction partners of S-SCAM, such as NMDA (N-methyl-D-aspartate) receptors, neuroligin-1 and SAPAP, are best characterised at excitatory synapses (Hirao et al 1998). NL2, IgSF9b and β-dystroglycan are cell adhesion molecules of inhibitory synapses that interact with S-SCAM (Sumita et al 2007, Woo et al 2013). It is interesting to note that each of the interacting molecules occupies individual binding sites on S-SCAM. S-SCAM binds to dystroglycan through its WW domains, to NL2 through its WW domains and the second PDZ domain, and to IgSF9b through its PDZ domains 4 and 5 (Sumita et al 2007, Woo et al 2013). As described above (see 1.4.4.4), S-SCAM can thus serve as a link between different subsynaptic domains (Mishra et al 2014). Furthermore, it can serve as a link to the cytoskeleton by binding to intracellular signalling proteins such as SynARFGEF (Fukaya et al 2011). In patients with epilepsy (Marshall et al 2008) and schizophrenia (Karlsson et al 2012), mutations in MAGI2, the gene coding for S-SCAM, were identified. Further investigation of the specific effects of S-SCAM loss on inhibitory synapses is very difficult due to its localisation on inhibitory and excitatory synapses.

1.6 Interacting molecules of the scaffold

1.6.1 Collybistin

CB, a brain specific GEF, was described for the first time in ascidian embryos and named posterior end mark 2 (PEM-2) due to its polarized localization (Satou & Satoh 1999). Later, a homology search to identify other GEFs of the Dbl family for small Rho GTPases led to the discovery of the human homologue hPEM-2 on the X chromosome. The domain structure (see Figure 6) of an N-terminal src homology 3 (SH3) domain and a tandem of a Dbl homology (DH) and a pleckstrin homology (PH) domain was also characterized.

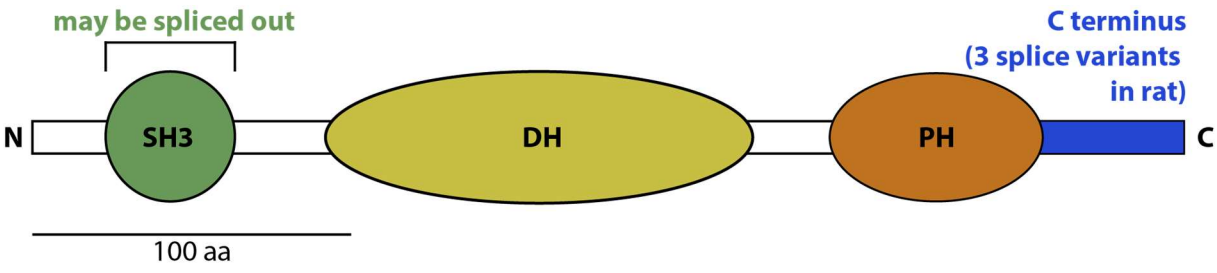

Figure 6 Domains of Collybistin (CB)
N-terminal src homology 3 (SH3) domain, Dbl homology (DH) domain and pleckstrin homology (PH) domain.

Furthermore, it was shown using biochemical and morphological approaches that Cdc42 is specifically activated by hPEM-2 in cells (Reid et al 1999). In a yeast 2-hybrid screen aimed at discovering new gephyrin-binding proteins, two different transcripts of the same gene were identified in a cDNA library generated from brains of newborn rats (Kins et al 2000). The protein sequences of the newly identified transcripts showed 93% identity with the hPEM-2 sequence. Derived from the ancient Greek

“κολλυβιστής” for a person who changed small coins, the new protein was named "collybistin" due to its presumed function as a GEF (Kins et al 2000). The difference between the two splice variants is the presence or absence of the C-terminal SH3 domain (Kins et al 2000). Furthermore, upon co-expression of the longer SH3 domain-containing variant CBI with gephyrin, an accumulation of both proteins in cytoplasmic aggregates could be observed. These aggregates are also formed by gephyrin alone. In contrast, co-expression of the shorter SH3-domain-lacking variant with gephyrin led to the formation of plasma membrane-associated clusters in which both proteins colocalized (Kins et al 2000). This fundamental work by Kins and colleagues (2000) demonstrated the potential role of CB in the regulation of gephyrin, associated neurotransmitter receptor targeting to the plasma membrane and neurotransmission at inhibitory synapses.

1.6.1.1 Expression of CB

Expression, alternative splicing and localization of CB were previously described in many studies (Chiou et al 2011, Harvey et al 2004b, Kins et al 2000, Kneussel et al 2001, Patrizi et al 2012, Reid et al 1999). CB is mainly expressed in the brain, whereas only low levels have been detected in the heart and skeletal muscles (Kins et al 2000, Reid et al 1999). In an *in situ* hybridization study, it was shown that CB mRNA can be detected in postmitotic neurons of different brain regions at a time of neuronal death (Kneussel et al 2001). Both recombinantly and endogenously expressed CB show a subcellular localization at inhibitory postsynapses and in the cytoplasm (Chiou et al 2011, Harvey et al 2004a). Immunohistochemical studies using an antibody against the C-terminal domain of CB3 showed that the longest splice variant is colocalized with 40-80% of gephyrin positive synapses in different brain regions (Patrizi et al 2012). Interestingly, CB3 was also found to be colocalized with dystroglycan-positive, gephyrin-deficient synapses of the cerebellum (Patrizi et al 2012). Colocalization of CB3 with all $GABA_AR$ α subunits, as well as the GlyR in the spinal cord, has also been documented (Patrizi et al 2012). The examination of the mRNAs of all three CB variants showed that $CB2_{SH3+}$ and CB3 are the most abundant isoforms in the adult rat brain (Harvey et al 2004a). Interestingly, co-expression of gephyrin with $CB2_{SH3+}$ in HEK293 cells did not result in the formation of submembranous microclusters of gephyrin (Harvey et al 2004a, Kins et al 2000). Furthermore, expression of either $CB2_{SH3-}$ or $CB2_{SH3+}$ in hippocampal neurons has different effects on inhibitory postsynapses (Chiou et al 2011). For example, $CB2_{SH3-}$ expression significantly increases gephyrin and $GABA_AR$ γ2 subunit cluster size and leads to an increase in the amplitude of miniature IPSCs (mIPSCs). In contrast, expression of $CB2_{SH3+}$ causes an increase in the density of gephyrin and $GABA_AR$ γ2 subunit clusters in dendritic structures (Chiou et al 2011).

In addition, the results of Chiou et al., 2011 described above were further supported by another study, in which $CB2_{SH3-}$ was shown to induce mainly synaptic and $CB2_{SH3+}$ mainly extrasynaptic gephyrin clusters (Tyagarajan et al 2011).

1.6.1.2 Loss of CB affects the formation of inhibitory synapses

In CB KO mice, the specific loss of synaptic gephyrin and γ2 subunit-containing $GABA_ARs$ in the hippocampus was described, demonstrating the importance of CB for inhibitory synaptogenesis (Papadopoulos et al 2007). Furthermore, electrophysiological analyses of brains derived from CB KO animals indicated both defects in hippocampal GABAergic neurotransmission and changes in

hippocampal synaptic plasticity, as compared to controls (Papadopoulos et al 2007). Moreover, CB KO mice showed increased anxiety-levels and defects in spatial learning, as compared to controls (Papadopoulos et al 2007). In addition, CB was shown to be essential for both the formation and the maintenance of GABAergic postsynapses in the hippocampus (Papadopoulos et al 2008). Contrary to expectations, no changes in gephyrin or GlyR clustering in the spinal cord or neuromotoric defects were observed in CB KOs, although CB is localized in the spinal cord and has the ability to trigger GlyR clustering together with gephyrin in non-neuronal cells (Papadopoulos et al 2007). This suggests that there must be other signaling proteins that take over the role of CB in the unaffected glycinergic synapses of CB KO animals.

1.6.1.3 The importance of CB for gephyrin-dependent clustering of $GABA_ARs$

Despite numerous studies aimed at unraveling the molecular mechanism by which CB recruits gephyrin to the plasma membrane and thus induces clustering of $GABA_ARs$, a detailed mechanistic understanding of the CB-dependent formation of inhibitory synapses is not yet available. Previous studies defined a CB-based protein interaction network that controls the gephyrin content at inhibitory postsynapses (Kilisch et al 2020, Mayer et al 2013, Papadopoulos et al 2015, Poulopoulos et al 2009, Soykan et al 2014). Within this network, CB can adopt open/active and closed/inactive conformations to act as a switchable adaptor that links gephyrin to plasma membrane phosphoinositides (Kilisch et al 2020, Soykan et al 2014).

The most abundant isoforms of CB in the brain are SH3-domain-containing ones (Harvey et al 2004a). However, SH3 domain-containing isoforms do not have the ability to initiate gephyrin clustering in non-neuronal cells (Kins et al 2000). Previous studies identified NL2 as the first protein capable of interacting with the SH3 domain of CB, thereby stabilizing the open/active conformation of CB at the postsynaptic plasma membrane by competing with an intramolecular interaction in CB that favors the closed/inactive conformation (Poulopoulos et al 2009, Soykan et al 2014). In addition, NL4 (Hoon et al 2011), the α2 subunits of $GABA_ARs$ (Saiepour et al 2010) or the small Rho-like GTPase TC10 (Mayer et al 2013), are capable of interacting with either the SH3 domain (NL4, $GABA_AR$-α2) or the PH domain (TC10) of CB, thereby stabilizing its open/active conformation (Soykan et al 2014).

The DH domain of CB catalyzes the GDP-GTP exchange on small Rho-like GTPases. Based on biochemical assays with the three Rho-like GTPases, Cdc42, Rac1 and RhoA, mouse CB and its human ortholog were initially described as Cdc42-specific GEFs (Reid et al 1999). However, gephyrin and $GABA_AR$ clustering is not affected by forebrain-specific deletion of Cdc42 in mice, indicating that CB may also activate other Rho-like GTPases in the brain (Reddy-Alla et al 2010). Accordingly, the small Rho-like GTPase TC10, which is closely related to Cdc42, has been previously shown to induce CB-dependent clustering of gephyrin and $GABA_ARs$ at inhibitory postsynaptic sites (Mayer et al., 2013). Moreover, GTP-bound TC10 maintains an interaction with the PH domain of CB as a GTPase-effector complex (Mayer et al., 2013). This active TC10-CB complex is capable of inducing a phospholipid affinity switch in the PH domain of CB, which allows CB to specifically interact with phosphoinositide species present at the plasma membrane (Kilisch et al 2020). Interestingly, a series of missense mutations in the human CB gene (R290H, R338W and R356Q) that are linked to epilepsy and intellectual disability were shown to disrupt phospholipid binding of CB and to result in defective gephyrin clustering in neurons (Chiou et al 2011, Kalscheuer et al 2009, Long et al 2015, Papadopoulos et al 2015).

1.7 The cytoskeletal system of synapses

A complex meshwork of microtubules, actin microfilaments, intermediate filaments and many associated proteins form the neuronal cytoskeleton, which is responsible for determining neuronal morphology and for the transport and anchoring of cellular components (Allison et al 2000). A highly complex interplay of regulatory enzymes, adaptors, molecular motors, scaffolding proteins and the cytoskeletal system is required to achieve the desired localization of postsynaptic proteins (Allison et al 2000).

In small actin-rich projections, the dendritic spines, more than 90% of the excitatory glutamatergic synapses in the mammalian brain are localized (Harris & Kater 1994). Despite their similar structure, consisting of longitudinal actin filaments in the neck and a lattice of actin filaments in the head, spines show differences in their size and morphology (Cohen et al 1985, Fifkova 1985, Landis & Reese 1983). In all glutamatergic synapses, the individual components of the PSD may be anchored to actin-, tubulin- or neurofilament-based cytoskeletal systems, or their localization may be independent of these complex systems (Brenman et al 1998, Ehlers et al 1998, Niethammer et al 1998, Shen et al 1998). For example, the synaptic accumulation of NMDA receptors has been shown to be largely independent of F-actin, whereas the synaptic accumulation of AMPA receptors in pyramidal cells of the hippocampus is dependent on the actin system (Allison et al 1998).

Inhibitory synapses are primarily localized to cell bodies and the shafts of dendrites and axon initial segments (Allison et al 2000). In these synapses, $GABA_AR$ is bound to the microtubule skeleton via gephyrin and/or GABARAP [GABAR adopter protein; (Essrich et al 1998, Kirsch & Betz 1995, Wang et al 1999) Furthermore, gephyrin is able to bind to microtubules *in vitro* and to thereby determine the synaptic localization of $GABA_AR$ in hippocampus (Essrich et al 1998, Kirsch et al 1991, Kneussel et al 1999).

1.7.1 Gephyrin and its interaction with the cytoskeleton

As mentioned in the section above, a highly complex interaction of numerous components is often necessary to achieve and maintain the localization of neurotransmitter receptors in the postsynaptic membrane (Allison et al 2000). The interaction of the cytoskeleton with scaffold proteins such as gephyrin also plays an important role.

The role of the actin cytoskeleton in the formation of the gephyrin scaffold was previously discussed but has not been clarified yet (Allison et al 2000, Kirsch & Betz 1995, Kirsch et al 1995). In contrast, biochemical analyses and transfection studies have shown that gephyrin binds cooperatively to polymerized tubulin with high affinity (Kirsch et al 1991). Furthermore, depolymerization of the microtubule network by demecolcin leads to impaired synaptic localization of gephyrin and the glycine receptor in spinal cord cultures (Kirsch & Betz 1995, Kirsch et al 1991). Furthermore, a complex formation between gephyrin and the microtubule motor protein dynein (Dlc-1/-2) was demonstrated (Fuhrmann et al 2002).

Another cytoskeleton-organizing protein that interacts with gephyrin is profilin (Mammoto et al 1998). Profilin stimulates the ADP-ATP exchange reaction of the actin monomer, which leads to a promotion of the incorporation of G-actin into F-actin filaments (Lambrechts et al 1995). Furthermore, profilin 1 is able to bind to phosphatidylinositol-3,4,5-trisphosphate (PIP_3) (Lambrechts et al 1995) and to enabled vasodilator stimulated phosphoprotein (ena/VASP) (Reinhard et al 1995). Furthermore, a role of profillin in endocytosis and vesicle recycling was previously discussed (Witke et al 1998). So far,

4 isoforms of profilin have been identified in mammals. Profilin is known to be expressed in numerous tissues, whereas profilin 2 is expressed exclusively in the brain and skeletal muscle (Witke et al 1998). The protein ena/VASP is also a ligand of gephyrin and can influence the organization of the microfilament system (Giesemann et al 2003). It belongs to a protein family derived from the Drosophila protein enabled (Ena), the corresponding mammalian homologue Mena (mammalian enabled) and VASP (Gertler et al 1996, Niebuhr et al 1997). All members of this family share a tripartite domain structure that includes an N-terminal ena/VASP homologous domain 1 (EVH1), a proline-rich region (similar to gephyrin) and the EVH2 domain in the C-terminal region (Gertler et al 1996, Niebuhr et al 1997). The protein mediates the recruitment of profilin-actin complexes to plasma membranes with active microfilament synthesis (Huttelmaier et al 1998). Here, ena/VASP often binds to proline-rich regions, such as those found in the linker region of gephyrin (Krause et al 2003, Mammoto et al 1998). Furthermore, ena/VASP can also bind to profilin, and this interaction is also mediated by the proline-rich region (Mammoto et al 1998). Gephyrin and profilin colocalize at inhibitory synapses as well as in recombinant expression systems (Giesemann et al 2003). This is an interesting observation as it indicates that gephyrin and G-actin compete for the same binding site on profilin, while interaction with VASP occurs at the C-terminal E-domain of gephyrin (Giesemann et al 2003).

2 Materials and Methods

2.1 Material

Table 1 Material

Name	Company	Head Office
1 ml syringe	BD Plastipak TM	Franklin Lakes, New Jersey, USA
1.5 ml tubes	Eppendorf AG	Hamburg, Germany
10 cm dishes (falcon)	Corning, Inc.	New York, USA
12 well cell culture plates	Greiner Bio-one International GmbH	Kremsmünster, Austria
15 ml falcon	BD falcon	Franklin Lakes, New Jersey, USA
2.0 ml Deep Well plates	Thermo Fisher Scientific Inc.	Waltham, Massachusetts, USA
50 ml falcon	BD falcon	Franklin Lakes, New Jersey, USA
Clean gate Kit	nexttec™ Biotechnologie GmbH	Hilgertshausen, Germany
Coverslips (Menzel-Gläser, 24x50 mm)	Thermo Fisher Scientific Inc.	Waltham, Massachusetts, USA
Coverslips (Menzel-Gläser, Ø 18 mm)	Thermo Fisher Scientific Inc.	Waltham, Massachusetts, USA
Electroporation cuvettes	Bio-Rad Laboratories, Inc.	Hercules, California, USA.
Microscope slides (Menzel Gläser, ground edges 45°, frosted end)	Thermo Fisher Scientific Inc.	Waltham, Massachusetts, USA
Microscope slides (Menzel Gläser, Superfrost Plus)	Thermo Fisher Scientific Inc.	Waltham, Massachusetts, USA
20G needle	BD Microlance TM 3	Franklin Lakes, New Jersey, USA
Tissue filter	BD falcon	Franklin Lakes, New Jersey, USA

2.1.1 Reagents

Table 2 Reagents

Name	Company	Head Office
10× REDTaq® PCR reaction Buffer	Sigma Aldrich GmbH	St. Louis, Missouri, U.S.A.
6x Loading Dye	Thermo Fisher Scientific Inc.	Waltham, Massachusetts, USA
Ampicillin	Hoffmann-La Roche AG	Basel, Switzerland
B-27 Supplement	Gibco by life technologies (Thermo Fisher Scientific)	Waltham, Massachusetts, USA
Bacto Agar	BD (Becton, Dickson and Company)	Franklin Lakes, New Jersey, USA
Bacto R peptone	Difco Laboratories GmbH (by BD (Becton, Dickinson and Company))	Franklin Lakes, New Jersey, USA
Bacto TM Yeast extract	BD (Becton, Dickson and Company)	Franklin Lakes, New Jersey, USA
Blasticidin S HCl	Invitrogen (by Thermo Fisher Scientific Inc)	Waltham, Massachusetts, USA
Buffer B	nexttec™ Biotechnologie GmbH	Hilgertshausen, Germany
Carbenicillin	Invitrogen (by Thermo Fisher Scientific Inc)	Waltham, Massachusetts, USA
DAPI solution (4‘, 6-Diamidino-2-phenylindol)	Thermo Fisher Scientific Inc.	Waltham, Massachusetts, USA
Dulbecco's Modified Eagle's medium (DMEM)	Gibco by life technologies (Thermo Fisher Scientific)	Waltham, Massachusetts, USA
DNA ladder 100bp	Thermo Fisher Scientific Inc.	Waltham, Massachusetts, USA
DNA ladder 1kb	Invitrogen (by Thermo Fisher Scientific Inc)	Waltham, Massachusetts, USA
dNTPs (2.5mM)	Bioline GmbH	London, UK
Fetal Calf Serum (FCS)	Gibco by life technologies (Thermo Fisher Scientific)	Waltham, Massachusetts, USA

Name	Company	Head Office
GC-Melt Ragent (5M)	Clontech Laboratories, Inc (Takara Bio USA, Inc.)	Kyoto, Japan
Gel red	Biotium, Inc.	Fremont, CA, USA
Glycerol	Sigma Aldrich GmbH	St. Louis, Missouri, U.S.A.
Goat serum	Gibco by life technologies (Thermo Fisher Scientific)	Waltham, Massachusetts, USA
Hank's Balanced Salt Solution (HBSS) (no calcium, no magnesium)	Gibco by life technologies (Thermo Fisher Scientific)	Waltham, Massachusetts, USA
HBSS (with calcium, magnesium)	Gibco by life technologies (Thermo Fisher Scientific)	Waltham, Massachusetts, USA
Hygromycin B in PBS (50mg/ml)	Invitrogen (by Thermo Fisher Scientific)	Waltham, Massachusetts, USA
L-Glutamine 200mM	Gibco by life technologies (Thermo Fisher Scientific)	Waltham, Massachusetts, USA
Lipofectamin 2000	Invitrogen (by Thermo Fisher Scientific Inc)	Waltham, Massachusetts, USA
Neurobasal medium	Gibco by life technologies (Thermo Fisher Scientific)	Waltham, Massachusetts, USA
nexttec™ 1-Step Plasmid Isolation Kit	nexttec™ Biotechnologie GmbH	Hilgertshausen, Germany
Optimem	Gibco by life technologies (Thermo Fisher Scientific)	Waltham, Massachusetts, USA
Paraformaldehyde (PFA)	Sigma Aldrich GmbH	St. Louis, Missouri, U.S.A.
Penicillin/Streptomycin (10000 Units/ml Penicillin, 10000µg/ml Streptomycin)	Gibco by life technologies (Thermo Fisher Scientific)	Waltham, Massachusetts, USA
Phosphate buffered saline (PBS)	Gibco by life technologies (Thermo Fisher Scientific)	Waltham, Massachusetts, USA
Poly L Lysin	Sigma-Aldrich GmbH	St. Louis, Missouri, U.S.A.
Prep Agraose	Biozym Scientific GmbH	Hessisch Oldendorf, Germany
QIAGEN Endofree Plasmid Maxi Kit	QIAGEN N.V.	Venlo, Netherlands

Name	Company	Head Office
RedTaq ® DNA Polymerase	Sigma Aldrich GmbH	St. Louis, Missouri, U.S.A.
Sodium Chloride (NaCl)	Merck KGaA	Darmstadt, Germany
TET	Sigma-Aldrich GmbH	St. Louis, Missouri, U.S.A.
Trypsin -EDTA (0.05%)	Gibco by life technologies (Thermo Fisher Scientific)	Waltham, Massachusetts, USA
UltraPure TM Agarose	Thermo Fisher Scientific Inc.	Waltham, Massachusetts, USA
ZymoPURE Midi Prep kit	Zymo Research Corp	California, USA

2.1.2 Equipment

Table 3 Equipment

Name		Company ; Head Office
Centrifuges	Biofuge pico	Heraeus GmbH, Hanau, Germany
	Megafuge 3.0R	Heraeus GmbH, Hanau, Germany
	Sigma 2	Sigma Laborzentrifugen GmbH, Osterode am Harz, Germany
Electrophoresis	Electrophoresis power supply EPS 301	Amersham pharmacia biotec/ GE Healthcare, Chicago, Illinois, United States
Electrophoresis	Gel electrophoresis apparatus horizon 11 14	Life technologies/ gibco BRL horizontal (Gel Company, Inc.), San Francisco, CA, USA
Incubator	Hera Cell 240	Heraeus GmbH, Hanau, Germany

Name		Company ; Head Office
Microscope	Zeiss Imager. Z1	Carl Zeiss AG, Oberkochen, Germany
	Leica TCS SP2	Leica Microsystems GmbH, Wetzlar, Germany
Neubauer Chamber	Neubauer Chamber	Carl Roth GmbH + Co.KG, Karlsruhe, Germany
Photometer	Ultrospec™ 3100 pro	Amersham Biosciences/GE Healthcare, Chicago, Illinois, United Stat
Pipettes	Pipetman	Gilson, Villiers-le-Bel, France
Pipettboy	Pipetboy acu	Integra Biosciences GmbH, Fernwald, Germany
Shaking incubator	Innove 4000	New Brunswick Scientific, Edison, New Jersey, USA
Sterile bank	Haraueus GmbH, Hanau, Germany	Sterile bank
Water bath	Certomat WR	B. Braun Biotech International GmbH, Melsungen, Germany
Vortex	Vortex Genie 2	Bender & Hobein AG, Switzerland

2.1.3 Cell lines and primary cells

Cell Lines:

The following is a list of all cell lines and associated required media (Thermo Fisher Scientific) and solutions used in this work.

HEK 293 FT (R700-07; Thermo Fisher Scientific, Germany) cells were used to produce AVV and Adenovirus particles.

Flp-In T-Rex HEK 293 cells (R780-07) were purchased from Thermo Fisher Scientific, Germany.

Flp-In T-Rex-GFP-gephyrin HEK 293 cells were provided by Dr. Theofilos Papadopoulos (Papadopoulos et al 2017).

COS-7 cells (CRL-1651; ATCC, LGC Standards GmbH, Germany) were used in verify the results obtained with Flp-In T-Rex-GFP-gephyrin HEK 293 cells.

HEK293 FT and COS-7 Culture Medium

DMEM	445 ml
FBS	50 ml
P/S	5 ml

Flp-In T-Rex-GFP-gephyrin HEK 293 cells were used to perform the cDNA library screen. A special feature of this cell line is that it expresses GFP-Gephyrin upon TET administration (Papadopoulos et al 2017).

Flp-In T-Rex-GFP-gephyrin HEK 293 Culture Medium

HEK 293 FT-Culture Medium	50 ml
Blasticidin	50 µl (Stock: 15 mg/ml)
Hygromycin B	200 µl (Stock: 50 mg/ml)

Galantine Solution

Gelantine	0.1 % (w/v)
PBS	

Poly-D Lysine Solution

Poly-D Lysine	10 % (v/v)
PBS	

Induction Solution

TET	40 µl (Stock: 2 mg/ml)
HEK 293 FT Culture Medium	20 ml

Primary Cell Cultures:

This section lists all solutions and media that were necessary for the preparation and cultivation of the hippocampal mouse neurons.

Papain Stock Solution

Cysteine	0.2 mg/ml
$CaCl_2$	1 mM
EDTA in DMEM	0.5 mM

Papain Working Solution

Papain	20 Units
Papain Stock Solution	1 ml

➔ *Solution was saturated with carbogen (95% oxygen, 5% carbondioxide) until Papain was resolved, and then it was sterilized using a 0.22 µm filter (Millipore).*

Stop Solution

BSA	2.5 mg/ml
Trypsin inhibitor	2.5 mg/ml
FBS	10 % (v/v)
DMEM	

Complete Neurobasal Medium

GlutaMAX	1 % (v/v)
B-27 supplement	2 % (v/v)
P/S	0.2 % (v/v)
Neurobasal A	

2.1.4 Bacterial strains

Table 4 List of bacteria strains used in this study

Strain	Application	Company
E. coli XL-1 Blue electrocompetent cells	cloning	Stratagene
E. coli 5-alpha high efficiency chemically competent cells	cloning	NEB
E. coli BL21 Rosetta electrocompetent cells	protein expression	Stratagene
E. coli Stable high efficiency chemically competent cells	AAV particles	NEB

2.1.5 Buffers and Media

2.1.5.1 Buffers for protein biochemistry

10 % SDS Solution

SDS	10 % (w/v)
H_2O	

Separating Gel Buffer

Tris-HCl	1.5 M
SDS	0.4 %
H_2O	

➔ *Adjust pH to 8.8*

Stacking Gel Buffer

Tris-HCl	0.5 M
SDS	0.4 %

➔ *Adjust pH to 6.8*

APS Solution

APS	10 % (w/v)
H_2O	

5x SDS-PAGE Loading Buffer

DTT	500 mM
SDS	10 % (w/v)
Glycerine	50 % (v/v)
Tris/HCl pH 6.8	250 mM
Bromophenol blue	0.5 % (w/v)

SDS-PAGE Separating Gel

	7.5 %	10 %	12 %
H_2O	4.8 ml	4 ml	3.3 ml
Separating gel buffer	2.5 ml	2.5 ml	2.5 ml
10 % SDS	100 µl	100 µl	100 µl
30 % Acrylamide	2.5 ml	3.3 ml	4 ml
10 % APS	100 µl	100 µl	100 µl
TEMED	10 µl	10 µl	10 µl

SDS-PAGE Stacking Gel

	4 %
H_2O	3.6 ml
Stacking gel buffer	1.5 ml
10 % SDS	60 µl
30 % Acrylamide	800 µl
10 % APS	60 µl
TEMED	10 µl

10X TBS (Tris Bufferd Saline)

Tris-Base	0.2 M
NaCl	1.5 M
H_2O	

➔ *Adjust pH to 7.6*

1x TBS

10x TBS	10 % (v/v)
H_2O	

10x SDS PAGE Running Buffer

Tris	250 mM

Glycine	2 M
SDS	1 % (w/v)

1x SDS PAGE Running Buffer

10x SDS PAGE Running Buffer	10 & (v/v)
H_2O	

Coomassie Brilliant Blue (1 l)

- Dissolve 2,6 M $(NH_4)_2SO_4$ in 500 ml H_2O
- Slowly add 310 ml methanol while stirring continuously
- Allow time for the ammonium sulfate, dropping out of solution after each addition, to dissolve.
- Towards the end, the ammonium sulfate won't go back into solution → solution is milky
- Add 3,6 % (v/v) phosphoric acid while stirring continuously → solution becomes clear
- Add H_2O up to a total volume of 970 ml
- Add 0,2% (w/v) g of Coomassie G250 to a 50 ml reaction tube (Falcon) and dissolve completely in 10 ml methanol
- Transfer the 10% Coomassie solution into the prepared 970 ml
- Make up volume to 1 l

Blotting Buffer

SDS PAGE Running Buffer	10 % (v/v)
Methanol	20 % (v/v)
H_2O	

10x PBS

Na_2HPO_4	80 mM
NaH_2PO_4	25 mM
NaCl	1.5M
H_2O	

1x PBS

10x PBS	10 % (v/v)
H_2O	

→ *Adjust pH to 7.2*

Lysis Buffer for Protein Purification (25 ml)

$MgCl_2$	1 mM
Lysozyme	300 µg/ml
DNAse I	1 µg/ml
EDTA-free protease inhibitor cocktail tablets (Roche)	2
PBS	25 ml

➔ *Always prepare fresh solution at the beginning of the experiment*

Wash Buffer for Protein Purification

Tris-HCl	20 mM
NaCl	500 mM
Triton X100	0.5 % (v/v)
PBS	

➔ *Adjust pH to 8.0*

Elution Buffer for Protein Purification

Tris-HCl	20 mM
NaCl	150 mM
EDTA	2 mM
DTT	1 mM
Glycerol	10 % (v/v)
PBS	

Lysis Buffer for protein homogenate from mouse brain tissue (10 ml)

Tris-HCl	25 mM
NaCl	150 mM
EDTA-free protease inhibitor cocktail tablets (Roche)	2
PBS	

➔ *Adjust pH to 7.4*

2.1.5.2 Buffers for histology

10x PBS

Na_2HPO_4	80 mM
NaH_2PO_4	25 mM
NaCl	1.5M
H_2O	

1x PBS

10x PBS	10 % (v/v)
H_2O	

➔ *Adjust pH to 7.2*

Sodium-Citrate-Buffer

$Na_3C_6H_5O_7$	10 mM
Tween-20	0.05 % (v/v)
H_2O	

➔ *Adjust pH to 8.0*

Sorensen Buffer

Na_2HPO_4	350 mM in 10 % H_2O of total volume
NaH_2PO_4	50 mM in 75 % H_2O of total volume

➔ *Mixed together and filled up to final volume; pH should be between 7.5 to 7.6 and cannot be corrected*

PFA-Stock Solution

PFA	8 % (w/v)
H_2O	

Sterile filtration and storage at 4 °C

Fixation Buffer (40 ml)

H_2O	10 ml
Sorenson Buffer	10 ml

PFA-Stock Solution	20 ml

Permeabilisation Buffer

Goat Serum	4 % (v/v)
Triton X-100	0.3 % (v/v)
1x PBS	

Blocking Buffer

Goat Serum	10 % (v/v)
Triton X-100	0.1 % (v/v)
1x PBS	

2.1.6 DNA molecular weight standards

GeneRuler™ 100 bp Plus DNA Ladder (Thermo Fisher Scientific)

GeneRuler™ 1 kb Plus DNA Ladder (Thermo Fisher Scientific)

2.1.7 Protein molecular weight standards

PageRuler prestained protein ladder (Thermo Fisher Scientific)

PageRuler Plus prestained protein ladder (Thermo Fisher Scientific)

2.1.8 Vectors and Plasmids

The cDNA libraries were kindly provided by Dr. Ann-Marie Craig [(Vancouver, Canada), (Linhoff et al 2009)]

pRK5_HA-WAVE3 and peGFP-N1-WAVE2 were kindly provided by Dr. Laura Machesky [(Glasgow, England), (Stovold et al 2005)]

2.1.9 Primers

Table 5 Oligonucleotide primers *Abbreviations: forward, fwd; reverse, rev.*

Primer ID	Sequence (5' – 3')	Direction
05443	GAGCCACACATCCAGCGCCTT	rev
36839	ATGGATCCGGCACAGCGGCTGAGCTCAAGATGCGCGTG	fwd
36840	CCGAATTCTCACTCCAGCCAGTCTACTTCATCGAACTC	rev
37130	TATTGGTCTATATATTTATACCCATACGATGTTCCAGATTACGCTTGATAAACCATTTCCGTTTG	fwd
37131	CAAACGGAAATGGTTTATCAAGCGTAATCTGGAACATCGTATGGGTATAAATATATAGACCAATA	rev
37407	GGCATTATATTGTAAATGAAACAAC	fwd
37562	GCATACATGGACCAGTGAACATGAC	rev
37581	GGAATAAATCACAGAGCTCGTCAGTTCTCTCAGACACACTCTCAAGGTTTCATGATTAATCCTCAAATCAAATCCACGCTGTGCTTCCAATAACTTCGTATAATGTATGCTAT	fwd
37582	GAAATATATTGTACTATGTAAAGTAGTAACTGTGGTTAGTAAATATTTGTAAATATACATCATTTAAAAATTAGATGGTTTTAAACCAAGGTTATAACTTCGTATAGCATACATTAT	rev
37583	GGCTGGCCCACAGACACGCTCACCACACAGGTAAGGATCTCTCTAGCCTATCCATCATAGCCAGAGAAGGCCCGAATGCCCTTTCTATAACTTCGTATAATGTATGCTAT	fwd
37584	GGTAACTTTAATCTGCTAAGCAGCAGGTTGTTCTGAAACCAATTACTTGAATCTATTTTTAAGTCAAAGATACATGGCAAGGAAGGGCCAACGGCATAACTTCGTATAGCATACATTAT	rev
37585	CAGGAGGTAAAAACCATGATTAATACGACTCACTATAGGGTTTAAACGCACTTTGGGATATTTACATTTATTC	fwd
37586	TCTGACGTCATTATTATCAGTTTAAACCTATAACCAAAGAGAACAGCAATC	rev
37587	CTGACGAGCTCTGTGATTTATTCCT	rev
37588	CTACTTTACATAGTACAATATATTTCTTCC	fwd
37589	GTGTGGTGAGCGTGTCTGT	rev
37590	CTGCTGCTTAGCAGATTAAAGTTACC	fwd
37594	TCAACATTAATTTAGGTTACTATTTAGGTT	rev
37595	GGTTGGTTAATCAGTTGACTATTATTC	Fwd

Primer ID	Sequence (5’ – 3’)	Direction
37596	GGTATAAATATATAGACCAATATATAACATTG	rev
37597	GCTTTAAGAATCAATGACAAATATGCATAC	fwd
37598	CAGGAGGTAAAAACCATGATTAATACGACTCACTATAGGGTTTAAACCTGACAGCTTTATCTTTATGTTGCCTC	fwd
37599	TCTGACGTCATTATTATCAGTTTAAACGCATTATGTTATGAGTTGGCTGTAC	rev
37600	CCTAAATAGTAACCTAAATTAATGTTGATTCATGCATTATCTCTTAGACAAATTAATAAAAAAAAAAGCCCATTCAAATAACTTCGTATAATGTATGCTAT	fwd
37601	GAATAATAGTCAACTGATTAACCAACCAGAATAATTAGACATTTAAGAAGGCTCTGATACTTTGCCCAAATAACAAGGCTAATACCAATAACTTCGTATAGCATACATTAT	fwd
37602	TTCCTAGCAATATATTGCATTTTGGATGCCACTTGATTATAATAAAATACAGCACCTTACTTTTGAATGGCAGCATGACCCTGTAAATAACTTCGTATAATGTATGCTAT	fwd
37603	GTATGCATATTTGTCATTGATTCTTAAAGCACTATGCTCAATATACATACATCTATCTATCTATCTCACAGTCGGTGCACAGACTATAACTTCGTATAGCATACATTAT	rev
37604	CAATGTTATATATTGGTCTATATATTTATACCCATACGATGTTCCAGATTACGCTTGATAAACCATTTCCCTTTGTATGAAATACAGCACCATTTCATTGT	fwd
37605	AGTGGCATCCAAAATGCAATATATTGCTAGGAAAATGCAAAGTTTCCACAGATCAGCAATTATGAATTGCATTGGTCACAATGAAATGGT	rev
38484	GCAGCGGCCGCCATGCCGTTAGTAACGAGGAACATC	fwd
38485	GCATCTAGATCAGTCGGACCAGTCGTTCTC	rev

2.1.10 gRNA

Table 6 gRNAs for CRISPR; Abbreviations: forward, fwd; reverse, rev

gRNA ID	Sequence (5’ – 3’)	PAM sequence
38/fwd	CACGCTGTGCTTCCAAACCT	TGG
53/fwd	CCGAATGCCCTTTCTGCCGT	TGG
85/rev	ACAAGGCTAATACCATTGAA	TGG
163/rev	GTCGGTGCACAGACTTTACA	GGG

2.1.11 Antibodies

Table 7 Primary Antibody; Abbreviations: immunocytochemistry, ICC; immunohistochemistry, IHC; Western Blot, WB; Catalog number, Cat. Nr.

Epitope	Species	Company (Cat. Nr.)	Dilution	Application
c-Myc (polyclonal)	rabbit	Sigma (C3956)	1:2000	ICC
gephyrin (mAB7a, monoclonal)	mouse	Connex	1:3000/1:2000	ICC/IHC
gephyrin (3B11, monoclonal)	mouse	Synaptic Systems	1:3000	WB
HA (monoclonal)	mouse	Covance (MMS-101R-500)	1:2000	ICC
parvalbumin (PV 27, polyclonal)	rabbit	Swant	1:4000	IHC
VIAAT (vesicular inhibitory amino acid transporter, polyclonal)	guinea-pig	Synaptic Systems (131 004)	1:2000	IHC
V5 (polyclonal)	rabbit	Millipore (AB3792)	1:1000	WB
c-Myc (polyclonal)	rabbit	Sigma (C3956)	1:2000	ICC
WAVE2 (monoclonal)	mouse	Santa Cruz (sc-373889)	1:500	WB
WAVE3 (monoclonal)	mouse	Santa Cruz (sc-515303)	1:500	WB

Table 8 Secondary Antibodies; Abbreviations: immunocytochemistry, ICC; immunohistochemistry, IHC; Western Blot, WB.

Epitope	Species	Company	Dilution	Application
anti-guinea pig Alexa 555 conjugate	goat	Thermo Fisher Scientific Inc.	1:2000	IHC
anti-mouse Alexa 488 conjugate	goat	Thermo Fisher Scientific Inc.	1:2000	ICC/IHC
anti-mouse Alexa 555 conjugate	goat	Thermo Fisher Scientific Inc.	1:2000	ICC
anti-rabbit Alexa 555 conjugate	goat	Thermo Fisher Scientific Inc.	1:2000	ICC/IHC
anti-rabbit Cy5 conjugate	goat	Thermo Fisher Scientific Inc.	1:1000	IHC
Anti-mouse-HRP-conjugate	goat	Dianova	1:10.000	WB
Anti-rabbit-HRP-conjugate	goat	Dianova	1:10.000	WB

2.2 Methods

2.2.1 Molecular biological methods

2.2.1.1 Fast DNA-Plasmid purification

The plasmid DNA mini preparation was carried out by using the ZymoPURE Plasmid Miniprep Kit (Zymo Research) according to the manufacturer's instructions. DNA was resuspended in 30 µl ultrapure water.

For purification of high amounts of endotoxin free DNA the EndoFree Plasmid Kit (Quiagen) was used according to the manufacturer's instructions. DNA was resuspended in 150 µl ultrapure water and the concentration determined. Final concentration was adjusted to 1 µg/µl with ultrapure water.

2.2.1.2 DNA concentration measurements

For DNA concentration measurements by the UltraSpec 3100pro (Amersham) the DNA sample was diluted 1:100 using ultrapure water and UV absorbance at 260 nm and 280 nm was measured. To ensure a high-quality DNA solution the ratio of A_{260}/A_{280} with a value between 1.8 to 2.0 was accepted.

2.2.1.3 Polymerase chain reaction

For the amplification of DNA sequences of interest, a PCR mixture with a total volume of 50 µl containing the double stranded DNA template (100 ng), oligonucleotide primers (7 pmol per primer), dNTPs, DNA polymerase and the appropriate buffer was prepared. For cloning, the Pfu polymerase (Cloned Pfu Polymerase AD, Agilent Technologies) was used, for genotyping the Red-Taq DNA polymerase (Sigma Aldrich). The amplification was performed in a cycler (GeneAmp PCR System 9700) using the following program:

95 °C	5 min	
95 °C	30 sec	30x
Annealing temperature	1 min	
72 °C	x min	
72 °C	30 min	
10 °C	∞	

The applied annealing temperature is at least 5°C lower than the melting temperature determined by SnapGene. An extension time of 1 minute was calculated for every 250 base pairs to be amplified.

Mouse genotyping

For the genotyping of the WAVE1 mouse line the primers 37404, 37405, 16119 and 16120 (PrimerSet PS0408_WAVE1_NEO) were used in the following PCR master mix:

9.8 µl H2O

4.0 µl 5 x MyTaq Reaction Buffer with 5 mM dNTPs, 15 mM $MgCl_2$

1.0 µl 50 mM $MgCl_2$

0.2 µl MyTaq_HS DNA Polymerase, 5 units/µl (Bioline, BIO-21113)

4.0 µl PrimerSet PS0408_WAVE1_NEO (1 pmol/µl each)

1.0 to 02.0 µl DNA

20.0 µl total

For the amplification of the DNA fragments the cycler (GeneAmp PCR System 9700) with the following program was used:

96 °C	3 min	
94 °C	30 sec	32x
62 °C	1 min	
72 °C	1 min	
72 °C	7 min	
12 °C	∞	

For the detection of the wild-type allele a DNA fragment with a size of 356 bp and for the KO allele with a size of 222 bp was expected.

CB PCR screening

To test the cDNA pools for CB the primers 36397 and 36398 were used in a PCR master mix with a total volume of 25 µl. This consisted of the corresponding volume 10x red Taq buffer, 0.5 µl red Taq,

oligonucleotide primers (7 pmol per primer), dNTP's and 2 µl of DNA. For the amplification, the following cycler program was used:

94 °C	3 min	
94 °C	30 sec	25x
55 °C	30 sec	
72 °C	1 min	
72 °C	5 min	
10 °C	∞	

Under these conditions a PCR fragment with a size of 360 bp was amplified.

2.2.1.4 Sequencing of DNA constructs

All sequencing of DNA constructs was performed by the DNA core facility of the Max Planck Institute of experimental medicine on an Applied Biosystems 373 DNA Sequencer.

2.2.1.5 Digestion of DNA with restriction enzymes

Restriction enzymes from NEB were used in all digestions carried out and performed in a total volume of 50 µl, at 37 °C for 2 hours. Depending on the manufacturer's instructions, the appropriate buffers were used and heat inactivations were performed.

2.2.1.6 De-phosphorylation of 5'-DNA ends

In order to prevent religation of the cut plasmids, de-phosphorylation of the 5' ends was carried out. For this purpose 1 µl shrimp alkaline phosphatase (NEB) and 2 µl the corresponding buffer were added to the plasmid DNA (total volume 20 µm) and incubated for 1 h at 37 °C, followed by heat inactivation at 65 °C for 20 minutes.

2.2.1.7 Gel-electrophoresis of DNA

Gel electrophoresis was used to separate DNA by size and to check the quality of the sample. For this purpose, 1 µl of the sample was mixed with 10 µl application buffer and applied to the agarose gel containing 0.1 % Gel Red (Biotium). The separation was carried out in 1-2 % TBE buffer. The visualization was done with the UV light system (Intas).
Gel electrophoresis was also used to separate DNA according to size in order to purify a PCR product or digested DNA. For this purpose, the entire sample was mixed with the corresponding amount of 6x Application Buffer and applied to the agarose gel containing 0.1 % Gel Green (Biotinum). The separation was carried out in 1-2 % TBE buffer with application of 100 V for 1 hour. The visualization was done with blue light.
To estimate the size of the DNA bands a DNA size standard 100 bp or 1 kB (Fermentas) was used.

2.2.1.8 DNA extraction and purification from agarose gels

After the electrophoretic separation of PCR products or digestion reactions the DNA band of the corresponding size was cut out with a scalpel and extracted from the gel and purified with ISOLATE Kit II (BIOLINE) according to the manufacturer's instructions. Depending on the amount of DNA in the band, the DNA was eluted in 20 - 30 µl ultrapure water.

2.2.1.9 Ligation of DNA molecules

For the ligation of DNA molecules the LigaFast Rapid DNA Ligation System (Promega) was used according to the manufacturer's specifications. The incubation of the ligation reaction was performed at 16 °C overnight.

2.2.1.10 TOPO cloning

A TOPO cloning kit (pCR2.1-TOPO-TA; Invitrogen) was used for the subcloning of PCR products that are difficult to ligate. The instructions of the manufacturer were followed during the procedure.

2.2.1.11 Transformation of electrically competent E. coli bacteria

For the electroporation of electrically competent cells (see 2.1.4) the Bio-Rad *E.coli* Pulser at 1.8 kV, 25 µF with pulse controller set at 200 Ω was used. The determined time constant, which should be greater than 4, was used as a measure for the quality of the performed transformation. After thawing the cells as quickly as possible, 1-2 µl of the ligation reaction were pipetted to the cells and stored on ice. This mixture was transferred bubble-free into the pre-cooled electroporation cuvette (0.1; cm Bio-Rad).

After the electrical pulse the cells were transferred into 800 µl LB medium and incubated for 1-2 minutes on ice. Subsequently, the cells were incubated at 37 °C for 1 hour while shaking. After incubation, the cells were centrifuged at 10000 g for 1 min, resuspended in 100 µl LB medium and plated out on the appropriate selection medium. The LB plates were then incubated overnight at 37 °C.

2.2.1.12 Transformation of chemically competent E. coli bacteria

For the chemical transformation of DNA into chemically competent bacteria (see 2.1.4), the manufacturer's (NEB) instructions were followed. Briefly, he cells were slowly thawed on ice before the DNA to be transformed was added. The DNA-cell mixture was incubated on ice for 20 minutes and then subjected to heat shock at 42 °C for 30 - 60 seconds. Growth medium was then added to the cells, which were then incubated for 1-2 minutes on ice. The cells were then incubated for 1 hour at 37 °C with shaking, before the cells were plated on appropriate selective medium. The LB plates were then incubated overnight at 37 °C.

2.2.1.13 Overnight cultures of bacteria in a suspension culture

Suspension cultures were prepared for plasmid preparation and heterologous expression of proteins. To ensure optimal growth of the cultures, a preculture (5 ml LB medium with appropriate antibiotic) was inoculated with a colony of the bacteria to be cultivated. This was incubated for 6 to 10 hours at 37 °C and 210 rpm. Subsequently, 100 µl of this preculture were inoculated into the overnight culture. The incubation was carried out for 12 to 16 hours at 37 °C and 210 rpm.

2.2.1.14 Cloning strategies for constructs generated in this study

All clones shown here were amplified with Pfu Polymerase (Cloned Pfu Polymerase AD, Agilent Technologies) (2.2.1.1 - 2.2.1.3 and 2.2.1.4)

<u>pKH3_HA-WAVE1</u>

WAVE1 was amplified from the pcDNA3.1_WAVE1 construct of the screened cDNA library using primers 36839 and 36840 (62 °C annealing temperature) and inserted into pKH3_HA using BamHI and EcoRI.

<u>pGEX4T1_GST-WAVE1</u>

WAVE1 was amplified from the pcDNA3.1_WAVE1 construct of the screened cDNA library using primers 36839 and 36840 (62 °C annealing temperature) and inserted into pGEX4T1 using BamHI and EcoRI.

pRK5_HA-WAVE2

WAVE2 was amplified with the primers 38484 and 38485 (62 °C annealing temperature) from the peGFP-N1-WAVE2 plasmid and cloned into the pRK5_HA-WAVE3 plasmid using NotI and XbaI.

pcDNA3_GlyRβ-HA

Site-directed mutagenesis was performed using primers 37130and 37131. Further processing of the PCR products obtained was carried out as described in 2.2.1.1, 2.2.1.7, 2.2.1.8 and 2.2.1.11. A final check of the correct integration of the c-terminal HA tag was confirmed by sequencing (see 2.2.1.4).

2.2.2 Protein biochemical methods

2.2.2.1 Production of protein homogenate from mouse brain tissue

For the production of brain homogenates, the mice were anaesthetised and decapitated. The prepared brains were transferred to a Teflon glass homogenizer (Sartorius) precooled on ice, mixed with 2 ml homogenization buffer and homogenized by rotating the potter. The samples were then centrifuged for 10 min at 2000 g and 4 °C. The supernatant was transferred to a 2 ml reaction tube (Eppendorf), made up to 2 ml with homogenization buffer and TritonX 100 with a final concentration of 1% was added. The homogenate is incubated for 30 min at 4 °C with overhead shakers before the samples were centrifuged at 12.000 g for 30 min and 4 °C. The supernatant was aliquoted into new 1.5 ml reaction tubes (Eppendorf; 50 µl each), shock frozen in liquid nitrogen and stored at - 80 °C.

2.2.2.2 Protein concentration determination

To determine the protein concentration of the samples (see 2.2.2.1) a Bradford protein assay (BioRad) was performed according to the manufacturer's specifications. For this purpose, 2 µl of the sample were incubated with 200 µl of Bradford reagent for 1 min at room temperature. In parallel, a standard curve was prepared using BSA. The adsorption at 560 nm wavelength was then measured, the calibration curve with the corresponding function determined and the protein concentration calculated (Bradford 1976).

2.2.2.3 Preparation of protein homogenates from cell cultures

To isolate proteins for SDS-PAGE, the culture medium was removed from the neuron culture at the appropriate time, 200 µl 2x SDS buffer was added, the cells were detached from the coverslip using a

cell scraper and transferred to a 1.5 ml reaction tube (Eppendorf). Further sample processing was performed as described above (see 2.2.2.7, 2.2.2.8 and 2.2.2.9).

2.2.2.4 Protein expression in bacteria

Transformation of the corresponding constructs expressing the desired proteins was performed as described in 2.2.1.11. Subsequently, a 100 ml over-night culture was added to 900 ml LB medium, and the resulting 1 L culture was incubated at 37 °C and 210 rpm up to an OD_{600} of 0.8 - 0.9. The culture was then cooled down on ice for 20 minutes. Protein expression was induced by addition of IPTG (0.5 mM final concentration) and the culture was incubated overnight at 150 rpm at room temperature.

2.2.2.5 Purification of GST-fusion proteins

To achieve the highest possible quality of purified proteins, all steps were performed on ice and the solutions used were pre-cooled on ice. Cultures described in 2.2.2.3. was used as the basis for purification. The culture was centrifuged for 20 min at 4000 g and 4 °C. The supernatant was discarded, the pellet resuspended in 25 ml lysis buffer and transferred to a 50 ml reaction tube (FALCON). After 15 min incubation on ice, sonification was performed under continuous cooling with ice (VS-70, 2 times one minute, cycle 2 at 100 %). TritonX-100 with a final concentration of 1 % was added and the sample incubated for 20 min at 4 °C in an overhead shaker. This was followed by a 30 min centrifugation at 10.000 g at 4 °C. The supernatant was transferred to a new reaction tube and 500 µl glutathione beads were added (Thermo Fisher Scientific) prepared by washing three times with 1 ml of PBS. The GST beads/protein mixture was incubated for 3 h at 4 °C in an overhead shaker. Centrifugation for 5 minutes at 4 °C and 1000 g was performed. The supernatant was discarded and the proteins bound to the glutathione beads were transferred to a 2 ml reaction tube (Eppendorf). Subsequently, the beads were washed three times with PBS, followed by three washes with wash buffer and two washes with elution buffer, 1 ml each, and centrifugation at 1000 g. After the last washing step, the supernatant was completely removed and a GST bead/protein mixture with a total volume of about 1 ml with elution buffer was prepared. 50 µl aliquots of the eluate were prepared in pre-cooled 1.5 ml reaction tubes (Eppendorf), shock-frozen in liquid nitrogen and stored at - 80 °C.
Quality control of the purified GST fusion proteins was performed by SDS-PAGE of the samples followed by Coomassie brilliant blue staining of the SDS gel (see 2.2.2.7 and 2.2.2.8)

2.2.2.6 GST-pulldown assay

For GST-pulldowns, 100 µl glutathione beads (Thermo Fisher Scientific) were transferred into a 15 ml reaction tube (FALCON) and washed 3 times with PBS. Centrifugation was performed at 1000 g for 2 minutes. Subsequently, the purified GST proteins (see 2.2.2.4.) were added to the beads and filled up to 8 ml total volume with 1 % TritonX 100 (v/v) in PBS. After a 4 hour incubation at 4 °C in an overhead

shaker, the beads were washed 3 times, as described above and the interaction partner to be tested was added and the sample was filled up to 8 ml total volume with 1 % Triton (v/v) in PBS. In this step 80 µl were taken, mixed with 20 µl 5xSDS buffer and stored at - 80 °C (total sample). Incubation was performed for 2 h at 4 °C in an overhead shaker. The beads were washed 3 times with 0.5 % TritonX 100 (v/v) and centrifuged at 1000 g for 2 min. After the last washing step all liquid was removed and the beads were transferred to 100 µl 3xSDS buffer. The samples were stored at - 80 °C. Subsequently, SDS-PAGE and Western blots were performed to check for direct interactions between proteins (see 2.2.2.7, 2.2.2.8 and 2.2.2.9).

2.2.2.7 SDS-polyacrylamide gel electrophoresis (SDS-PAGE)

To separate proteins according to their molecular weight, corresponding samples were applied to an SDS gel under denaturing conditions and separated by applying a constant voltage. For sample preparation, these were placed in 5x SDS-loading buffer and incubated for 30 min at 70 °C with shaking. Subsequently, the denatured samples were applied to a two-layer polyacrylamide gel. The separation of the proteins was carried out in a Mini Protean Tetra System (BioRad) at the beginning with a voltage of 60 V. When the run front had moved from the stacking gel to the separation gel, the voltage was increased to 120 V and maintained until the running front exited the gel (Laemmli 1970).

2.2.2.8 Staining of SDS gels with Coomassie-Brilliant-Blue

After separation of the proteins using SDS PAGE, the gel was removed from the apparatus and the stacking gel was separated. The remaining separation gel was transferred to the Coomassie Blue solution and incubated overnight with moderate shaking. For a clear presentation of the bands, the gel was washed 3 times with ultrapure water after removal of the staining solution.

2.2.2.9 Western Blot

Proteins separated by SDS-PAGE were transferred to a nitrocellulose membrane (Protran 0.2 µm; GE Healtcare) by applying a constant voltage of 600 V for 90 minutes, and immunodetected using appropriate antibodies. The Western blot was performed in an Mini Protean Tetra System (BioRad) filled with blotting buffer and cooled with ice during the whole procedure (Towbin et al 1979).
Subsequently, the membrane was washed with ultrapure water and a MemCode (Thermo Fisher Scientific, Germany) staining was performed according to the manufacturer's instructions. After documentation of the results, the membrane was destained, again following the manufacturer's instructions, followed by incubation at room temperature in blocking buffer for 2 h under slight shaking. Subsequently, the membrane was incubated with the primary antibody (see 2.1.11) under the same conditions. After washing three times for 5 min with TBST, the secondary antibody (see 2.1.11) was

incubated for 45 min with gentle shaking at room temperature. Finally, the membrane is washed 3 times with TBST and once with TBS.
The membrane was incubated with ECL (GE Healthcare), according to the manufacturer's conditions, and the signal was detected using the ECL Chemo Star Plus Imager (INTAS). For quantitative blots, secondary antibodies coupled with fluorophores were used and the signals were detected with the Oddysey Infrared System (Li-COR).

2.2.2.10 Quantitative analysis of Western blots

For the quantitative analysis of Western blots, the protein to be investigated was normalized to the corresponding intensity of β-tubulin labeling. Densitometric analysis was performed using ImageJ/FIJI (NIH; Wayne Rasband).

2.2.2.11 Mass spectrometric analysis of WAVE1 fragments

WAVE1 fragments were separated on precast 10% Tris-glycine gels (TG PRiME, Serva) run in parallel in the same gel electrophoresis chamber. Proteins were either visualized by colloidal Coomassie staining or transferred onto nitrocellulose membranes and immunodetected as described above (see 2.2.2.9). Coomassie signals were detected with a conventional transmitted light scanner, while a CCD camera system (Intas) was used to detect total protein (MemCode, Thermo Fisher Scientific) and immunoreactive bands (ECL kit, GE Healthcare) on blotting membranes. The respective images were overlayed in Photoshop (Adobe) and false-colored in Fiji/ImageJ 1.52 to identify gel regions of interest, from which gel bands were excised manually. In-gel digestion with trypsin and generation of peptide mass fingerprint (PMF) and fragment ion mass spectra of the proteolytic peptides by matrix-assisted laser desorption ionization-time of flight mass spectrometry (MALDI-TOF MS; ultraFlextreme, Bruker) was essentially performed as described (Jahn et al., 2006; PMID: 16821028). For protein identification, database searches in the Swiss-Prot primary sequence database (UniProt release 2019_08; without or with taxonomy restriction to rat) were performed using the MASCOT Software version 2.3.02 (Matrix Science, London, UK). Carboxamidomethylation of Cys residues was specified as fixed and oxidation of Met residues as variable modifications. Trypsin was specified as protease and one missed cleavage was allowed. Mass tolerances were set to 100 ppm for PMF searches and to 100 ppm (precursor ions) and 0.7 Da (fragment ions) for MS/MS ion searches.

2.2.3 Cell biological methods

2.2.3.1 Freezing and thawing of eukaryotic cells

For freezing and storing eukaryotic cell lines, confluent 10 cm Petri dishes containing the cells to be cryopreserved were washed with PBS (Thermo Fisher Scientific, Germany) and the cells were detached

from the Petri dish by trypsinization (0.05% trypsin, incubation for 2 min at 37 °C and 5% CO2) and taken up in 10 ml culture medium. The cell suspensions were transferred to a 15 ml Falcon tube and centrifuged for 5 min at 800 g. The supernatant was discarded, the cell pellet resuspended in 1 ml medium and transferred to 1.5 ml tubes (Thermo Fisher Scientific, Germany). Freezing was performed in a container (Nalgene) filled with isopropanol at - 80 °C for 72 h.
Cells cryopreserved as described above, were thawed in a 37 °C water bath as quickly as possible and transferred to 10 ml culture medium. The cells were then centrifuged at 800 g for 5 min, the supernatant was discarded and the cells were resuspended in 1 ml culture medium. The cell suspension was transferred dropwise into a suitably prepared 10 cm Petri dish containing 10 ml culture medium.

2.2.3.2 Cultivation of HEK 293 FT and Cos-7 cells

The cells were cultivated in 10 cm Petri dishes for line maintenance and in 15 cm Petri dishes for lentivirus particle production. Cultivation was performed at 37 °C, 5 % CO_2 in DMEM medium (Thermo Fisher Scientific) with 10 % FBS and P/S. To split the cells, the medium was removed, the cells were washed once with PBS, and 2 ml Trypsin 0.05 % (Thermo Fisher Scientific) were added. After two minutes incubation at 37 °C and 5 % CO_2 in the incubator, 10 ml culture medium was added and the cells were resuspended. The corresponding volume was placed in a new Petri dish containing 10 ml culture medium for the desired dilution. Careful swivelling of the cells achieved an even distribution of the cells.

2.2.3.3 Cultivation of Flp-InT-Rex-GFP-gephyrin HEK 293 cells

Cultivation was performed at 37 °C and 5 % CO_2 in DMEM (Thermo Fisher Scientific) medium with 10 % FBS, P/S, Hygromycin (200 µg/ml) and Blasticidin (15 µg/ml) in 10 cm Petri dishes coated with gelatine (see 2.2.3.4). The cells were split as described in 2.2.3.2.

2.2.3.4 Gelantine coating of coverslips

The coverslips used for cell culture (24 mm for 12 well and x mm for 24 well plate) were autoclaved before use or baked for 3 h at 220 °C. The cover slips were covered with 1 ml or 0.5 ml 0.1 % gelatine solution and incubated for 1 h in an incubator at 37 °C and 5 % CO_2. After washing three times with PBS, cells could be seeded onto the gelatine-coated coverslips.

2.2.3.5 Poly-L-Lysine coating of coverslips

The sterilization of coverslips was performed as described in 2.2.3.4. Subsequently, the coverslips were incubated in a 12 well or 24 well plate with 10 % Poly-L-Lysine (Thermo Fisher Scientific) solution for one hour at 37 °C and 5 % CO_2 in the incubator. After washing 3 times with PBS (Thermo Fisher Scientific) the coverslips were ready to be seeded with cells.

2.2.3.6 Calcium phosphate transfection of hippocampal neurons

The calcium-phosphate transfection of the hippocampal neurons was performed at DIV 4. For this purpose, 50 µl of solution A, consisting of 2 µg of the DNA to be transfected and 6 µl 2M $CaCl_2$ in milliQ water, were added to 50 µl of solution B, consisting of 2x HBS, under vortex and incubated for 15 min at room temperature. During this time the coverslips with the neurons were transferred into pre-incubated (5 % CO2, 37 °C) Neurobasal A Medium (Thermo Fisher Scientific). The transfection mix was then applied dropwise to the cells and the cells were incubated for 20 min at 37 °C and 5 % CO2. After checking for the presence of a precipitate, the coverslips were transferred to pre-incubated (10 % CO2, 37 °C overnight) HBSS medium (Thermo Fisher Scientific) and incubated for 10 min at 5 % CO2 and 37 °C. Here, a check was made to see whether the precipitate had disappeared. If so, the coverslips were returned to the conditioned culture medium. If precipitate was still present, the cells were incubated in HBBS medium until the precipitate had disappeared, but for a maximum of 15 min total time.

2.2.3.7 Lipofectamin transfection of eukaryotic cells

Cell lines transfected in this study were always seeded on Poly-L-lysine coated coverslips 24 h before transfection. Lipofectamin 2000 (Thermo Fisher Scientific) was used for the transfection according to the manufacturer's instructions. Briefly, the culture medium was removed and replaced by 300 µl OPTIMEM Medium (Thermo Fisher Scientific) to which the transfection mix was added. After 8 hours incubation 1 ml of culture medium was added.

2.2.3.8 Preparation of hippocampal primary continental cultures

For culturing hippocampal neurons, pregnant mice were killed by decapitation. The embryos were removed at embryonic day 18 (E18) and decapitated. The brains were collected and the hippocampi were isolated in a plate containing HBSS. Subsequently, the hippocampi were transferred into pre-cooled 15 ml Falcon tubes filled with HBSS (without calcium and magnesium; Thermo Fisher Scientific). All further steps were performed under a laminar flow hood. After the hippocampi were sedimented by gravity, they were washed 3 times with 10 ml HBSS, whereby the supernatant was always carefully aspirated up to 2 ml. After the last washing step, the volume was aspirated up to 1.8 ml and 200 µl of

2.5 % (w/v) Trypsin [(Thermo Fisher Scientific; final concentration 0.25 % (w/v))] was added, swivelled slightly and incubated for 15 min at 37 °C in a water bath. Subsequently, a 4-times washing with HBSS was performed as described above. The volume was then aspirated up to 1 ml and the cells were transferred into a sterile 1.5 ml reaction tube (Eppendorf). The same pipette tip was used to homogenize the hippocampi by pipetting up and down 10 - 20 times. After settling the cell clusters, the supernatant was transferred through a tissue filter (Cellstrainer 40 µm from FALCON) into a sterile 50 ml falcon tube and the filter was washed with 1 ml preheated DMEM containing 10 % FCS, P/S and glutamate. From the same medium, 1 ml was added to the cell clusters and carefully homogenized with a 20G 1 1/2 " cannula. The cells were allowed to settle and 1 ml of the supernatant was transferred through the filter into the 50 ml reaction tube and the filter was washed. This procedure was performed twice more. Finally, the filter was washed with DMEM, as described above, until 20 ml total volume was present in the 50 ml reaction tube. After swivelling the reaction tube, 10 µl were removed and the neurons were counted in a Neubauer counting chamber. The cell density was adjusted to 160.000 cells/ml and 500 µl/well of this solution was added to the prepared (see 2.2.3.5) 12 well plates filled with 500 µl DMEM medium per well. Incubation was performed at 5% CO_2 and 37 °C overnight in an incubator before the medium was removed and replaced by 2 ml complete neurobasal medium. Further incubation was also performed at 37 °C and 5 % CO_2.

2.2.3.9 Preparation of hippocampal primary autaptic cultures

Autaptic hippocampal neuron cultures were prepared according to a published protocol (Burgalossi et al 2012). Neurons from postnatal day 0 (P0) mice were used.

2.2.4 Histological methods

2.2.4.1 Preparation of PFA fixed mouse brains

The mice were anaesthetised and decapitated. The brain was removed from the skull as quickly as possible and placed in the fixation solution containing 4% PFA and incubated overnight at 4 °C. They were transferred into a 20 % (w/v) sucrose solution in PBS and incubated overnight at 4 °C. Once the brains had sunk to the bottom of the tube, they were removed, the hemispheres separated with a scalpel, transferred to embedding media (Leica) and frozen on dry ice. The completely frozen samples were stored at - 80 °C.

2.2.4.2 Preparation of fresh frozen mouse brains

The mice were anaesthetised and decapitated. The brain was removed from the skull as quickly as possible, the hemispheres were separated with a scalpel and frozen on dry ice. As soon as the brains were completely frozen (about 5 min) they were kept at - 80 °C.

2.2.4.3 Performing cryostat sections of PFA fixed mouse brains

Before the brains were cut at - 18 °C on cryostat (Leica) with a thickness of 40 µm, the samples were equilibrated for about 30 min in the cryostat. The sections were transferred to a 6 well plate, which was also pre-cooled and placed in the cryostat. After cutting the sections about 2 ml PBS per well were added. The sections were then transferred to slides with a brush, air dried and processed as described in 2.2.4.5.

2.2.4.4 Performing cryostat sections of fresh frozen mouse brains

Before the brains were cut at - 18 °C in a cryostat (Leica) with a thickness of 12 µm, the samples were equilibrated for about 30 min in the cryostat. The sections were transferred directly to the slide, three per slide, and air dried. The samples were the processed as described in 2.2.4.5.

2.2.4.5 Indirect immunofluorescence staining of brain slices

The corresponding sections (see 2.2.4.3 and 2.2.4.4) were incubated with the fixing solution for 7 to 10 min and then washed twice with PBS and once with sodium citrate buffer. The slides were transferred to the pre-heated sodium citrate buffer and incubated for 30 min at 90 to 95 °C. They were then cooled down until the buffer was clear again, but for at least 20 minutes. After two washes with PBS the slides were incubated for 1 h at room temperature in the permeabilisation buffer. The subsequent blocking was performed overnight at 4 °C in the blocking buffer. The corresponding primary antibodies (see 2.1.11) were diluted in blocking buffer, added to the samples and incubated overnight at 4 °C. After washing three times with PBS, a one hour incubation with the corresponding secondary antibodies (see 2.1.11) at room temperature followed. Subsequently, the samples were washed three times in PBS and a nuclear staining was performed using 4'6-diamidino-2-phenylindole (DAPI; 1:10.000 in PBS) for 10 minutes. After final three thorough washes in PBS, Aqua-Poly/Mount (Polysciences) was applied to the brain sections and they were covered with a glass slide.

2.2.4.6 Microscopy techniques

All microscopic images of the stained brain slices were taken on a LEICA SP2 LASER scanning microscope with a 405 nm solid state laser, 488 argon laser and 561 nm solid state laser, using a 63x objective and 2x digital zoom. The same number of animals from each group (WT and KO) were recorded on one day to ensure a comparable performance of the apparatus. On each day of recording the off set was adjusted. All other settings, i.e. laser power, gain of the PMCs, the resolution of 1024 x 1024 pixels, as well as the digital zoom, remained constant over all recordings. The z-stacks were shot in line to line mode, whereby the number of z-levels was automatically set by the LEICA software (setting: optimal). The first z-plane was acquired at the beginning of the signal with excitation of the 488 nm LASER and the last z-plane at the end of the signal with the 488 nm LASER.

2.2.4.7 Analysis of single-scan confocal images

Single-scan confocal images were analysed using FIJI/ImageJ (NIH; Wayne Rasband). A manual threshold was determined for each experiment and applied to the images. The image was then binarized and the watershed tool was applied to separate closely spaced spots. The processed image was then quantified using the "analyze particles" tool. The number, average area and diameter of a spot was determined.

2.2.4.8 Analysis of 3D confocal images

3D confocal images were analysed using IMARIS (bitplane). The IMARIS converter was used to convert the z-stacks in LEICA format into IMARIS 3D files, which were then used as the basis for the evaluation. For the quantification of the different stained and detected protein puncta the spot tool of the software was used. At the beginning of the analyses the corresponding thresholds were defined for each protein of a stain and applied to all quantifications. The quality of the spots (signal), which describes the intensity at the centre of the spot in the channel the spot was detected, as a discriminatory criterion. The intensity in the spot tool is the intensity of the channel Gaussian filtered by ¾ of spot radius.

In this way the number as well as the average area, diameter and volume of the spots were determined. The density of the spots (spots per 100 μm^3) was calculated on the basis of the number and the total volume of the image.

2.2.5 Generation of genetically modified mice using CRISPR/Cas9

2.2.5.1 Generation of conditional GlyRβ KO mice

The CRISPR/Cas9 method (Jinek et al 2012, Pennisi 2013) was used to generate conditional GlyRβ KO mice. An HDR fragment was created using Gibson assembly [(Thermo Fisher Scientific), (Gibson et al 2009a)]. The DNA fragments required for the HDR fragment were generated by PCR using the primer pairs 37585/37587, 37581/37582, 37588/37589, 37583/37584 and 37590/37586 with an annealing

temperature of 58 °C (for sequences see 2.1.9) and purified as described in 2.2.1.2 - 2.2.1.8. For the amplification the following program was used:

96 °C	3 min	
94 °C	30 sec	33x
58 °C	60 sec	
72 °C	60 sec	
72 °C	7 min	
10 °C	∞	

Isolated DNA from a WT mouse (C57Bl6/J) as template and the master mix as described in 2.2.1.3 with Pfu DNA-polymerase (Thermo Fisher Scientific) was used for amplification.
The necessary gRNAs were synthesized and provided by the DNA Core facility of the institute. Selection of the gRNA sequences was performed using the CRISPOR (www.crispor.tefor.net) tool. DNA microinjection was performed by the animal facility of the institute.

2.2.5.2 Generation of C-terminally tagged GlyRβ-HA knock in mice

The CRISPR/Cas9 method (Jinek et al 2012, Pennisi 2013) was used to generate a conditional GlyRβ-HA knock in (KI) line. An HDR fragment was created using Gibson assembly. The DNA fragments required for this were generated by PCR using the primer pairs 37598/37594, 37600/37601, 37595/37596, 37604/37605, 37602/37603 and 37597/37599 with an annealing temperature of 58 °C (for sequences see 2.1.9) and purified as described in 2.2.1.2 - 2.2.1.8. For the amplification the following program was used:

96 °C	3 min	
94 °C	30 sec	33x
58 °C	60 sec	
72 °C	60 sec	
72 °C	7 min	
10 °C	∞	

Isolated DNA from a WT mouse (C57Bl6/J) as template and the master mix as described in 2.2.1.3 with Pfu DNA-polymerase [(Thermo Fisher Scientific), (Gibson et al 2009a)] was used for amplification.
The necessary gRNAs were synthesized and provided by the DNA Core facility of the institute. Selection of the gRNA sequences was performed using the CRISPOR (www.crispor.tefor.net) tool. The provision of the recipient animals as well as the DNA microinjection were performed by the animal facility of the institute.

2.2.6 cDNA library screen

The cDNA library used in this work was kindly provided by Prof. Dr. Ann Marie Craig. It is an unamplified cDNA library prepared from mRNA isolated from a rat forebrain (Linhoff et al 2009). The library was provided in the form of 3 aliquots, each of which represented a cDNA pool (10.000 different cDNAs) with different gene insert sizes. Based on these aliquots the screen of the pools with an insert size of 2-3 kB, 3-4 kB and 4-5 kB was performed.

To ensure the most uniform growth of the different clones of a pool a liquid gel amplification was performed. Briefly, 200 ml 2x LB-Soft-Agar were prepared and autoclaved. After cooling the freshly autoclaved LB-soft-agar to 37 °C in a water bath, carbenicillin (100 µg/ml final concentration) and the respective pool were added and thoroughly mixed. The solution was then transferred to 1 ml/well in deep well plates (Biozym), incubated for 30 min in an ice water bath and sealed with an air-permeable membrane. Finally, these preparations were incubated for 40 hours at 30 °C.
After this growth phase, the deep well plates were centrifuged for 10 min at 2000 g, the supernatant was discarded and the pellet was resuspended in 1 ml LB medium. 80 µl of this suspension was removed, mixed with 20 µl glycerol and stored at - 80 °C. The remaining suspension was centrifuged as described above, the supernatant discarded and subsequently, nexttec Plasmid 1-step DNA isolation was performed in 96 well plates (Biozym) following the manufacturer's instructions. Each DNA preparation from a well thus consisted of 50 different cDNAs of the corresponding size. To verify successful and high-quality purification, 1 µl of each purified DNA was mixed with 10 µl application buffer, applied to a 0.75 % gel and separated electrophoretically for 20 min at 80 V.

To test the pools for possible new interaction partners of gephyrin, a HEK cell based assay was used (Papadopoulos et al 2017). Each pool was transfected into Flp-In T-Rex-GFP-gephyrin HEK 293 cells seeded on 24 mm coverslips (see 2.2.3.7). 24 h later the GFP-gephyrin expression was induced by addition of TET (4 µg/ml final concentration). 24 h later, the cells were fixed and placed on slides with mounting medium. GFP-gephyrin clusters could be detected by excitation at 488 nm. If there was a redistribution of large GFP-gephyrin aggregates to smaller GFP-gephyrin clusters, the transfected pool was confirmed as positive and again transfected to verify the effect. Subsequently, this pool was tested for the presence of CB by PCR (see 2.2.1.3). Thus, positive, CB-free pools could be identified. Subsequently, 50 µl of each 1:50.000 dilution of the corresponding glycerol stock was plated onto 6 Carbenicillin-LB plates and incubated overnight at 37 °C. After incubation 576 clones were picked and transferred to a 96 deep well plate filled with 1 ml Carbenicillin-LB-medium each and incubated overnight at 37 °C. The DNA was then prepared, as described above, using nexttec Plasmid 1-step DNA Isolation (Biozym), according to the manufacturer's instructions. 12 samples, 25 µl each, were combined to subpools and transfected according to the procedure described above. The samples were screened for phenotypic changes in GFP-Gephyrin. Finally, the individual cDNAs of the positive subpool were transfected according to the established method, examined and the cDNAs thus determined as positive were sequenced (see 2.2.1.4).

3 Results

3.1 Control Experiments for cell line establishment

For the cDNA library screen described in 2.2.6., the published cell line Flp-In T-Rex-GFP-gephyrin HEK 293 was used, which expresses GFP-gephyrin upon TET treatment (Papadopoulos et al 2017). The expressed GFP-gephyrin accumulates in large intracellular aggregates within the cell. If additional gephyrin interacting proteins, such as the CB_{SH3-} isoform of CB, are expressed, GFP-gephyrin is redistributed into numerous sub-membranous microclusters (Papadopoulos et al 2017). This phenotypic change in the GFP-gephyrin distribution was used to identify new gephyrin interaction partners. The cDNA library used in our screen was previously described (Linhoff et al 2009). To ensure a reliable screen of the cDNA library, a homogeneous expression of GFP-gephyrin in as many cells as possible and a very high transfection efficiency of the cDNA had to be achieved. For this purpose, the cells were seeded in 12 well plates, 24 hours later a part of the wells were transfected with an mCherry expressing plasmid and 24 hours later GFP-gephyrin expression was induced with TET. One day after GFP-gephyrin induction, the cells were fixed and microscopic images were taken.

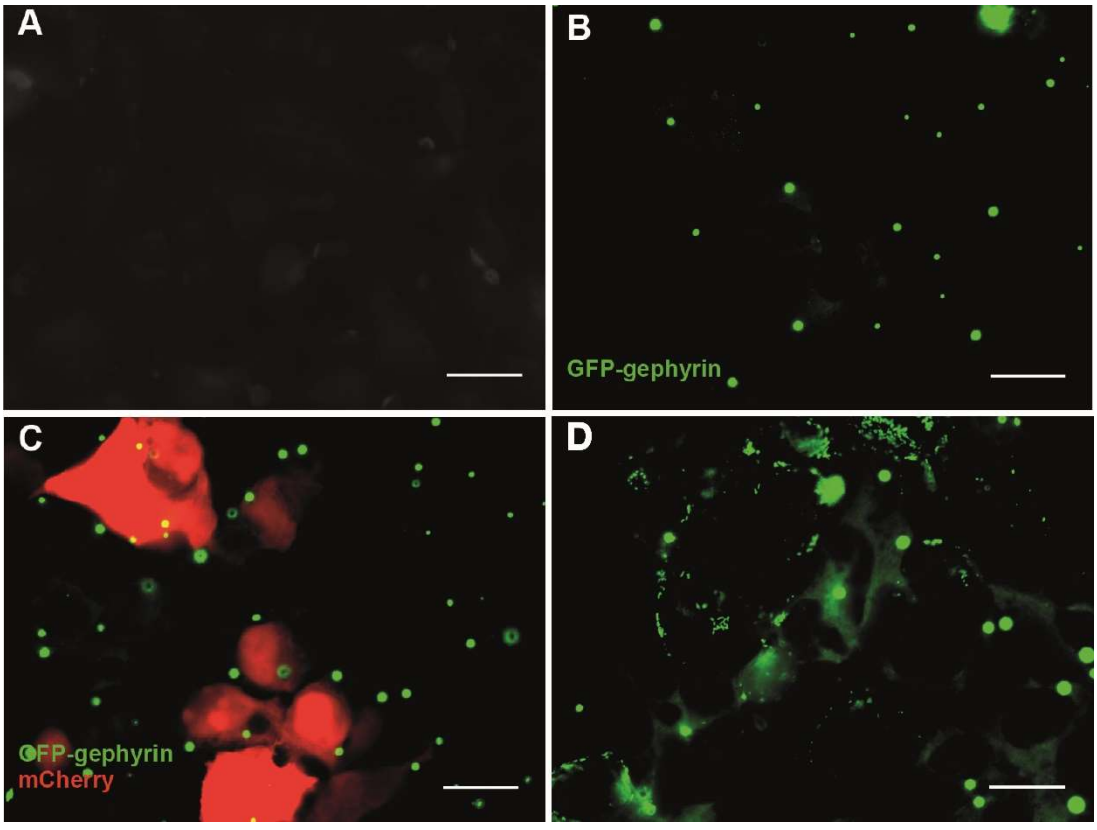

Figure 7 TET-Induced GFP-gephyrin expression in Flp-In T-Rex-GFP-gephyrin HEK 293 cells
A-D. Flp-In T-Rex-GFP-gephyrin HEK 293 cells treated under different conditions. **A.** Control untransfected and without TET treatment. **B.** Untransfected and treated with TET. **C.** Transfected 24 h after seeding with 200 ng mCherry-expressing plasmid DNA. **D.** Transfected 24 h after seeding with 50 ng CB_{SH3-} expressing plasmid DNA. GFP-gephyrin expression was induced 24 h after transfection by TET treatment. Scale bars: 20 µm

The experiment showed that GFP-gephyrin was only expressed upon TET treatment and accumulated in large intracellular aggregates within the cell (Figures 3B and 3C). In contrast, under the control conditions shown in **Figure 7**A, no GFP-gephyrin expression was visible. Furthermore, high transfection efficiency of about 60 - 70 % could be achieved under the selected conditions (see **Figure 7**C). In agreement with previous publications, redistribution of GFP-gephyrin into submembranous microclusters was also observed in this experimental approach by cotransfecting CB_{SH3-} and GFP-gephyrin (see **Figure 7**D). This phenotypic change, which is not observed when GFP-gephyrin is expressed alone, is consistent with previous observations reported in the literature (Harvey et al 2004a, Kins et al 2000).

3.2 Screening of the cDNA libraries

For screening of proteins capable of inducing a redistribution of GFP-gephyrin from large intracellular aggregates into microclusters, a previously described, size-selected cDNA expression library of the postnatal day 11 (P11) rat brain was used (Linhoff et al., 2009). This cDNA library was of highest quality and included aliquots of cDNA pools with the size of 2-3 kb, 3-4 kb and 4-5kb, respectively. The library was kindly provided by Prof. Dr. Ann-Marie Craig (Vancouver, Canada) in the form of glycerol stocks, as previously described (Linhoff et al 2009). Each of the stocks provided, contained approximately 10.000 CFU. Initially, we aimed to create pools of approximately 50 different cDNAs and amplified them by liquid gel amplification. Subsequently, the DNAs in the cDNA pools were purified using nexttex^{TM} 1-step DNA isolation kit for plasmids. This resulted in 192 cDNA pools of 50 cDNAs per insert size, and an aliquot of each pool was always kept as glycerol stock at -80 °C. In the following steps over 30.000 different cDNAs were analyzed. This was achieved by transfecting each pool into the Flp-In T-Rex-GFP-gephyrin HEK 293 cell line and, 24 h later, by inducing GFP-gephyrin expression using 20 µm TET. 24 h after GFP-gephyrin induction, the cells were fixed and analyzed with a Zeiss Imager Z1 microscope. The cells were screened for the previously described phenotypic redistribution of GFP-gephyrin. Such redistributions of GFP-gephyrin were very difficult to automatically screen due to the low concentration of each individual cDNA in a pool of 50 cDNAs. Therefore, each coverslip had to be carefully and manually inspected by eye, in order to identify the few cells that exhibit a phenotypic change in GFP-gephyrin distribution. In this first step of our unbiased screen, 7 different pools of cDNAs were identified as positive, i.e. to contain candidates capable of triggering a phenotypic redistribution of GFP-gephyrin. Subsequently, a PCR with all positive pools was performed to check whether the cDNA of CB was present in the particular pools. Our PCR-analysis indicated that all of the identified cDNA pools were negative for CB-cDNA. The glycerol stocks of the respective pools were thawed, aliquots of the bacteria were diluted 1:50.000 and plated onto agar plates containing carbenicillin. Subsequently, 576 single clones (6x96) per pool were picked, transferred into 96 well plates, and the cDNAs were isolated as described above. Sub-pools of aliquots containing 12 different cDNAs were collected, and additional screens of the resulting 48 sub-pools were performed in Flp-InT-Rex-GFP-gephyrin HEK 293 cells, as described above. Using this approach, we were able to identify positive sub-pools of each initial pool rated to be positive in containing candidate proteins capable of redistributing GFP-gephyrin. Finally, all 12 individual cDNAs of a positive sub-pool were analyzed by using the same cell-based assay. Positive cDNAs were sequenced and a sequence analysis was performed using the NCBI nucleotide BLAST database. It should be noted that each positive cDNA of a sub-pool led to the same result in the sequence analysis, which again indicates the robustness of our screen and our analysis. In Figure 8, the phenotypic redistributions of GFP-gephyrin upon expressing of the individual candidate proteins are shown.

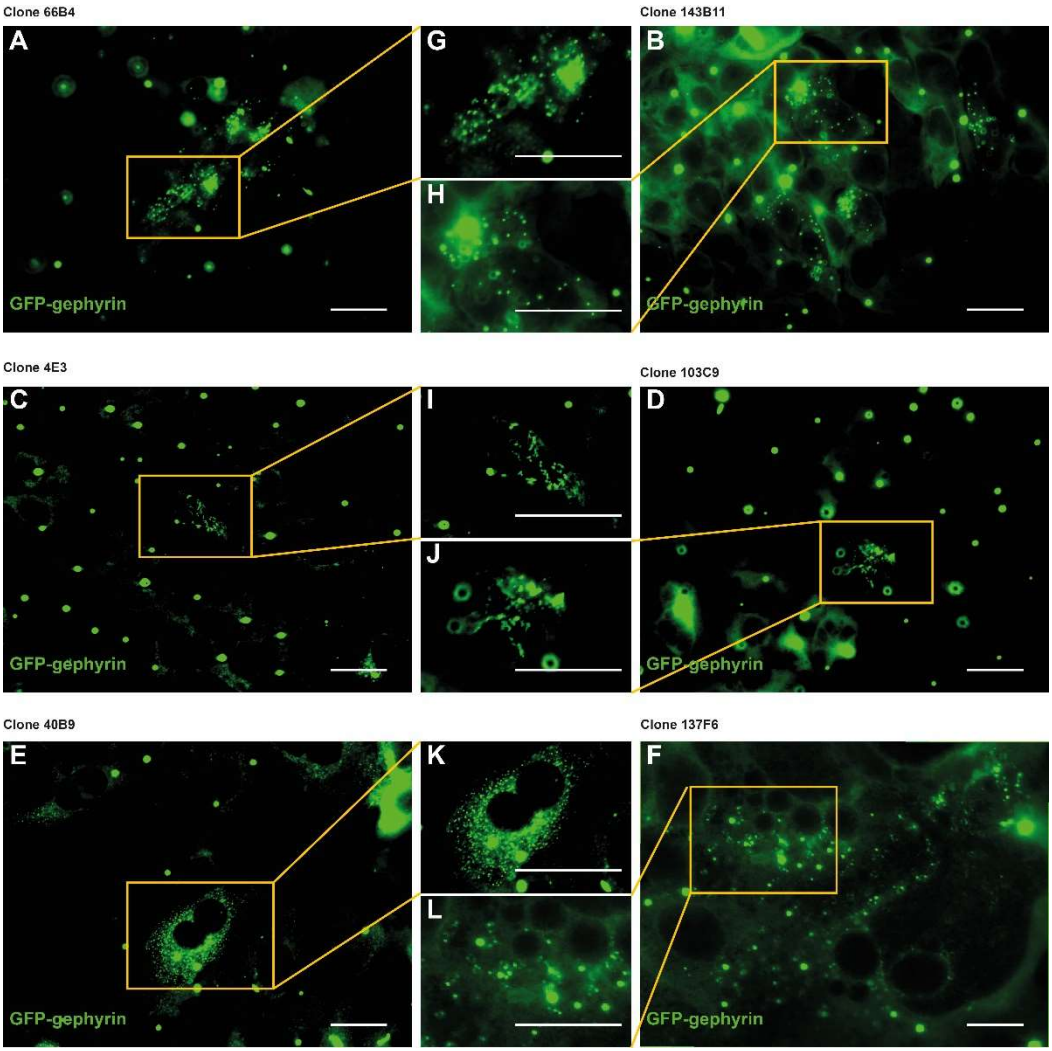

Figure 8 Phenotypic redistribution of the GFP-gephyrin of all positive clones from the cDNA library screen
A-B. Positive clones of the 2-3 kB cDNA library. **C-D.** Positive clones of the 3-4 kB cDNA library. **E-G.** Positive clones of the 4-5 kB cDNA library. **A.** The protein corresponding to the positive clone B4 of the pool 66 from the 2-3 kb library is β-actin; **G.** Zoom in on the phenotype of GFP-gephyrin redistribution. **B.** The protein corresponding to the positive clone B11 of the pool 143 from the 2-3 kb library is WAVE1; **H.** Zoom in on the phenotype of GFP-gephyrin redistribution. **C.** The protein corresponding to the positive clone E3 of the pool 4 from the 3-4 kb library is the glycine receptor β-subunit (GlyRβ); **I.** Zoom in on the phenotype of GFP-gephyrin redistribution. **D.** The protein corresponding to the positive clone C9 of the pool 103 from the 3-4 kb library is Neuroligin 2; **J.** Zoom in on the phenotype of GFP-gephyrin redistribution. **E.** The protein corresponding to the positive clone B9 of the pool 40 from the 4-5 kb library is protein tyrosin phosphatase receptor type N2 (PTPRN2); **K.** Zoom in on the phenotype of GFP-gephyrin redistribution. **F.** The protein corresponding to the positive clone F6 of the pool 137 from the 4-5 kb library is huntingtin interacting protein 1 related (HIP1R); **L.** Zoom in on the phenotype of GFP-gephyrin redistribution. Scale bars, 20 µm

Clone B4 from pool 66, as well as clone B11 from pool 143, were the sub-pools of the 2-3 kb cDNA library, that were identified as positive, leading to a redistribution of GFP-gephyrin from intracellular aggregates into microclusters. After sequence analysis by BLAST, the two clones were identified as β-actin (66B4) and WAVE1 (143B11). Both proteins were able to induce numerous GFP-gephyrin microclusters, which were distributed throughout the cell (**Figure 8**A-B). Furthermore, both proteins, WAVE1 and β-actin, induced mainly intracellular GFP-gephyrin microclusters.

The clone E3 from pool 4, as well as the clone C9 from pool 103 are the ones from the corresponding pools of the 3-4 kb cDNA library that were identified as positive in redistributing of GFP-gephyrin into

microclusters. After sequence analysis by using BLAST, the two clones were identified as the GlyRβ (4E3) and NL2 (103C9). In both cases, it can be clearly seen in the **Figure 8** that numerous microclusters form, but these accumulate into elongated patches. Again, numerous samples were viewed and, in the case of NL2, no submembranous localization of GFP-gephyrin microclusters was detected. However, the microclusters induced by GlyRβ appear to be located just below the cell membrane. To analyze this in detail, further investigations were necessary, which will be described and evaluated in more detail in chapter 3.3.

Clone B9 from subpool 40, as well as clone F6 from subpool 137 and clone A8 from subpool 171 correspond to the pools of the 4-5 kb cDNA library, that were identified as positive in redistributing GFP-gephyrin into microclusters. After sequence analysis by BLAST of the two clones were identified as protein tyrosine phosphatase receptor type N2 [PTPRN2 (40B9)], Huntingtin interacting protein 1 related [HIP1R (137F6)] and N-ethylmaleimide sensitive factor [NSF (171A8)]. Again, numerous samples and microscopic images were viewed and no submembranous clusters were observed with any of the identified candidates. In **Figure 8**E it is clearly seen that PTPRN2 causes numerous microclusters distributed throughout the cell. This redistribution is comparable to the type observed upon expression of WAVE1 and β-actin (clones 143B11 and 66B4, respectively).

In comparison, HIP1R induces fewer microclusters (**Figure 8**F). The microclusters seen in **Figure 8**F induced by NSF are predominantly localized at the cell edge and form elongated patches. This phenotype is comparable to that observed upon expression of GlyRβ or neuroligin 2 (compare clone 171A8 with clones 4E3 and 103C9, respectively).

Table 9 Overview of the identified candidate proteins in the different pools of our cDNA library

Gene	Protein Name	Known Functions	Gene	Protein Name	Known Functions
WASF1 Pool: 2-3 Kb	Wiskott-Aldrich Syndrome Protein (WASP) Family Member 1 (WAVE1)	Member oft he WASP family scaffold proteins.(Miki et al 1998) Actin-regulatory protein.(Miki et al 1998) Directs signals from Rac1 ro Arp2/3.(Miki et al 1998, Miki & Takenawa 1998, Nakagawa et al 2001)	PTPRN2 Pool: 4-5 Kb	Protein Tyrosin Phosphatase Receptor Type N2 (Phogrin)	Neurosecretory vesicle protein. (Wasmeier & Hutton 1996) Functions as a phosphatidylinositol phosphatase. (Caromile et al 2010) Dephosphorylates PI(3)P and PI(4,5)P_2. (Caromile et al 2010)
ACTB Pool: 2-3 Kb	β-actin	One of the two nonmuscle cytoskeletal actins.a(Harborth et al 2001, Vandekerckhove & Weber 1978) Is involved in cell motility, structure and integrity.(Khaitlina 2001, Le et al 1998, Peckham et al 2001)			

GLRB Pool: 3-4 Kb	Glycine Receptor Subunit β (GlyR-β)	GlyRs are ligand-gated chloride channels composed of 2 α- and 3 β-subunits.(Kuhse et al 1995) They mediate synaptic inhibition.(Kuhse et al 1995) GlyR-β is a known gephyrin-binding protein.(Kirsch & Betz 1995)	HIP1R Pool: 4-5 Kb	Huntingtin Interacting Protein 1 Related	Is involved in vesicle trafficking. (Yang et al 2018) Binds 3-phosphoinositides via its Epsin-N-terminal homology (ENTH) domain. (Hyun et al 2004)
NLGN2 Pool: 3-4 Kb	Neuroligin 2 (NLGN2)	Cell-adhesion protein on the postsynaptic membrane of inhibitory synapses.(Varoqueaux et al 2004) NLGN2 is a known gephyrin-binding protein.(Poulopoulos et al 2009)	NSF Pool: 4-5 KB	N-ethylmaleimide sensitive factor	ATPase involved in numerous membrane fusion events. (Furst et al 2003) The GluA2-NSF interaction is necessary for maintaining synaptic AMPARs. (Araki et al 2010)

3.3 Studies on the localisation of GlyRβ-induced gephyrin microclusters

Considering that the microclusters induced by GlyRβ appeared to be localized close to the plasma membrane of the cells, we aimed to determine their subcellular localization. To achieve this, the cell adhesion protein IgSF9b was used as a marker for the plasma membrane (Babaev et al 2018). For this purpose, IgSF9b-Myc was used, which has an N-terminal Myc tag located in the extracellular region of the protein. Thus, it was possible to perform immunolabeling without permeabilization of the cells.

It first had to be excluded that IgSF9b is not able to trigger a redistribution of GFP-gephyrin. In this control experiment, IgSF9b alone was transfected into the Flp-In T-Rex-GFP-gephyrin HEK 293 cells and 24 h later GFP-gephyrin expression was triggered by TET treatment. Analysis of the cells 24 h after the onset of GFP-gephyrin expression showed no evidence that IgSF9b causes a redistribution of GFP-gephyrin into microclusters.

In a next step Flp-In T-Rex-GFP-gephyrin HEK 293 cells were transfected with IgSF9b-Myc, as well as with clone 4E3 (GlyRβ). 24 hours later, gephyrin expression was induced by TET treatment. Upon TET-induction, cells were allowed to express GFP-gephyrin for additional 24 hours. Subsequently, the cells were fixed and immunocytochemistry was performed, as described in the 2.2.4.6 section. Cells were analyzed using the Leica TCS SP2 confocal microscope. For this purpose, z-stacks of the cells were acquired to generate 3D projections as shown in the **Figure 9**.

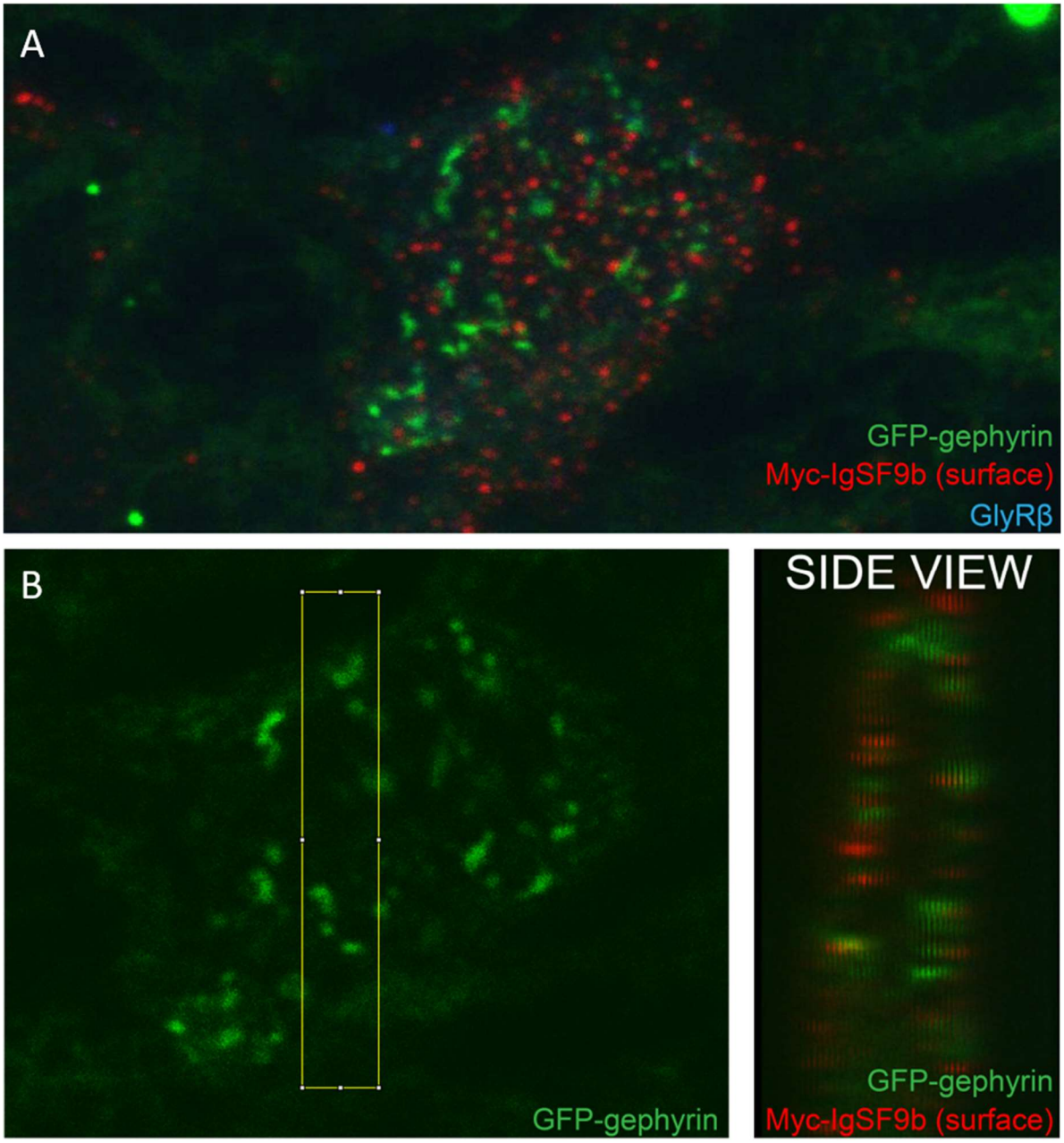

Figure 9 Co-expression of GFP-gephyrin and GlyRβ leads to the formation of submembranous microclusters of GFP-gephyrin

A. Maximum intensity projection of confocal z-stacks of Flp-In T-Rex GFP-gephyrin HEK293 cells transfected with IgSF9b-Myc (red) and the GlyRβ clone 4E3 (blue). 24 h after transfection, GFP-gephyrin (green) expression was induced by TET treatment. **B.** GlyRβ-induced microclusters of GFP-gephyrin. Yellow rectangle indicates the selected area for 3D reconstruction of the side view. Scale bar: 10 µm

This experiment shows that GlyRβ induces submembranous microclusters of GFP-gephyrin. In **Figure 9**A, a maximal intensity projection of the recorded stack is provided, which clearly shows the phenotypic change induced by GlyRβ. Furthermore, the plasma membrane marker IgSF9b-Myc is shown in red. **Figure 9**B shows the selection area for the 3D projection of the side view, in which it can be that some GFP-gephyrin microclusters colocalize with the IgSF9b immunoreactive spots. Furthermore, all GFP-gephyrin microclusters are very close to the plasma membrane labeled by IGSF9b. Thus, it can be concluded that the GFP-gephyrin microclusters induced by GlyRβ are plasma membrane-associated

microclusters. In the images obtained, only a very weak staining of GlyRβ is visible (blue), which may be due to low expression as well as rather poor antibody quality.

3.4 Studies on the localisation of GlyRβ in Flp-InT-Rex -GFP-gephyrin HEK 293 cells

In the previous chapter 3.3, GlyRβ was shown to lead to a redistribution of GFP-gephyrin into submembranous microclusters. These results motivated us to also determine the subcellular localization of GlyRβ.

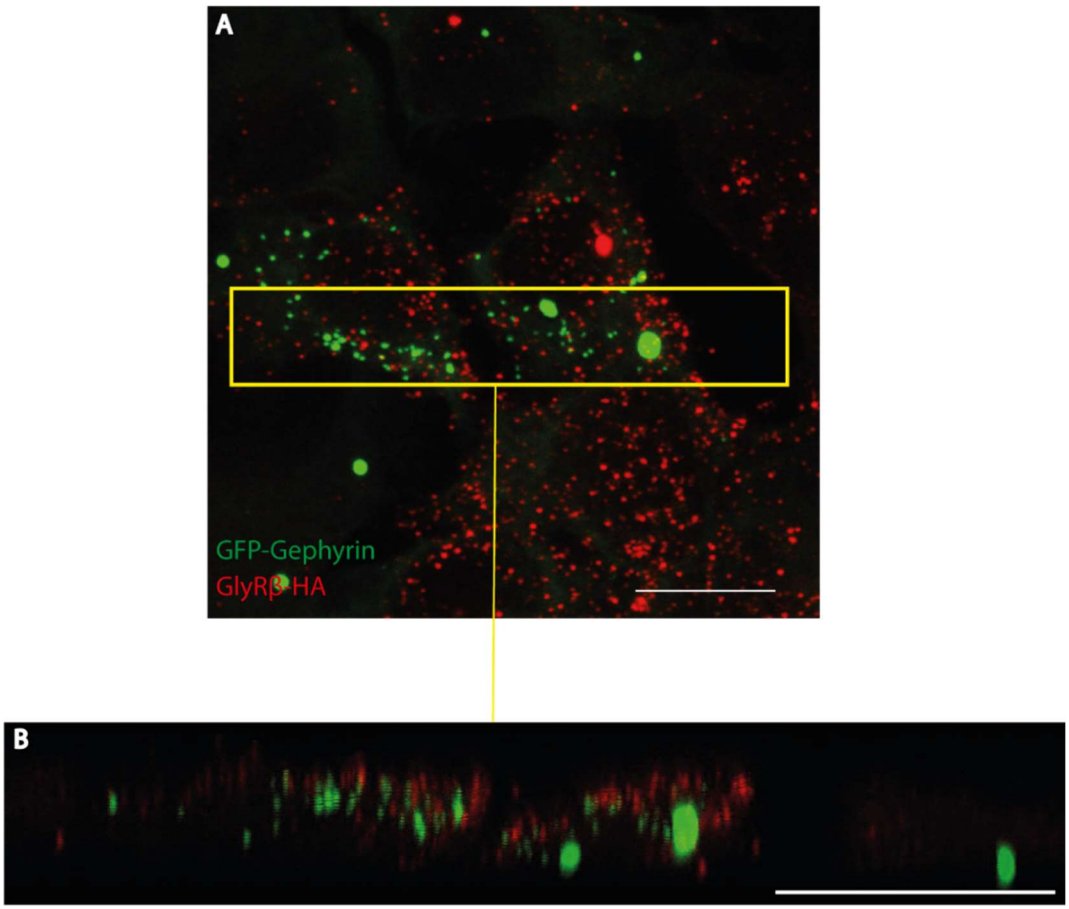

Figure 10 Co-expression of GFP-Gephyrin with GlyRβ leads to localization of GlyRβ in the plasma membrane
A. Maximum intensity projection of confocal z-stacks of Flp-In T-Rex-GFP-Gephyrin HEK293 cells transfected with GlyRβ (red). 24 h after transfection, GFP-Gephyrin (green) expression was induced by TET treatment. The Yellow rectangle indicates the selected area for (**B**) **B.** 3D reconstruction of the side view. Scale bar: 10 µm

For this purpose, PCR was used to amplify the cDNA of GlyRβ from the pcDNA3.1 vector of the cDNA library, which was then cloned into the pKH3 vector so that a GlyRβ-HA fusion protein is expressed. The C-terminal HA tag added in this way is localized in the extracellular region of the protein. This makes detection of the HA tag possible without permeabilization of the cells if the receptor is located in the cell membrane. Cells were transfected with the GlyRβ-HA construct as described in 2.2.3.7. 24 h later, GFP-gephyrin expression was initiated by TET treatment and further 24 h later the cells were fixed by PFA. Subsequently, immunocytochemistry was performed as described in 2.2.4.5, skipping the

permeabilization step. Cells were analyzed using the Leica TCS SP2 confocal microscope. For this purpose, z-stacks of the cell were acquired to generate 3D projections as shown in **Figure 10**.

For a clear representation, the maximum intensity projection of the recorded stack is shown in **Figure 10**A. Here again, the GFP-gephyrin (green) sub-membranous microclusters induced by GlyRβ-HA can be seen. In addition, a very good staining of GlyRβ-HA can be observed. When these images are compared to the **Figure 9**A, a much clearer staining of GlyRβ is seen in **Figure 10**A. This indicates a problem with the available antibodies against GlyRβ. Only by using the GlyRβ-HA construct a good and reliable detection by ICC was possible. By this experimental approach, we could show that the HA-labeled GlyRβ variant also led to a redistribution of GFP-gephyrin into submembranous microclusters (see **Figure 10**B) as well as that GlyRβ localized at the plasma membrane.

3.5 Generation of GlyRβ-KI mice using CRISPR/Cas9

The results obtained in the previous chapters 3.3 and 3.4 showed that GlyRβ, under the chosen conditions, is localized at the plasma membrane and able to trigger a redistribution of GFP-gephyrin into sub-membranous microclusters. These two new findings identify a previously unknown role of GlyRβ in promoting sub-membranous clustering of gephyrin indepedently of additional proteins. In order to perform further studies, the aim of this work was to generate two new mouse lines using CRISPR/Cas9.

3.5.1 Generation of conditional GlyRβ KO mice

For further studies, a conditional GlyRβ KO was generated using CRISPR/Cas9. The strategy used for this (see **Figure 11**) flanks exons 8 and 9 of the Glrb gene with loxP sequences for the conditional Glrb KO. The mouse line was generated using CRISPR/Cas9 and a HDR fragment (**Figure 11**A). The mouse line will allow conditional Glrb gene KO in different brain regions (e.g. forebrain), via crossing the mice with corresponding Cre-expressing mouse lines (see **Figure 11**A). The HDR fragment was integrated into the Glrb locus using two gRNAs. By using primers FP2 and RP, a WT fragment with the size of 297 bp (**Figure 11**B panel top left) is generated. After successful integration of the HDR fragment, the size increases to 332 bp; **Figure 11**B panel bottom left), due to the introduced lox-P site. In the generated founder animals, both the WT allele and the "floxed" (fl) allele were detected (**Figure 11**B panel top right). The electropherograms show a successful integration of the HDR fragment and thus the generation of founder animals. First, the founder mice were mated with WT animals (C57Bl6/J) to reveal germline transmission. The animals of the F1 generation (fl/+) were mated with each other to obtain homozygous fl/fl animals. To test the functionality of the newly generated mouse line, fl/+ animals were crossed to the "general deleter" line EIIα-Cre. Which expresses the Cre-recombinase at the zygote-state (Lakso et al 1996).

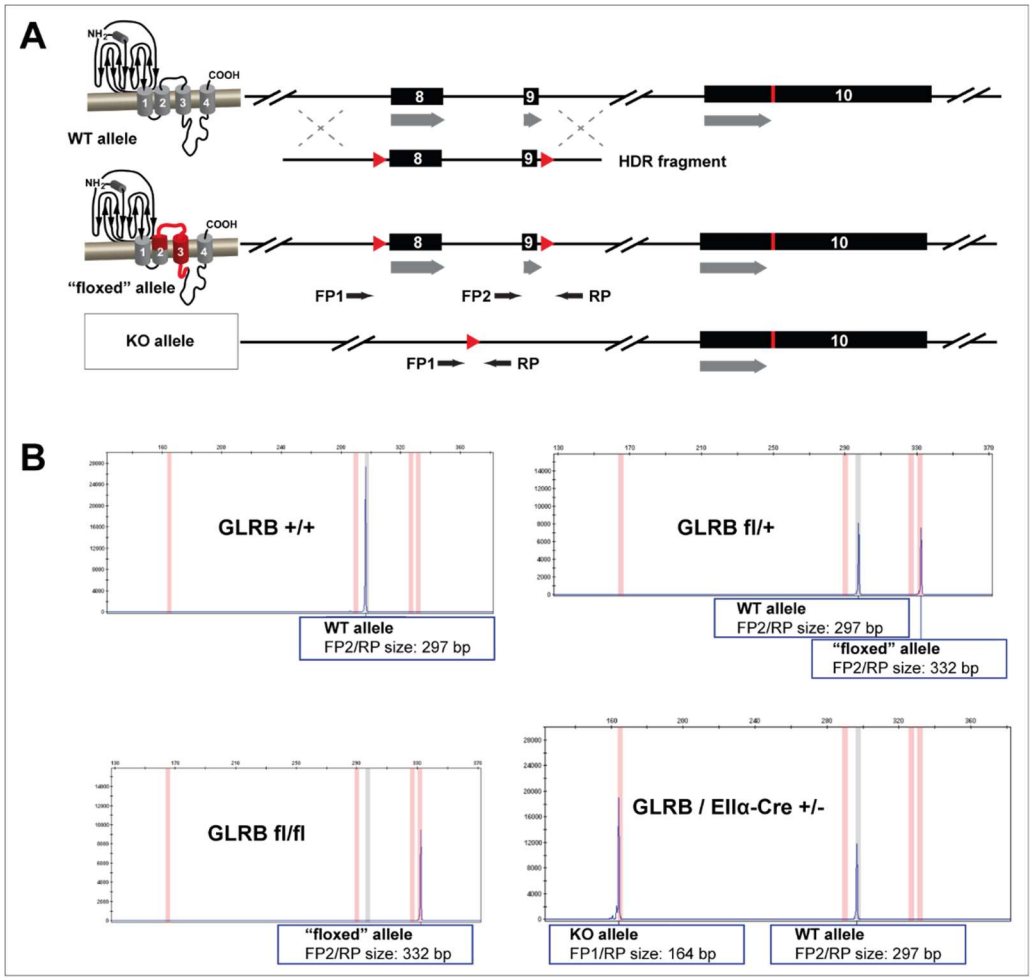

Figure 11 Schematic representation of the CRISPR/Cas9 strategy to create a conditional GlyRβ KO and the corresponding PCR strategy to detect founder animals and determine the genotype.
A. The HDR fragment generated by Gibson assembly contains the exons 8 and 9 and flanking lox-P sites (red triangles). It was integrated into the Glrb locus using 2 guide RNA. Founder animals were identified using the PCR strategy shown (FP1, FP2, RP). B. Electropherograms obtained using the PCR strategy shown upper panel the detection of the possible genotypes.

By using the primers FP1 (37407) and RP (05443) it was possible to detect the expected +/- allele (see Figure 11B panel bottom right; - allel: FP1/RP= 164 bp). This shows that the CRISPR/Cas9 strategy was successfully implemented and could be verified by PCR. This new conditional GlyRβ KO line should allow for further investigations of the role of GlyRβ in the development of inhibitory postsynapses in the mouse forebrain.

3.5.2 Generation of GlyRβ-HA KI mice

One of the best-studied interaction partners of gephyrin is GlyRβ (Kim et al 2006, Kirsch et al 1991, Schrader et al 2004). Gephyrin has been previously shown to bind to the intracellular loop of GlyRβ (Sola et al 2004). To further elucidate the role of GlyRβ-gephyrin interaction, we generated a GlyRβ-HA KI mouse. Based on our KI strategy, an insertion of a loxP-site in the intronic region upstream of the last exon 10, an insertion of an HA tag directly upstream of the STOP codon, and the insertion of another loxP-site in the untranslated region of exon 10 (see **Figure 12**A) was planned. The mouse line was generated using CRISPR/Cas9, a HDR fragment, and the use of two gRNAs.

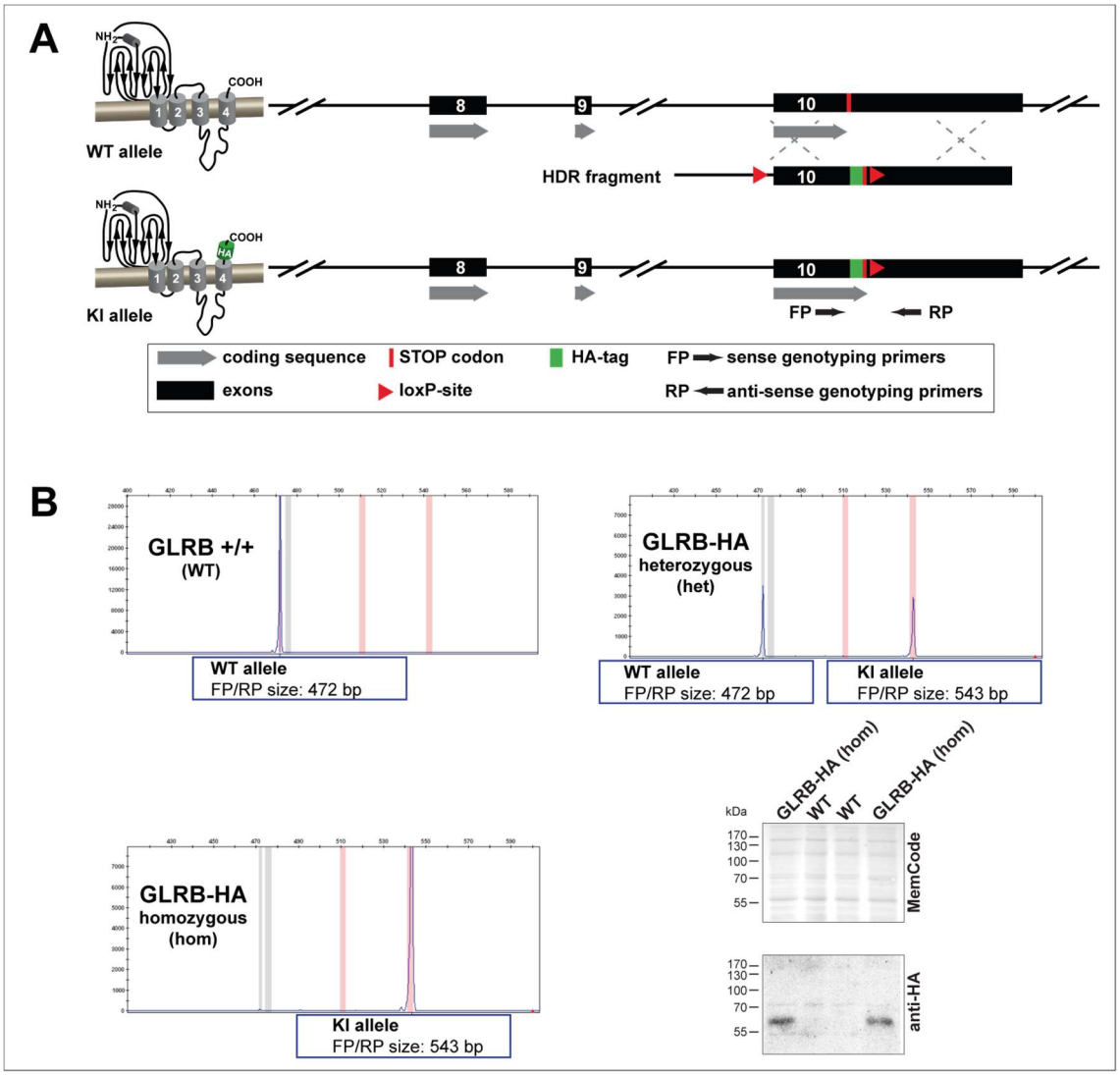

Figure 12 Schematic representation of the CRISPR/Cas9 strategy to create an GlyRβ-HA KI and conditional KO of Exon 10 and the corresponding PCR strategy to detect founder animals and determine the genotype.
A. The HDR fragment generated by Gibson assembly contains the exon 10 and lox-P sites (red triangles) and a HA tag in the untranslated region, which was integrated into the Glrb locus using 2 guide RNA. Founder animals were identified using the PCR strategy shown (FP and RP). **B.** Electropherograms obtained using the PCR strategy shown upper panel the detection of the possible genotypes. Panel bottom right shows the detection of the HA tagged GlyRβ from mouse brain lysate, using anti HA antibody.

Based on the experiments described above using Flp-In R-Rex-GFP-gephyrin HEK 293 cells (see Figure 6), which indicated, that the C-terminally tagged GlyRβ is capable of redistributing GFP-gephyrin into sub-membranous microclusters, we decided to perform our CRISPR/Cas9-mediated KI in a way that an HA-tag was introduced in the C-terminus of the endogenous GlyRβ protein. As described in chapter 3.3, reliable detection of GlyRβ using antibodies is not possible. In the absence of antibodies that allow specific detection of the GlyRβ protein in immunohistochemistry, this mouse line should allow immunohistochemical analysis of GlyRβ expression in the mouse forebrain, using the inserted HA tag.

Using the primers FP (37595) and RP (37562) it was possible to check the alleles and thus the success of the generation of the mouse lines. Initially, the founder animals were identified by PCR, which show a KI/+ genotype and generate a WT PCR fragment with the size of 472 bp and a KI PCR fragment with the size of 543 bp (see **Figure 12**B). The increase in fragment size is derived from the insertion of the HA-tag, as well as the inserted lox P-site. Initial PCR-based screening for homologous recombination in mice indicated the absence of the loxP-site upstream of exon 10 in the KI allele (**Figure 12**B). The founder animals were then crossed with WT animals (C57Bl6/J) to check for germline transmission. The F1 generation animals (KI/+; see top right panel) were then mated with each other to generate homozygous animals (KI/KI) (**Figure 12** bottom left panel). To verify the success of the KI generation, brain lysates of KI/KI animals and WT animals were analyzed by Western blot. As can be seen in **Figure 12**B (panel bottom right), only in the samples of KI/KI animals a protein with a size corresponding to GlyRβ-HA can be detected by using an HA-specific antibody. Together, these results show a successful generation of the described KI mouse with the exception of the missing loxP site. The KI mouse created in this way can already be used for immunohistochemical studies, since successful insertion of the HA tag has occurred. For further in-depth studies of the GlyRβ-gephyrin interaction *in vivo*, the introduction of the second loxP site is necessary.

3.6 Redistribution of GFP-gephyrin by WAVE2 and WAVE3 in COS-7 cells

In addition to WAVE1, the WAVE protein family consists of the members WAVE2 and WAVE3, which have a similar structure as WAVE1 (Soderling & Scott 2006). This led us to the assumption that also WAVE2 and WAVE3, like WAVE1 (**Figure 8**), might be capable of inducing a redistribution of GFP-gephyrin into microclusters. To test this, COS-7 cells were co-transfected with GFP-gephyrin and either WAVE1, WAVE2 or WAVE3. 24 h later, the cells were fixed and images were taken using the Zeiss Imager Z1 microscope (**Figure 13**).

As previously described (Kins et al., 2000), **Figure 13**A shows that GFP-gephyrin alone does not form microclusters within 24 h. This is also shown by the analysis of the size distribution of the clusters (**Figure 13** bottom panel), which indicates that the main fraction of the clusters has a size larger than 0.5 μm^2 (aggregates). As seen in the c-DNA library screen, WAVE1 triggers a redistribution of GFP-gephyrin within 24 h, generating microclusters (see **Figure 13**B). Thus, the size distribution (see **Figure 13** lower panel) shows that a shift in size to 0.1-0.2 μm^2 (microcluster) occurs. Here again, larger clusters can be seen, which have a size of more than 0.5 μm^2. However, the proportion of these clusters is significantly smaller. The same changes were also observed upon cotransfecting WAVE2 and WAVE3 with GFP-gephyrin. Redistributions of GFP-gephyrin were observed (see **Figure 13**C and 9D). Moreover, mainly microclusters were detected (see **Figure 13** bottom panel). Microclusters with a size of 0.1- 0.2 μm^2 are also formed when WAVE2 or WAVE3 are cotransfected with GFP-gephyrin. These results indicate that,

similar to WAVE1, the two additional members of the WAVE protein family, WAVE2 and WAVE3, are capable of triggering a redistribution of GFP-gephyrin into microclusters.

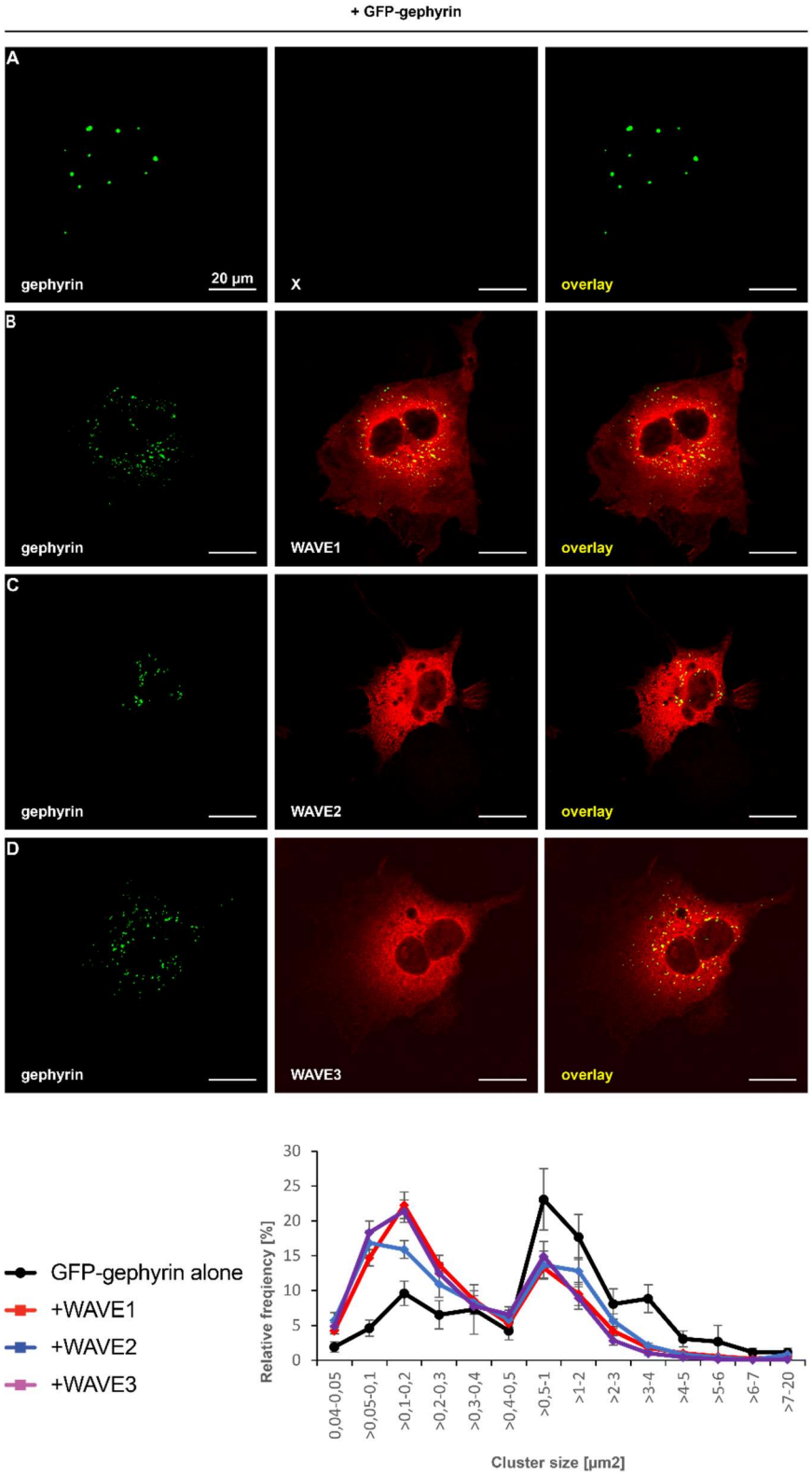

Figure 13 Like WAVE1, the WAVE family members WAVE2 and WAVE3 also induce a redistribution of GFP-gephyrin from aggregates to microclusters in COS-7 cells.

A. *COS-7 cell expressing GFP-gephyrin alone (green).* ***B.*** *COS-7 cells co-expressing GFP-gephyrin together with WAVE1 (red), WAVE2 (**C**, red) or WAVE3 (**D**, red). Scale bars 10 µm; Bottom panel: GFP-gephyrin clusters in COS-7 cells were binned according to their size, as indicated. X: not transfected*

3.7 Expression levels of WAVE2 and WAVE3 in cultured hippocampal neurons derived from WAVE1 KO mice

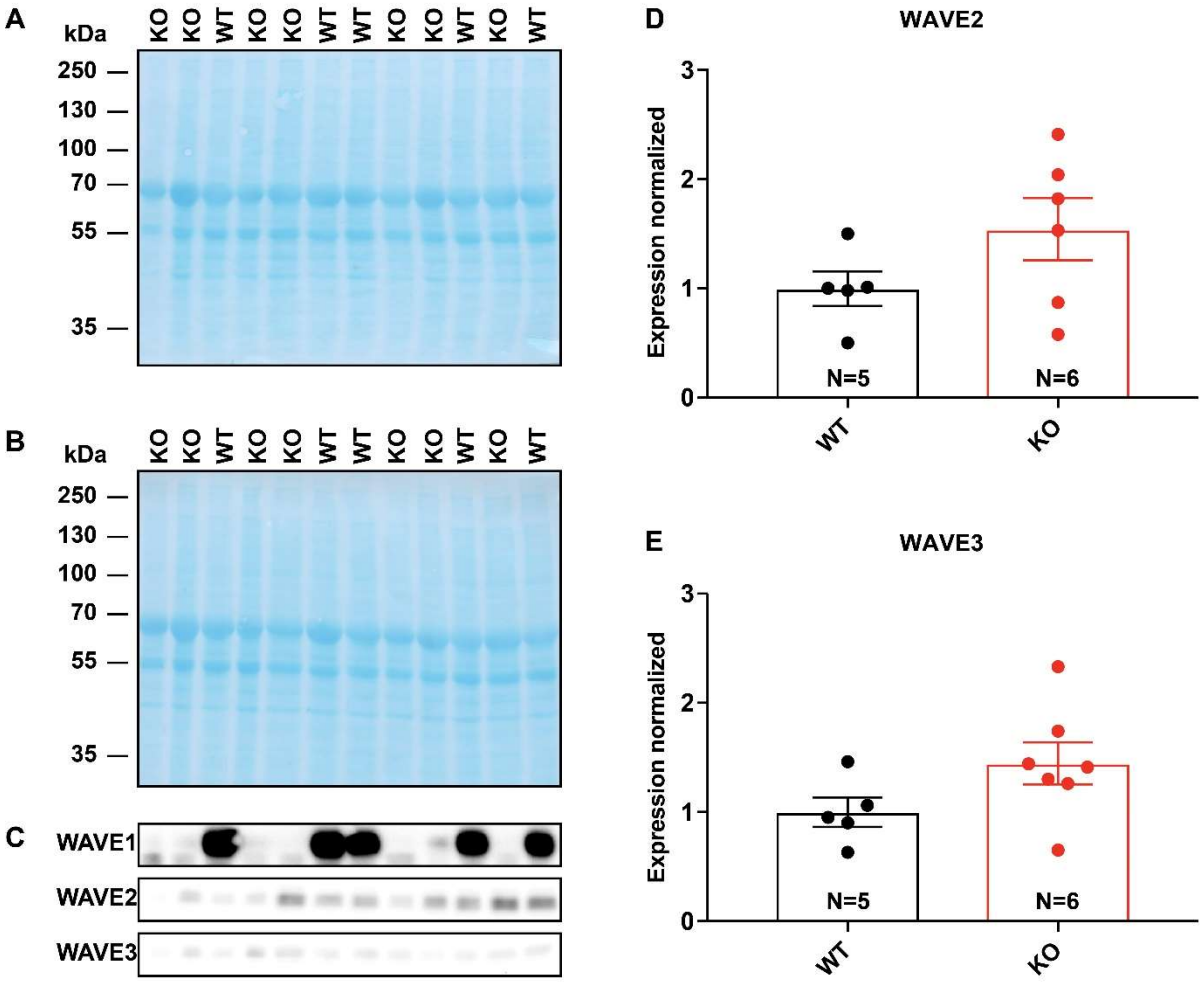

Figure 14 WAVE2 and WAVE3 expression is not significantly altered in hippocampal mass cultures derived from WAVE1 deficient mice.

*MemCode© staining of WAVE2 (**A**) and WAVE3 (**B**) Western blot membrane. For quantification of the relative protein levels of WAVE2 and WAVE3, a Western blot of hippocampal neuron cultures (DIV14) from WAVE1 deficient mice (black) and their littermate controls (red) was performed (**C**). For the calculation of relative expression, the Western blot signal of the samples was normalized to the MemCode© staining. The values obtained were normalized to the mean value of wild-type expression and then plotted in **D** and **E** with standard error of the mean. For statistical analysis, the unpaired students T-test was used. N= analyzed cultures*

The results shown in chapter 3.6 indicated that WAVE2 and WAVE3, similar to WAVE1, are able to redistribute GFP-gephyrin into microclusters. This led to the conclusion that WAVE2 and WAVE3 are not only structurally but also functionally related to WAVE1. To investigate possible compensation of the WAVE1 function in WAVE1-deficient mice by WAVE2 or WAVE3, expression analysis of WAVE2 and WAVE3 was performed at the protein level. To this end, hippocampal mass cultures of WAVE1 deficient mice, as well as of their WT littermates, were established. The WAVE1 deficient mice were described previously (Soderling et al 2003). After 14 days *in vitro* (DIV), cells were harvested and transferred to lysis solution. This was followed by separation of the samples using SDS-PAGE and detection of proteins by Western blot. The blotted membrane was stained using MemCode© and this staining was documented. Finally, treatment with WAVE1, WAVE2 and WAVE3 antibodies (primary antibodies) and horseradish peroxidase coupled antibodies (secondary antibodies) was performed. Detection of the

signal was performed using ECL and the INTAS Chemo Star Plus imager. In **Figure 14** the corresponding blots, as well as the MemCode stainings are shown.

To determine the relative expression levels, the Western blot signal (see **Figure 14**C) was normalized to the MemCode intensity (**Figure 14**A WAVE2 and **Figure 14**B WAVE3). The total MemCode intensity of the corresponding lane was used to compensate for variations in protein loading. This value was then normalized to the mean value of the WT. For WAVE2, the normalized expression increased from 1.0 ± 0.13 to 1.44 ± 0.19. For WAVE3, an increase from 1.0 ± 0.32 to 1.68 ± 0.43 was observed (see **Figure 14**D). However, despite a tendency towards higher WAVE2 and WAVE3 protein levels in neurons derived from WAVE1 deficient mice, the differences were not statistically significant (Figure 10 D and 10 E).

3.8 WAVE1 overexpression in cultured hippocampal neurons

The experiments described in the previous section showed that loss of WAVE1 in hippocampal mass cultures does not lead to substantial changes in the expression of WAVE2 and WAVE3. This motivated us to investigate the effects of WAVE1 overexpression on gephyrin clustering in hippocampal mass cultures. To this end, hippocampal neurons from C57Bl6/N P18 embryos were cultured in a mass culture. Subsequently, the cultures were transfected at DIV 3 with either HA-WAVE1 or mCherry (MOCK control) using the calcium phosphate method. At DIV 14, the neurons were fixed with PFA and immunocytochemistry was performed to identify transfected cells and examine gephyrin clustering. Subsequently, images were taken with a Zeiss Imager Z1 microscope, gephyrin clustering was quantified both in the somata and the dendrites of neurons, and data from neurons expressing WAVE1-HA and MOCK control neurons were compared. The quantifications obtained and also representative images are shown in **Figure 15**.

In the analysis performed on the first and second order dendritic structures, a highly significant reduction in gephyrin puncta densities was observed upon WAVE1 overexpression (10.92 ± 0.77 puncta/20µm in the MOCK transfected cells vs 5.24 ± 0.58 puncta/20µm in HA-WAVE1 overexpressing neurons). There was no significant change in gephyrin puncta size (MOCK: 0.36 ± 0.01 μm^2; WAVE1 overexpression: 0.38 ± 0.01 μm^2). The perisomatic areas also showed a similar effect of WAVE1 overexpression. MOCK transfected neurons had an average gephyrin puncta density of 4.52 ± 0.41 puncta/100μm^2, which was significantly reduced to an average of 2.48 ± 0.35 puncta/100μm^2 in WAVE1 overexpressing neurons. Again, no change in gephyrin puncta size (MOCK: 0.38 ± 0.01 μm^2; WAVE1 overexpression: 0.38 ± 0.01 μm^2) was detected. Thus, WAVE1 overexpression in mass cultures of hippocampal neurons leads to a reduction in gephyrin puncta density as compared to MOCK transfected neurons. Interestingly, the size of the gephyrin clusters remained unchanged despite their reduced density.

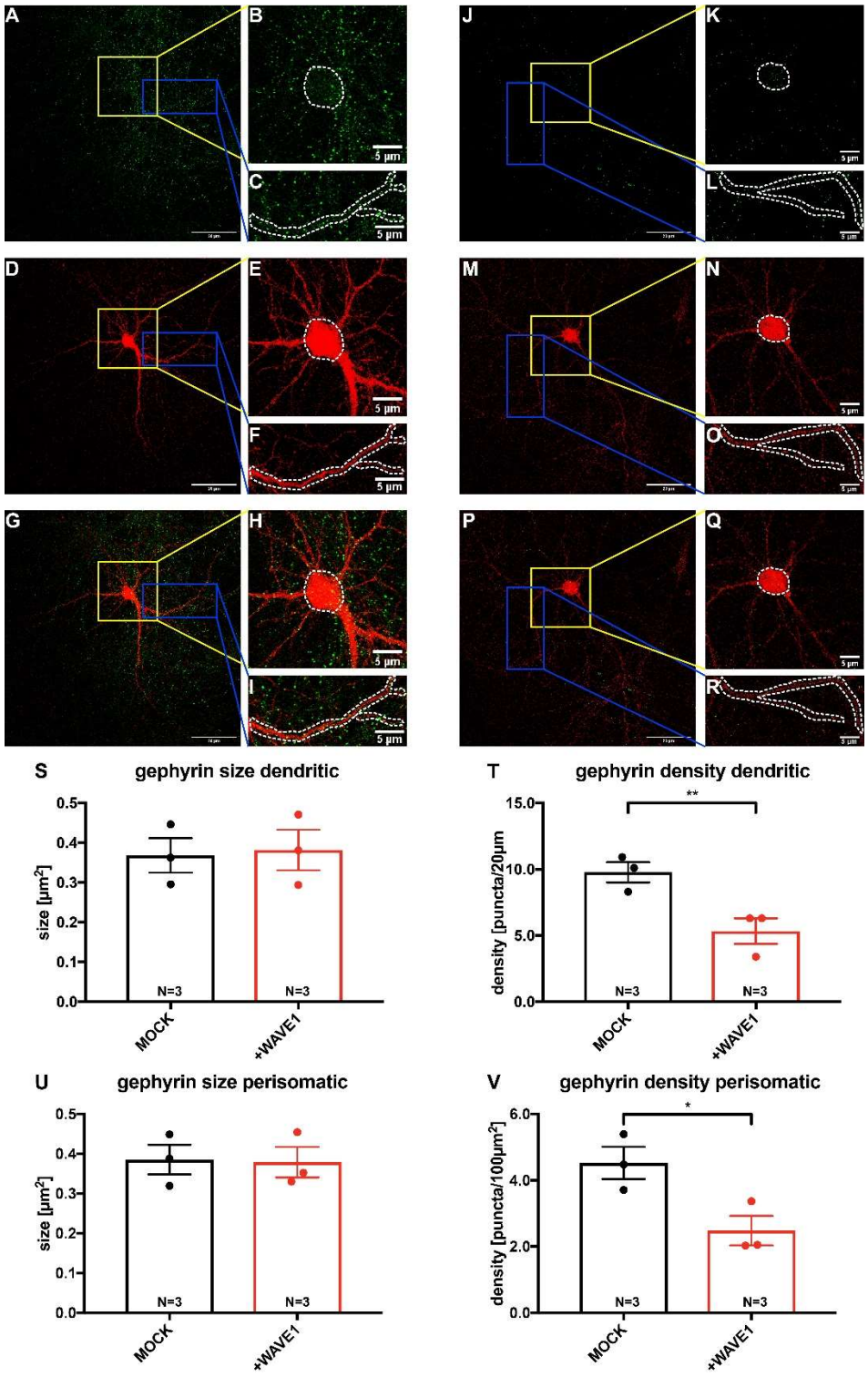

Figure 15 WAVE1 overexpression leads to significantly reduced somatic and dendritic gephyrin puncta densities in hippocampal mass cultures, whereas puncta sizes remain unchanged.

*The brains of C57Bl6/N wild-type embryos were isolated on day E18 and hippocampal cultures were prepared. The cultures were transfected at DIV 3 with a plasmid expressing HA-WAVE1 using the calcium phosphate method (**J-R**) or a control plasmid (mCherry; **A-I**). At DIV 14, the cultures were fixed using PFA and then immunocytochemistry was performed. Both groups were stained for gephyrin (green). The cells transfected with HA-WAVE1 (red; **D-F**) were additionally stained for the HA tag to exclusively visualize the HA-WAVE1 overexpression in cells. In the MOCK group, transfected cells were identified by the expression of the mCherry fluorescent signal (**M-O**). Epifluorescence images of both groups (WAVE1 overexpressing **A-I**; MOCK **J-R**) were acquired for analysis. ImageJ was used to quantify both the dendritic sizes (**S**) and densities (**T**), as well as the perisomatic sizes (**U**) and densities (**V**) of*

*immunoreactive gephyrin puncta. White dashed lines represent the structures selected for quantification. Yellow squares represent the area of enlargement of the perisomatic area (**B,E,H,K,N,Q**); blue rectangles represent the area of dendritic structures (**C,F,I,L,O,R**). For all quantifications, only transfected neurons were used, which in the case of WAVE1 overexpression could be identified by staining against the HA-tag of HA-WAVE1 (**Figure 15**D). The mock transfected neurons express mCherry and could be identified by the red fluorescence (**Figure 15**M). By manual selection in ImageJ, the somatic region of the transfected neuron was selected for quantification, as well as all first and second order dendrites of the neuron. In the figure above, regions for somatic (yellow square) and dendritic (blue rectangle) analysis are shown as examples. The statistical evaluation was carried out by applying the unpaired, two-tailed, students T-test. p<0.05 *, p<0.03 **; Values represent means ± s.e.m.; scale bars: 20 µm and 5 µm, as indicated. N= analyzed cultures*

3.9 Biochemical studies on possible interaction partners of WAVE1

3.9.1 Studies on the interaction of WAVE 1 with CB

The scaffolding protein WAVE1 mediates actin reorganisation by activating the Arp2/3 complex and is itself activated by the GTPase Rac in this process (Soderling et al 2002). An important regulator in this interaction is WRP, which can bind to the proline-rich region of WAVE1 via its SH3 domain and thus interfere with the WAVE1-Rac interaction (Soderling et al 2002). Previous experiments have shown that the WRP-WAVE1 interaction is important for a homeostatic process whose balance plays a central role in neuronal development and the fidelity of synaptic connectivity (Soderling et al 2007). These biochemical features of WAVE1 motivated us to investigate whether CB is also able to bind directly to WAVE1 through its SH3 domain. For this purpose, the respective proteins were expressed in bacterial cells and purified. In order to be able to use WAVE1 as a bait in this experiment, the GST-fusion of WAVE1 was cleaved using thrombin. In a subsequent pull-down assay, direct binding of the proteins was investigated. WAVE1 acted as bait in this experiment to test whether the corresponding proteins bind directly and can be detected by Western Blot after a pulldown (see **Figure 16**).

The results shown in Figure 12 indicate that the SH3 domain of CB2 (GST-SH3) is able to bind WAVE1. Similarly, the full-length variant of CB (GST-$CB2_{SH3+}$) is able to bind WAVE1. The SH3 domain lacking isoform of CB2 ($CB2_{SH3-}$) shows no binding to WAVE1. This confirms that the interaction of WAVE1 and CB2 is via the SH3 domain of CB2. As previously described, GST-WAVE1 was cleaved with thrombin to obtain the untagged WAVE1. This appears to result in the formation of truncated WAVE1 fragments, which are labeled in the **Figure 16** (3,4,6 and 7). These fragments are not only detectable in the input, but also in the pulldown with GST-SH3. Thus, it can be deduced that the SH3 domain of CB2 is able to bind to all labeled fragments. Interestingly, in the pulldown sample of $CB2_{SH3+}$ it was not possible to detect fragments 4, 6 and 7. Here, only the full length band (2), as well as a very weak band of fragment 3 appears.

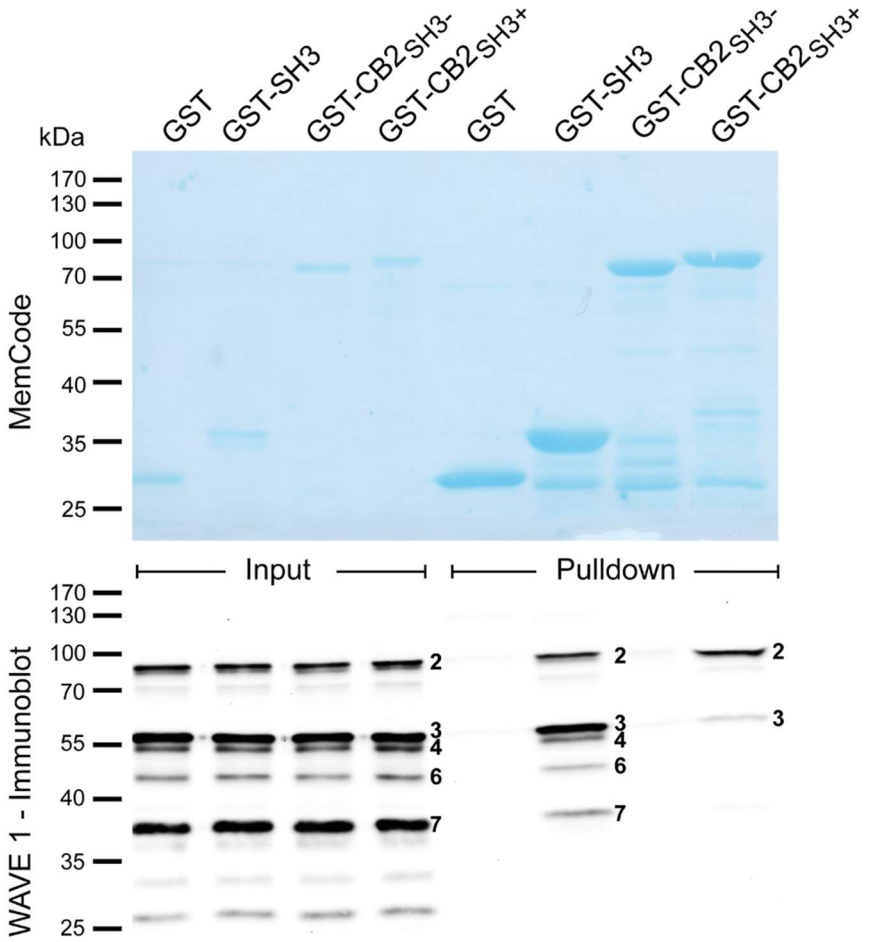

Figure 16 CB2 binds directly to WAVE1 via its SH3 domain.
MemCode stainings (top) and WAVE1-immunoblots (bottom) of the input (left) and the pulldown (right) samples, as indicated. WAVE1 and the different GST-tagged proteins were expressed and purified, as described in the 2.2.2.4 and 2.2.2.5. Note that WAVE1 interacts with GST-SH3 and GST-CB2$_{SH3+}$, but not with GST or GST-CB2$_{SH3-}$. In the upper panel, the input of the pulldown can be seen on the left side. In addition to the bands seen, purified WAVE1 was added, which was used as a bait and detected in the Western blot (lower panel of the figure). On the right side of the upper panel the enrichment of the GST proteins can be seen very well. WAVE1 was detected using Western blot, which can be seen in the lower panel on the right side of the figure, in order to investigate whether the GST proteins used are able to bind WAVE1. Experiments were performed by Theofilos Papadopoulos.

This result suggests that there are differences in the binding affinities of GST-SH3 and GST-CB2$_{SH3+}$ to the different WAVE1 fragments and to the full length WAVE1. In summary, this experiment demonstrated that CB2 is able to bind to WAVE1 and that this binding is mediated by the SH3 domain. Furthermore, possible different binding preferences of GST-CB2$_{SH3+}$ and GST-SH3 to WAVE1 and WAVE1 fragments, respectively, were detected.

3.9.2 Mass spectrometric analysis of the purified WAVE1 fragments indicates the SH3 domain of CB interacts with proline-rich sequences in WAVE1

The results shown in Figure 12 indicated that GST-CB2$_{SH3+}$ preferentially binds to full-length WAVE1, whereas GST-SH3 also binds to smaller WAVE1 fragments. In order to define which protein sequence corresponds to the different fragments of WAVE1 that were obtained upon unspecific cleavage of the

bacterially expressed WAVE1 protein through the protease thrombin, we performed a mass spectrometric analysis of the different fragments. In addition to the bacterially expressed and purified WAVE1, HA-WAVE1 expressed in HEK cells and subsequently purified via HA-Sepharose beads was used as an additional control. The different WAVE1 fragments were separated by using precast 10% Tris-glycine gels (TG PRiME, Serva). Proteins were either visualized by colloidal Coomassie staining (**Figure 17**A) or transferred to nitrocellulose membranes and immunodetected as described in 2.2.2.8 and 2.2.2.9 (**Figure 17**B). In-gel digestion with trypsin and generation of peptide mass fingerprint (PMF) and fragment ion mass spectra of the proteolytic peptides by matrix-assisted laser desorption ionization-time of flight mass spectrometry (MALDI-TOF MS; ultraFlextreme, Bruker) was essentially performed as described (Jahn et al 2006).

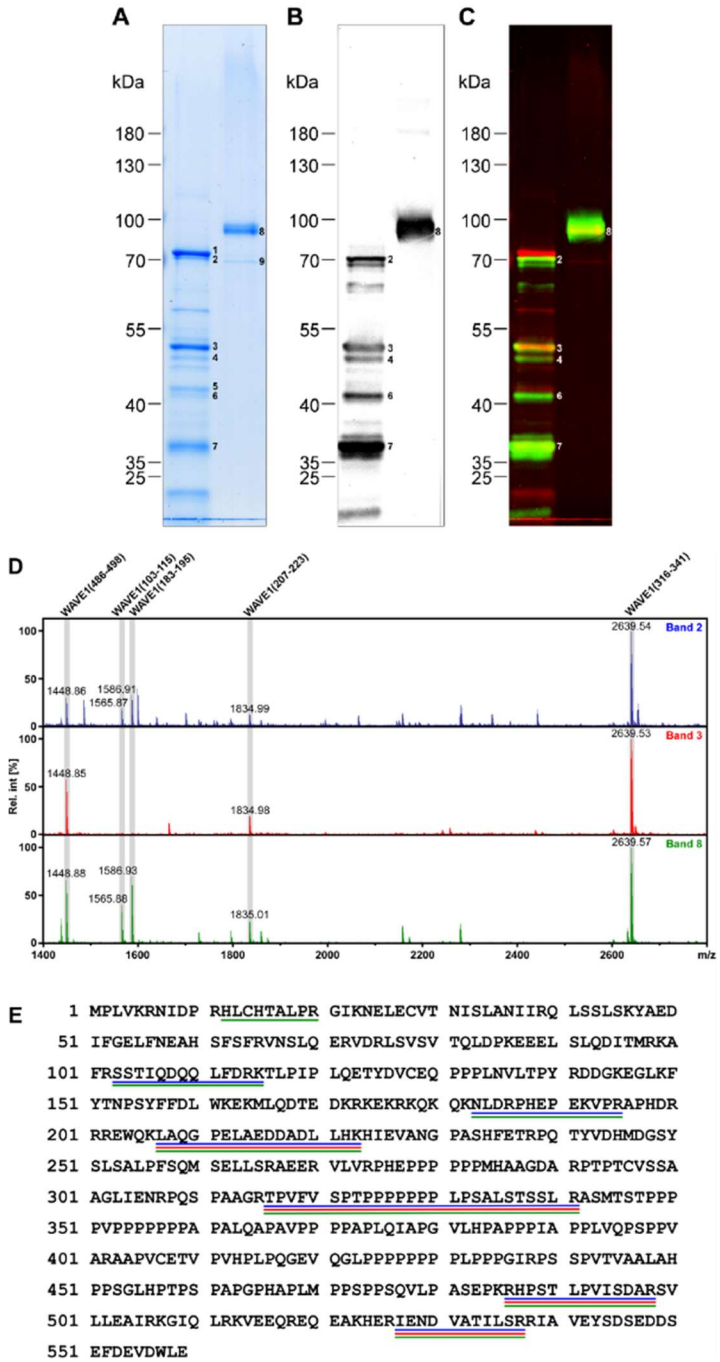

Figure 17 Mass spectrometric identification of the WAVE1 fragments involved in binding to full length $CB2_{SH3+}$.

A. *Coomassie-stained gel showing GST-WAVE1 purified from bacteria after thrombin cleavage (left lane) and HA-WAVE1 purified from HEK cells (right lane).* ***B.*** *Immunoblot showing the WAVE1 immunoreactive bands from the gel ran in parallel with the gel shown in* ***A*** *(same loading scheme).* ***C.*** *False-colored overlay of the Coomassie image shown in* ***A*** *(red) and the immunoblot shown in B (green). Gel bands subjected to mass spectrometric protein identification are numbered.* ***D.*** *Mass spectrometric analysis of trypsin digests of putative full-length WAVE1 (bands 2 and 8; blue and green mass spectrum) and its major thrombin cleavage product (band 3; red mass spectrum). Underlined in grey are the signals for the N-terminal tryptic peptides WAVE1(103-115) and WAVE1(183-195) and, for comparison, the signals for the central and C-terminal tryptic peptides WAVE1(207-223), WAVE1(316-341), and WAVE1(486-498). Note that the signals for the N-terminal tryptic peptides, but not for the central and C-terminal tryptic peptides are missing in the mass spectrum corresponding to the WAVE1 thrombin cleavage product in band 3 (middle panel).* ***E.*** *Amino acid sequence of WAVE1 (UniProtKB accession Q5BJU7). Peptides identified by MS are underlined according to the color code of the mass spectra in D (blue, green: peptides from putative full-length WAVE1 in band 2 and 8, respectively; red: peptides from WAVE1 thrombin cleavage product in band 3). Only peptides confirmed by mass spectrometric sequencing are shown. For the WAVE1 thrombin cleavage product in band 3, no such mass spectrometric evidence was found for sequences N-terminally of Lys-206, indicating N-terminal truncation. Experiments were performed by Olaf Jahn.*

In the first lane of figure **Figure 17** (A-C), the bacterially expressed, purified and thrombin-cleaved WAVE1 was applied and separated as in the previous experiment. Again, multiple fragments were observed. In comparison, in the second lane of figure **Figure 17**(A-C), HA-WAVE1 expressed and purified in HEK cells was applied and separated. Here, no fragmentation of WAVE1 was observed. One of the main differences between the two samples is the thrombin treatment of the sample in lane 1, so that the fragmentation was probably due to a non-specific activity of thrombin. In a next step, we aimed at analysing the fragments that were formed. These were evaluated in an MS analysis **Figure 17**D in cooperation with Dr. Olaf Jahn as described in 2.2.2.11. Since no fragmentation took place in the HA-WAVE1 sample used, this could be used as a control. The analysis indicated that both, the 80 kDa and the 50 kD fragments of WAVE1, which were pulled-down with full-length CB_{SH3+} or the isolated SH3 domain of CB (see **Figure 16**), contained the proline-rich regions within the following sequences of the WAVE1-protein: 316-TPVFVSPTPPPPPPPLPSALSTSSLR-341 and 421-QGLPPPPPPPPL-431. In addition, it was noticed that the fragments that arose showed a truncation of the N-terminal region. This underlines the conclusion that the fragmentation was caused by a non-specific activity of thrombin. Furthermore, the loss of certain N-terminal sequences could also be related to the altered affinity of WAVE1 for full-length CB compared to the SH3 domain of CB alone. Thus, this experiments shows that all WAVE1 fragments binding to CB have a proline-rich region.

3.9.3 No biochemical evidence for a direct interaction between WAVE1 and gephyrin

In this work, it was shown that WAVE1 is able to lead to a redistribution of gephyrin into microclusters. However, based on the phenotype observed in the cDNA library screen, no conclusion can be drawn about possible direct interactions of WAVE1 and gephyrin. To study whether the redistribution of gephyrin is based on a direct interaction with WAVE1, we performed *in vitro* binding assays. To this end, GST-WAVE1 purified from bacteria was used as bait. This was incubated either with His-gephyrin4xR (Saiyed et al 2007) purified from bacteria or with WRP-V5 expressed in COS 7 cells. The corresponding pulldowns were analysed by SDS-PAGE and subsequently Western blotted. The proteins to be tested were detected here by antibodies and the signals obtained are shown in **Figure 18**.

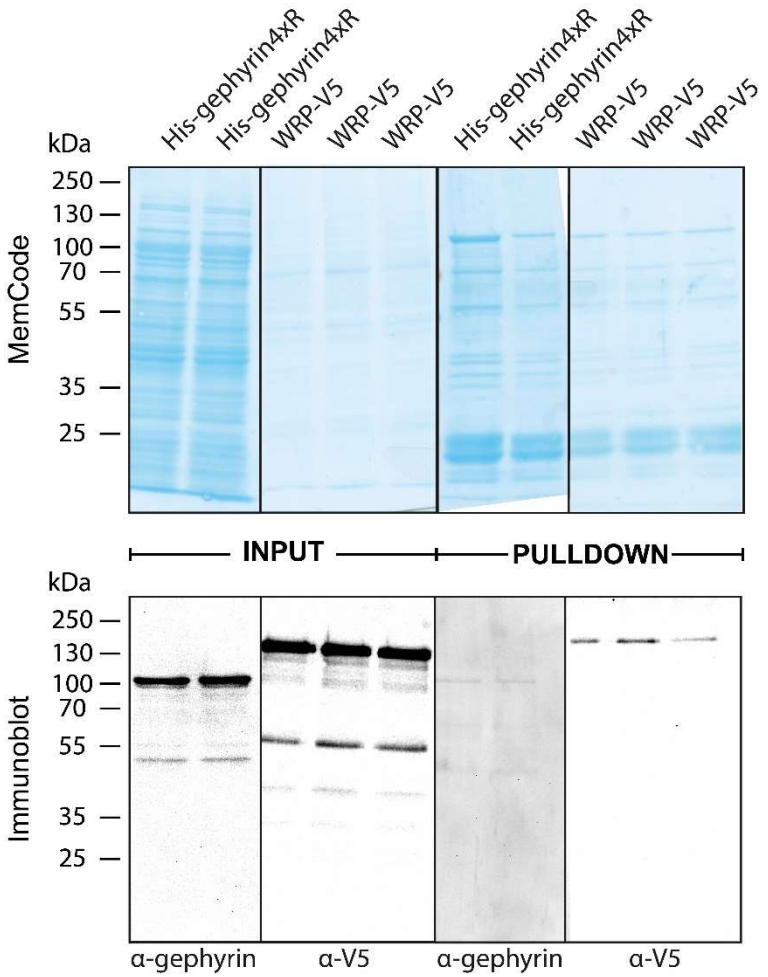

Figure 18 WAVE1 does not interact directly with gephyrin.
MemCode stainings (top) and anti-gephyrin and anti-V5--immunoblots (bottom) of the input (left) and the pulldown (right) samples, as indicated. In all samples, GST-WAVE1 was used as bait, which was incubated either with bacterially expressed and purified His-tagged gephyrin4xR protein, or with the cell homogenates of COS-7 cells expressing V5-tagged WRP.

Following a similar approach as that shown above for analyses of the interaction of CB with WAVE1, we further investigated whether gephyrin binds directly to WAVE1. To this end, GST-WAVE1 was used as bait (Figure 18). Bacterially expressed and purified His-gephyrin4xR was incubated together with GST-WAVE1. The mutant variant of gephyrin (4xR) used here harbours substitutions of 4 hydrophobic amino acid residues (F90R, L113R, L128R, and L168R) at the trimer interface, which due to hydrophilicity and charge abolishes the interactions required for trimerization (Saiyed et al 2007). This choice was made to avoid possible aggregation of gephyrin during pulldown and thus false positive results. In a second approach, COS-7 cells were transfected with the known WAVE1 interaction partner WRP-V5 (Soderling et al 2002) and 36 h after transfection, cell homogenates were prepared as described in 2.2.2.3 and incubated together with GST-WAVE1. Immunobloting was used to detect His-gephyrin4xR and WRP-V5 in the input (left) and pulldown (right) samples (Figure 18, bottom panel). As previously shown (Soderling et al 2002), our pulldown indicated that WRP-V5 binds directly to GST-WAVE1. In contrast, the immunoblots indicated no direct interaction between GST-WAVE1 and His-gephyrin4xR (Figure 14, bottom panel, pulldown). Together our results indicate that the WAVE1-mediated redistribution of GFP-gephyrin into microclusters, which was observed in our cell-based assay, is not due to a direct interaction of WAVE1 with gephyrin.

3.10 Immunohistochemistry of WAVE1 KO brain slices

The generation of WAVE1 KO animals was previously described (Soderling et al 2003). Previous analyses of the WAVE1 deficient mice indicated sensorimotor deficits, reduced anxiety levels and defects in learning and memory (Soderling et al 2003). Furthermore, previous studies showed that that WAVE-1 signaling complexes control certain aspects of neuronal morphogenesis and synaptic plasticity (Soderling et al 2007). However, most previous research has been limited to the role of WAVE1 in excitatory synapses. Based on the results described above (chapters 3.6-3.9), we used the WAVE1 KO to investigate whether WAVE1 has additional important roles at inhibitory synapses.

3.10.1 Analysis of gephyrin clustering in the cerebellum of WAVE1 KO mice

The most striking observations described in WAVE1 KO mice are the different behavioural abnormalities (Soderling et al 2003). These were shown in the rotarod, inclined-screen, and balance beam test, reflecting a disturbance of sensorimotor function and thus indicating perturbed cerebellar physiology. This association was demonstrated in mice with defects in Purkinje cells, which represent the sole synaptic output from the cerebellum (Caston et al 1995, Lalonde 1987a, Lalonde 1987b, Lalonde 1994). These observations motivated us to investigate the gephyrin clustering in WAVE1 deficient mice and to compare it with littermate controls. For this purpose, fresh frozen brain slices were prepared from 5-week-old animals and immunohistochemistry was performed as described in 2.2.4.4. The LEICA SP2 LASER scanning microscope was used to image z stacks, which were converted to a 3D model (see **Figure 19**A) using IMARIS software, and the resulting volume was analysed for size, diameter, volume and density of immunoreactive gephyrin puncta.

Figure 19A and B show a section of the cerebellum with stratum ganglionare (SG), which is characterised by the high density of Purkinje cells and the resulting high density of cell nuclei, and with stratum moleculare (SM), which consists mainly of neuropil and only very few cell nuclei. For the present analysis, the SM was selected by hand using the IMARIS volume tool and only this volume was quantified in terms of size (C), diameter (D), volume (E) and density (F) of Gephyrin puncta. In the visual comparison of WT (**Figure 19**A) and KO (**Figure 19**B), there is no noticeable difference in the Gephyrin staining, which was confirmed by quantification (**Figure 19**C-F). There is no statistically significant difference in the size (WT: 3.61 ± 0.10 μm^2; KO: 3.53 ± 0.07 μm^2), diameter (WT: 0.85 ± 0.02 µm; KO: 0.84 ± 0.01 µm), volume (WT: 0.66 ± 0.02; KO μm^3; KO: 0.64 ± 0.02 μm^3) and density (WT: 4.97 ± 0.49 puncta/100μm^3; KO: 6.13 ± 0.62 puncta/100μm^3) of the gephyrin puncta in the analysed volume between WT and KO samples. Thus, the loss of WAVE1 has no influence on the gephyrin clustering of the molecular layer of cerebellum.

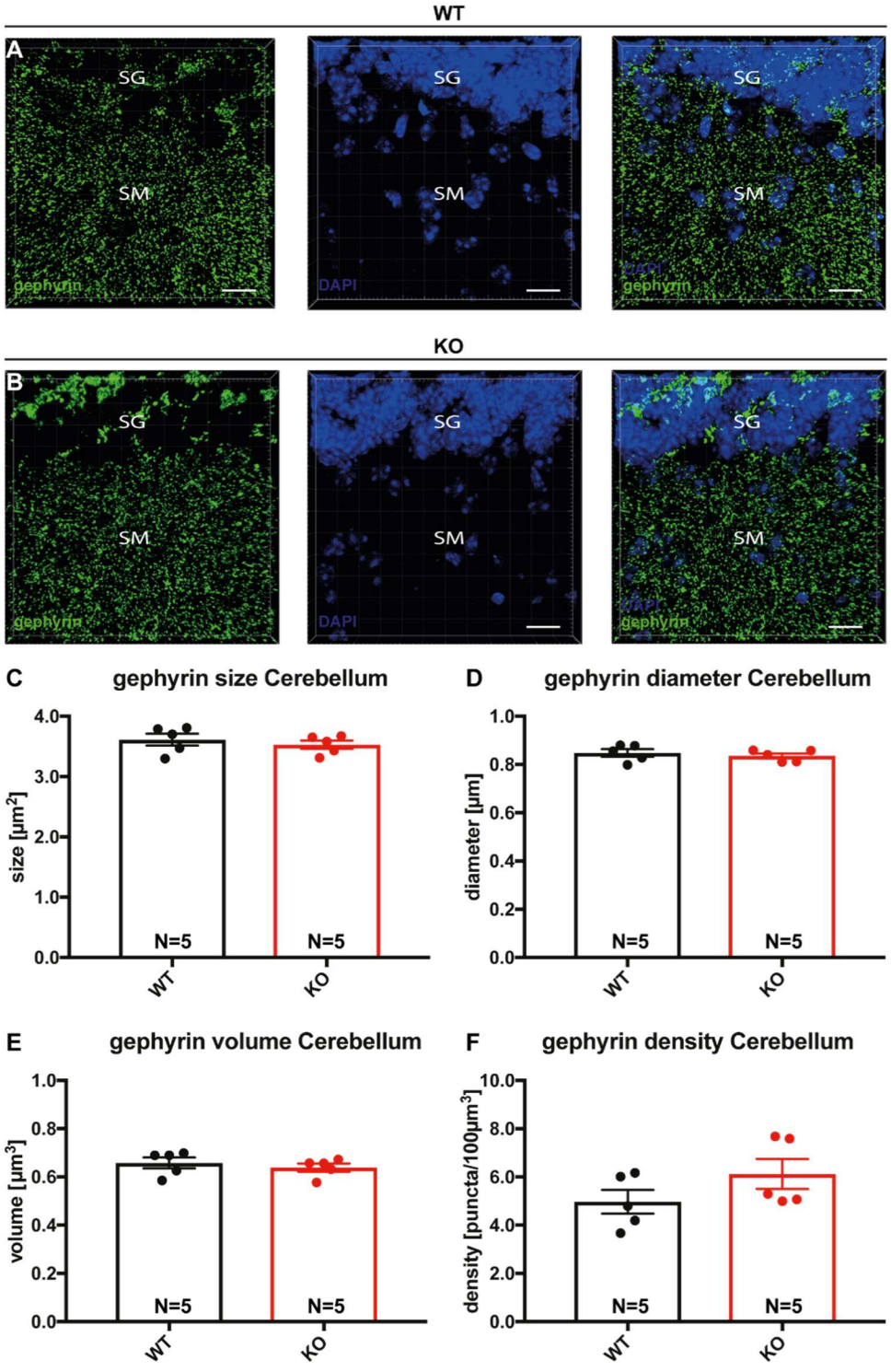

Figure 19 WAVE1-deficient mice show unchanged gephyrin clustering in the cerebellum.
*Representative 3D reconstructions of gephyrin (green) and DAPI (blue) stainings in the cerebella of WT (**A**) and WAVE1 deficient mice (**B**). Brains were fresh frozen and slices were cut, as described in 2.2.4.2. Immunohistochemistry was performed, as indicated. Z stacks were created on a confocal laser-scanning microscope and, subsequently, a 3D reconstruction was performed using IMARIS software. The quantification of the gephyrin cluster sizes (**C**), diameters (**D**) and the volume of the spots (**E**) within the captured volume was performed using the spot tool of the IMARIS software. The total number of detected spots per image was also determined, so that the spot density (**F**) could be calculated using the recorded volume. The statistical evaluation was carried out by applying the unpaired, two-tailed Student's T-test. Values represent means ± s.e.m.; Scale bars: 20 µm. N= analyzed animals (3 slices per animal)*

3.10.2 Quantification of the gephyrin immunoreactivity in the CA1 region of the hippocampus

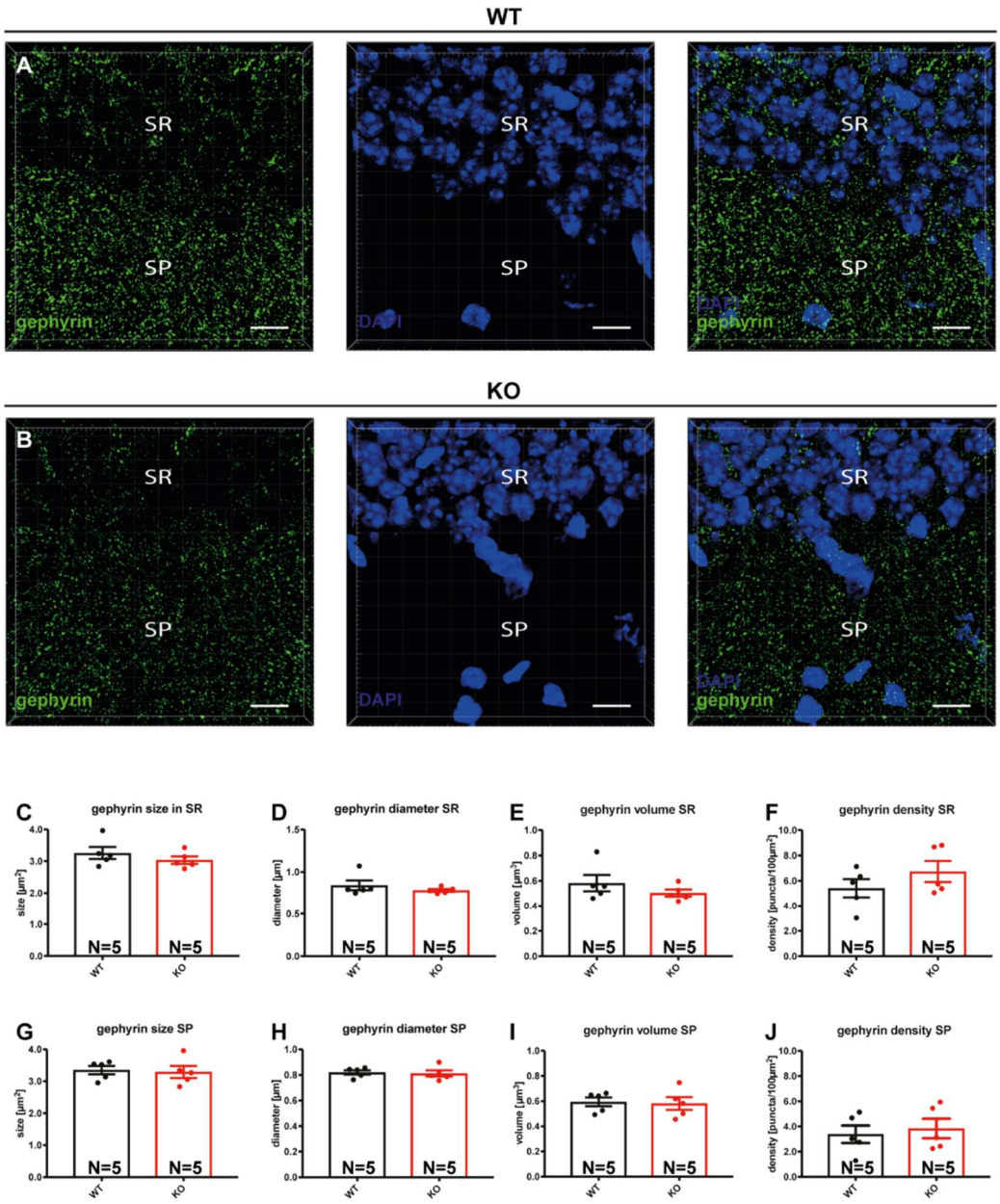

Figure 20 WAVE1-deficient mice show unchanged gephyrin clustering in the CA1 region of the hippocampus. *Representative 3D reconstructions of gephyrin (green) and DAPI (blue) stainings in the hippocampus of WT (**A**) and WAVE1 deficient mice (**B**). Immunohistochemistry was performed on brain slices, as indicated. Z stacks were generated on a confocal laser scanning microscope and a 3D reconstruction was performed using the IMARIS software. The quantification of the Gephyrin cluster sizes (**C+G**), diameters (**D+H**) and the volume of the spots (**E+I**) within the indicated volume of the stratum radiatum (**SR; C-F**) or stratum pyramidale (**SP; G-J**) was performed with the help of the spot tool of the IMARIS software. In order to be able to analyze the areas separately from each other, two separate volumes were defined by hand using the IMARIS volume tool. The total number of detected spots per brain area was also determined, whereby the spot density (**F+J**) was calculated using the volume previously defined. The statistical evaluation was carried out by applying the unpaired, two-tailed Student's T-test. Data represent means ± s.e.m.; Scale bars: 20 µm. N= analyzed animals (3 slices per animal)*

Characterisation of WAVE1-deficient mice revealed defects in learning and memory (Soderling et al 2003). The hippocampus is closely associated with these abilities (Bird & Burgess 2008, Jarrard 1993).

Therefore, we aimed to investigate whether the clustering of gephyrin is changed in the hippocampus of WAVE1 deficient mice.

A previous study indicated that the expression levels of WAVE1 vary greatly within the hippocampus. A high WAVE1 expression was shown in the CA1 region of the hippocampus, whereas the expression in the CA2 and CA3 regions is moderate to very low (Soderling et al 2003). We concluded that a possible effect would therefore manifest itself most strongly in CA1, the region with high WAVE1 expression.

A visual comparison of WT (**Figure 20**A) and WAVE1 KO sections (**Figure 20**B), indicated no obvious differences in the clustering of gephyrin between genotypes. This observation was confirmed in the quantification shown in **Figure 20**C-J. In the SR, there is no statistically significant difference in the sizes (WT: 3.26 ± 0.19 μm^2; KO: 2.90 ± 0.11 μm^2), diameters (WT: 0.84 ± 0.06 µm; KO: 0.78 ± 0.02 µm), volumes (WT: 0.582 ± 0.06 μm^3; KO: 0.50 ± 0.03 μm^3) and densities (WT: 5.41 ± 0.72 puncta/100 μm^3; KO: 6.74 ± 0.83 puncta/100 μm^3) of the gephyrin puncta in the analysed volumes. In addition, in the SP, no difference in sizes (WT: 3.35 ± 0.08 μm^2; KO: 3.29 ± 0.11 μm^2), diameters (WT: 0.82 ± 0.01 µm; KO: 0.81 ± 0.01 µm), volumes (WT: 0.59 ± 0.02 μm^3; KO: 0.58 ± 0.03 μm^3) and densities (WT: 3.38 ± 0.40 puncta/100μm^3; KO: 3.84 ± 0.45 puncta/100 μm^3) of the gephyrin puncta could be detected. Thus, the loss of WAVE1 has no effect on gephyrin clustering in the CA1 region of the hippocampus.

3.10.3 Quantification of gephyrin clustering in PV+ interneurons in the CA1 region of the Hippocampus

As described above, no significant differences in gephyrin clustering were detected in the CA1 region of the hippocampus of WAVE1 KO mice, as compared to the WT littermates. However, a closer inspection of the immunostainings in the sections of WAVE1-deficient mice indicated characteristic patterns of high-density gephyrin clustering in certain areas of the hippocampal CA1, which were not as evident in the corresponding areas of WT littermates. We therefore suspected that certain neuronal subpopulations within the hippocampal CA1 area of WAVE1 KOs might be affected with regard to clustering of gephyrin. Based on their topology and their immunolabeling pattern, we assumed that the neurons indicating increased gephyrin clustering in WAVE1 KO brains might be interneurons. A typical interneuronal subpopulation for the areas studied here are PV+ interneurons (Kosaka et al 1987, Nomura et al 1997). Therefore, we analysed the gephyrin clustering in PV+ interneurons of the CA1 region of the hippocampus. In order to optimize our staining conditions for the immunolabeling of PV+ cells, brains of 5 weeks old animals were first incubated overnight in a 4% PFA solution and, subsequently, immunohistochemistry was performed by using the sodium citrate treatment, as described in 2.2.4.5. Finally, gephyrin immunoreactive puncta in PV+ interneurons were quantified, as shown in **Figure 21** (C-F).

Our immunohistochemical analysis indicated that in PV+ CA1 cells of WAVE1-deficient mice, the densities of gephyrin puncta were increased, as compared to WT controls (control: 0.95 ± 0.13 puncta/100μm^3; WAVE1 KO: 2.21 ± 0.33 puncta/100 μm^3). In contrast, the sizes of gephyrin puncta (control: 1.01 ± 0.06 μm^2; WAVE1 KO: 0.82 ± 0.06 μm^2) and their diameters (control: 1.01 ± 0.03 µm; WAVE1 KO: 0.9 µm ± 0.03 µm) were significantly reduced, compared to controls

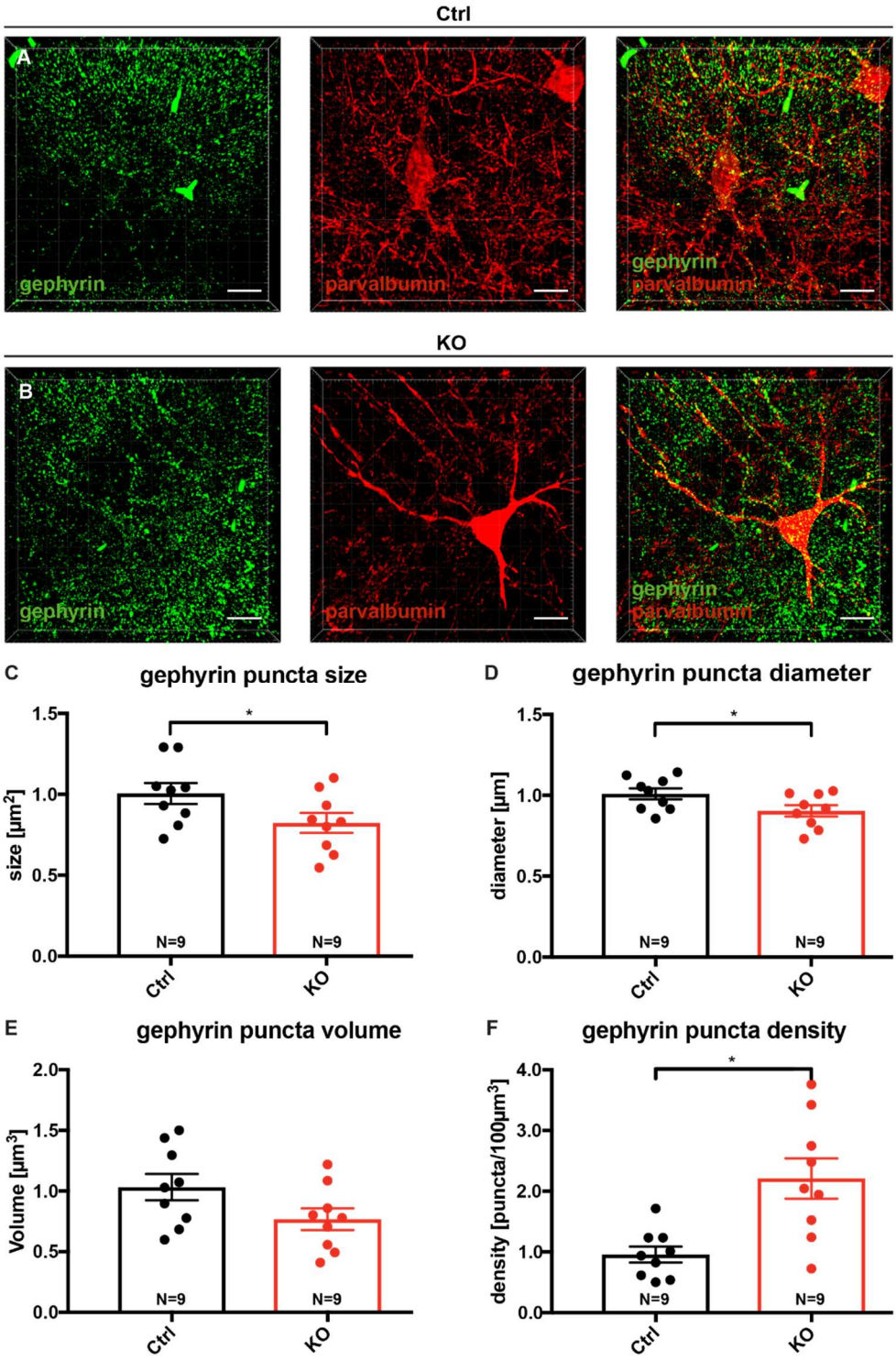

Figure 21 WAVE1-deficient mice show significant changes in the clustering of gephyrin in PV+ interneurons of the hippocampal CA1 area.

*Representative 3D reconstructions of gephyrin (green) and PV (red) stainings in the CA1 hippocampal area of control (**Ctrl; A**) and WAVE1 deficient mice (**KO; B**). Brain slices were immunostained, as indicated. Z stacks were generated using a confocal laser scanning microscope and 3D reconstruction was performed using the IMARIS software. Quantification of gephyrin cluster sizes (**C**), diameters (**D**) and volumes of spots (**E**) in PV+ neurons was performed using the spot tool of the IMARIS software. Areas of PV-immunoreactivitiy were selected manually with the help of the IMARIS volume tool. The total number of detected spots per brain area was also determined, whereby the spot density (**F**) could be calculated using the previously defined volume. The statistical evaluation was carried out by applying the unpaired, two-tailed Student's T-test. $p<0.05$*; Values represent means ± s.e.m. Scale Bars: 20 µm. N= analyzed animals (3 slices per animal)*

In order to investigate whether the increase in the densities of gephyrin puncta was paralleled by an equivalent increase in the synaptic localization of gephyrin, parallel sections were co-stained with antibodies against gephyrin and the presynaptic marker vesicular inhibitory amino acid transporter (VIAAT) (Todd & Sullivan 1990, Wojcik et al 2006) and analysed using IMARIS, as described 2.2.4.8 (see Figure 22A-D).

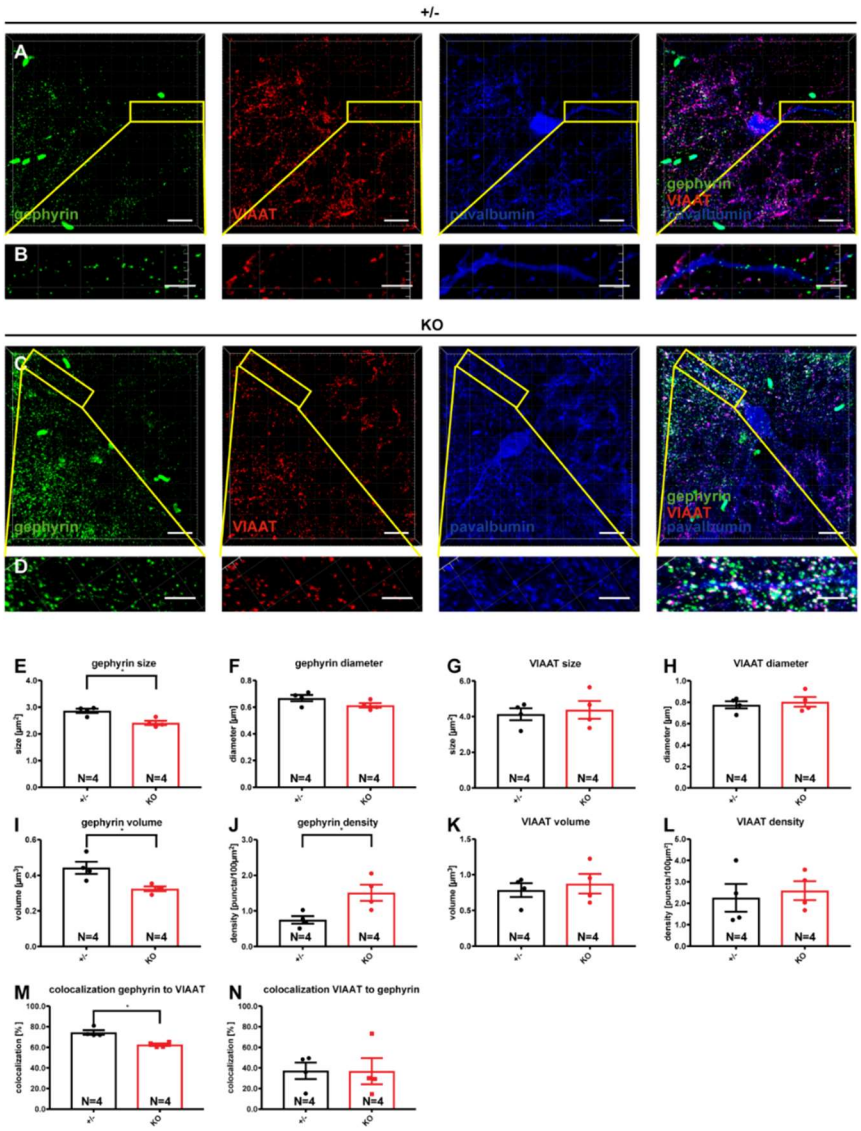

Figure 22 The increase in the density of gephyrin puncta in PV+ WAVE1 KO cells is accompanied by an increase in non-synaptic gephyrin.

*Representative 3D reconstructions of gephyrin (green), VIAAT (red) and PV (blue) stainings in the CA1 hippocampal area in the brains of heterozygous control (**A+B**) and WAVE1 KO mice (**C+D**). Panels in A and C show the entire field of view. The yellow rectangles indicate the areas of magnification shown in the corresponding panels in B and D. Brain slices of PFA-fixed brains were prepared, followed by immunohistochemistry, as indicated. Z stacks were generated by using a confocal laser scanning microscope and a 3D reconstruction was performed using the IMARIS software. Quantification of gephyrin puncta sizes (**E**), diameters (**F**) and volume of spots (**I**) in the dendrites of PV-positive interneurons was performed using the spot tool of IMARIS software. The same principle was used to quantify the sized of VIAAT puncta (**G**), as well as the corresponding diameters (**H**) and the volume of the spots (**K**). Dendrites of PV-positive interneurons were selected by hand using the IMARIS volume tool. The total numbers of detected spots per channel was also determined, whereby the densities of the gephyrin puncta (**J**) and VIAAT puncta (**L**) were calculated in the same selected volumes. Using the Colocalize Spot tool of the IMARIS software, the colocalization of the defined gephyrin (**M**) and VIAAT (**N**) was determined. The statistical evaluation was carried out by applying the unpaired, two-tailed Student's T-test. p<0.05 *; Values represent means ± s.e.m.; Scale Bars: 20µm. N= analyzed animals (3 slices per animal)*

In addition, the colocalization tool of IMARIS was used to determine the percentages of gephyrin immunoreactive puncta that were co-localizing with VIAAT puncta (**Figure 22**M, N).

The results shown in **Figure 22** indicated similar significant differences in the densities and sizes of gephyrin immunoreactive puncta in PV+ interneurons between WAVE1 KO and heterozygous controls, as those described between WAVE1 KO and their WT littermates (compare quantifications in **Figure 22** with quantifications in **Figure 21**). Accordingly, a significant reduction in the gephyrin puncta sizes in WAVE1 KO was detected, as compared to heterozygous controls (**Figure 22**E, control: 2.83 ± 0.08 μm^2vs WAVE1 KO: 2.41 ± 0.08 μm^2). Similarly, a reduction in the volume of gephyrin puncta was detected in WAVE1 KO mice (0.32 ± 0.01 μm^3), compared to the heterozygous controls (0.41 ± 0.03 μm^3). Furthermore, consistent with the results obtained by comparing WAVE1 KOs with WT controls, a significant increase in the densities of gephyrin puncta in WAVE1 deficient mice (1.51 ± 0.23 puncta/100μm^3) was detected, compared to the heterozygous animals (0.83 ± 0.11 puncta/100μm^3). However, the determined diameter of the gephyrin puncta remained unchanged between WAVE1 KOs and their heterozygous littermates (heterozygous controls: 0.65 ± 0.02 µm; WAVE1 KO: 0.61 ± 0.02 µm). Together, our comparative analyses of WAVE1 KOs with either their WT (Figure 17) or their heterozygous (**Figure 22**) littermates revealed similar changes, indicating that heterozygous mice are phenotypically indistinguishable from their WT littermates in gephyrin clustering.

Based on these results, we concluded that in the quantifications of the percentages of gephyrin immunoreactive puncta co-localized with VIAAT puncta, heterozygous mice can be used as WT-like controls. Dendrites of PV+ interneurons were manually selected and the IMARIS spot tool was used for the analysis. No statistically significant differences was found in the VIAAT puncta sizes (controls: 4.44 ± 0.33 μm^2 vs WAVE1 KO: 4.38 ± 0.50 μm^2), diameters (controls: 0.81 ± 0.03 µm vs WAVE1 KO: 0.80 ± 0.05 µm), volumes (controls: 0.88 ± 0.10 μm^3vs WAVE1 KO: 0.87 ± 0.14 μm^3), or the VIAAT puncta densities (control: 2.19 ± 0.65 puncta/100μm^3 vs WAVE1 KO: 2.59 ± 0.44 puncta/100μm^3). Thus, our results indicate that the immunoreactivities of the synaptic marker VIAAT are similar between genotypes.

Next, we determined the percentages of gephyrin immunoreactive puncta colocalized with VIAAT and, *vice versa*, the percentages of VIAAT puncta colocalized with gephyrin puncta. Since the quantifications of VIAAT and gephyrin referred to the same dendritic structures, the spots obtained in this way are analysed for colocalization using the "colocalize Spot Tool" of the IMARIS software. Here, no significant differences in the percentages of VIAAT puncta colocalized with gephyrin were detected between genotypes (**Figure 22**N; control: 44.61 ± 7.99 % vs WAVE1 KO: 36.88 ± 12.70 %). In contrast, the percentages of gephyrin puncta colocalized with VIAAT puncta were significantly reduced in WAVE1 KOs, as compared to controls (Figure 18 M; control: 75.34 ± 2.18 % vs WAVE1 KO: 62.61 ± 1.20 %). Together, the results shown in Figures 17 and 18 indicate, that the increase in the gephyrin clustering observed in PV+ interneurons located in the CA1 hippocampal area of WAVE1 KO animals reflects an increase in the percentage of the total gephyrin immunoreactive puncta localized at extrasynaptic sites.

4 Discussion

4.1 Candidates of the 2-3 kb cDNA library screen

4.1.1 WAVE1

WAVE1 belongs to the WASP (Wiskott-Aldrich syndrome protein) family of scaffolding proteins. It is one of many regulatory proteins involved in actin nucleation and lamellipodia formation (Miki & Takenawa 1998, Nozumi et al 2003). The pentameric protein complex WRC (WAVE Regulatory Complex) binds to the Scar homology domain (SHD) of WAVE1, leading to inhibition of its activity (Eden et al 2002). Interaction with the small Rho-like GTPase Rac1 leads to dissociation of WRC and, subsequently, to activation of WAVE1. Active WAVE1 directly binds and activates the Arp2/3 complex, thereby leading to Arp2/3 mediated actin nucleation (Bear et al 1998, Machesky et al 1999). In addition, WAVE1 binds, via its verprolin homology domain and a proline-rich domain, to G-actin monomers and profilin (Miki & Takenawa 1998). Notably, all members of the WAVE family (WAVE1-3), have basal actin nucleation activity (Machesky et al 1999). In contrast to the homologous WASP protein, the WAVE1-3 proteins have an N-terminal WAVE homology domain (WHD) instead of a GTPase binding domain (GBD) (Bear et al 1998). Furthermore, the proline-rich domain has been shown to contain numerous recognition sites for SH3 domains, including the Ableson tyrosine kinase (Abl) and the WAVE-associated Rac GTPase activating protein (GAP) called WRP [also known as MEGAP (mental disorder-associated GAP)/SrGAP3 (SLIT-ROBO Rho GTPase activating protein 3)] [(Soderling et al 2002, Westphal et al 2000)]; see Figure 23)]

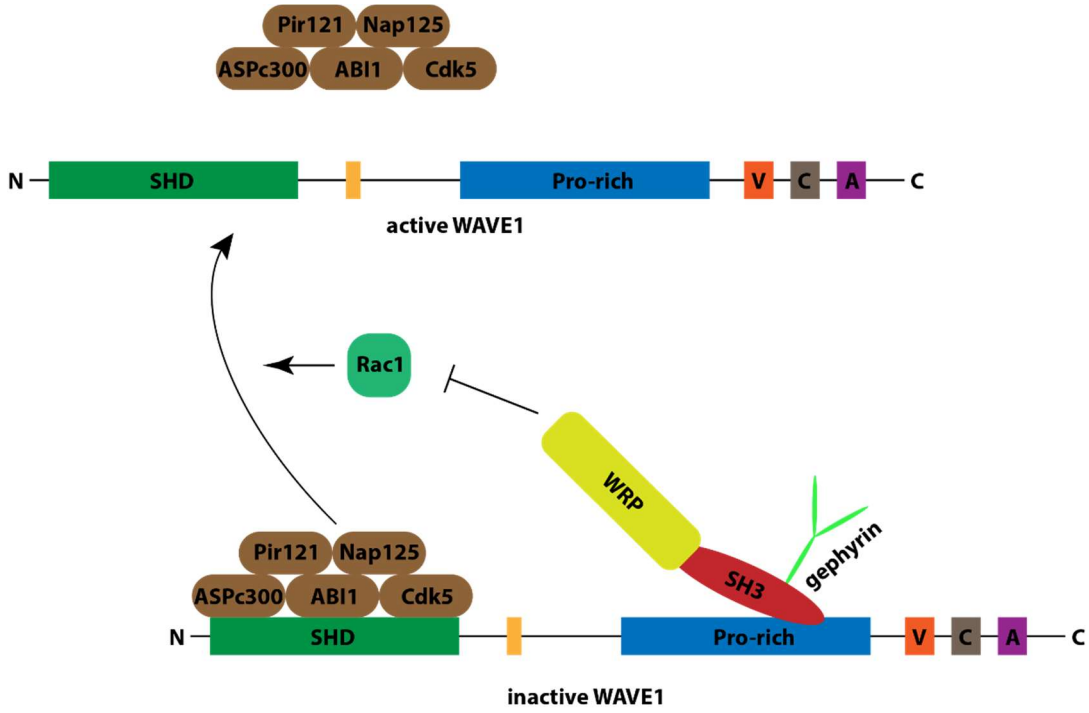

Figure 23 The WRP/Rac1/WAVE1 interaction model
For details see main text. Abbreviations: SHD, Scar homology domain; Pro-rich, proline rich region; V, verprolin homology; C, cofilin homology; A, acidic region.

Previous studies indicated that WAVE1 KO mice showed deficits in sensorimotor functions and performed poorly in cognitive tests (Soderling et al 2003). Patients with mental retardation of the 3p syndrome show analogous sensorimotor and cognitive deficits (Endris et al 2002). In those patients, a haploinsufficiency for WRP/MEGAP, a component of the WAVE-1 signaling network, could be detected (Endris et al 2002). In addition, WAVE1-deficient mice show altered neuronal growth cone dynamics and morphology, as well as altered spine densities and abnormal synaptic plasticity (Soderling et al 2007).

4.1.1.1 WAVE1 does not interact directly with gephyrin

As mentioned above, the Rac1-specific GTPase activating protein WRP is capable of binding directly, via its SH3 domain, to a proline-rich region of WAVE1. This interactions leads to the inhibition of the Rac1 activity [(Soderling et al 2002); **Figure 23**]. More recently, it was shown that WRP also binds to gephyrin via its SH3 domain and that the WRP-gephyrin interaction facilitates the clustering of gephyrin and $GABA_A$Rs at inhibitory postsynaptic sites (Okada et al. 2011). Thus, one of the aims of the current work was to elucidate the role of WAVE1 in the formation and stabilisation of the gephyrin scaffold at inhibitory synapses. In order to study whether gephyrin interacts directly with WAVE1, we performed *in vitro* binding assays. As a *proof-of-principle*, our binding assays (see **Figure 18**) confirmed the previously described direct interaction between WRP and WAVE1 (Soderling et al 2002). In contrast, no direct interaction between gephyrin and WAVE1 could be shown in our assays. This indicates that the phenotypic change in GFP-gephyrin distribution (i.e. from large intracellular aggregates into numerous microclusters) observed in our cell-based assay upon WAVE1 overexpression was not due to a direct interaction between gephyrin and WAVE1. Taking into account that WAVE1 is an actin-regulatory protein, and that overexpression of β-actin induces a similar redistribution of GFP-gephyrin into microclusters in our cell-based assay, our results together indicate that actin-cytoskeleton dynamics play a crucial role in gephyrin clustering.

4.1.1.2 WAVE1 interacts directly with CB

Previous studies indicated that the SH3 domain of WRP interacts directly with both WAVE1 (Soderling et al 2002) and gephyrin (Okada et al. 2011). In addition, unpublished work indicates that the SH3 domain of CB interacts directly with gephyrin (Dr. Theofilos Papadopoulos, personal communication). This prompted us to investigate whether the SH3 domain of CB is also capable of interacting directly with WAVE1. The *in vitro* binding assays performed in this study clearly show a direct and specific interaction between WAVE1 and the SH3 domain of CB (see **Figure 16**). In our *in vitro* binding assays, WAVE1 was first expressed in bacteria using a pGEX-4T-1 vector and purified as a GST-tagged protein. The purified protein contains a thrombin cleavage site that served to remove the GST tag upstream of the ATG start codon of WAVE1, thus allowing the isolation of an unlabeled WAVE1. This cleavage by the protease is non-specific and also resulted in fragmentation of WAVE1 in these experiments, which was observed in the immunoblots shown in **Figure 16** using a specific WAVE1 antibody. For a more detailed analysis of the WAVE1 amino acid sequences that directly bind to CB, a mass spectrometric analysis of the generated fragments was performed in collaboration with Dr. Olaf Jahn (Dept. of Neuroproteomics, Max Planck Institute for Experimental Medicine, Göttingen). This revealed that both the 80 kD and 50

kD fragments of WAVE1 detected with the full-length CB_{SH3+} or the isolated SH3 domain of CB contain proline-rich regions within the following sequences of the WAVE1 protein: 316-TPVFVSPTPPPPPLPSALSTSSLR-341 and 421-QGLPPPPPPL-431 (see Figure 17). Notably, a previous study indicated that deletion of these two sequences in mice led to effects implying that signal transduction through WAVE1 complexes is essential for neuronal plasticity and cognitive behavior (Soderling et al 2002). This raises the question of how the interactions of WAVE1 with the SH3 domains are regulated by both WRP and CB to promote the formation of the inhibitory postsynaptic scaffold. Here, additional work will be required to clarify the roles of WAVE1 in the formation of inhibitory synapses.

Furthermore, our *in vitro* binding assays and the mass spectrometric analysis also indicated that WAVE1 may have an additional, N-terminal, binding site for the full-length SH3 domain-containing CB. While the SH3 domain of CB alone binds to numerous fragments of WAVE1, CB_{+SH3} binds mainly to WAVE1 full length, suggesting that an additional binding site in the N-terminus of WAVE1, which is missing in the truncated WAVE1-proteins, may act synergistically in stabilizing the interaction of WAVE1 with the full-length CB. Here, additional studies are required to clarify whether the WAVE1-CB interaction is stabilized by a second binding site located in the N-terminus of WAVE1.

4.1.1.3 WAVE1 deficiency affects gephyrin clustering in PV+ interneurons of the CA1 hippocampal area

In the present study, the effect of WAVE1 deficiency on gephyrin clustering was investigated in the cerebellum and in the CA1 region of the hippocampus of WAVE1 KO mice, as compared to control littermates. To this aim, slices derived from brains of 5 weeks old mice were prepared, and immunohistochemistry, confocal microscopy, 3D-reconstruction and image-analysis were performed as described in materials and methods. Our results indicated no differences in gephyrin clustering between genotypes in both, the SR and the SP of the CA1 region of the hippocampus. Similarly, no differences in gephyrin clustering in the SM of the cerebellum were observed between WAVE1 KOs and controls. In contrast, clear differences in gephyrin clustering were found in PV+ interneurons of the CA1 region of the hippocampus. The significantly increased densities of gephyrin clusters in PV+ interneurons of WAVE1 KO brains, in combination with a significant reduction in their apparent mean sizes and their apposition to the presynaptic marker VIAAT, as compared to controls, indicates a role of WAVE1 in regulating the strength of the inhibitory postsynaptic scaffold. Thus, we here provide first evidence that WAVE1 acts as a regulator of gephyrin clustering in PV+ interneurons of the CA1 hippocampal area. The reasons for this highly specific effect of WAVE1 on the clustering of gephyrin in PV+ interneurons are currently unknown, but may be due to morphological and functional differences between neuronal subpopulations. In contrast to the CA1 glutamatergic neurons, CA1 GABAergic cells lack dendritic spines or are sparsely spiny, but many excitatory synapses form on the dendritic shaft. Particularly, CA1 PV+ cells receive 10-fold more excitatory than inhibitory inputs (Gulyas et al 1999). These anatomical differences between CA1 glutamatergic neurons and GABAergic interneurons may indicate distinct roles of WAVE1 in the formation of excitatory versus inhibitory synapses in those two cell types.

4.1.1.4 No changes in WAVE2 and WAVE3 expression levels in hippocampal neurons derived from WAVE1 deficient mice

In addition to WAVE1, the WAVE gene family includes two other members, WAVE2 and WAVE3, but all have a similar domain organization and comparable roles in actin polymerization and cytoskeleton remodeling processes (Soderling & Scott 2006). Furthermore, all three human WAVE genes, as well as their mouse orthologues, have been shown to be expressed in the brain (Sossey-Alaoui et al 2003). In addition, the expression of the various proteins in the cortex and hippocampus was shown to be unchanged across WAVE1 genotypes (WT, +/-, KO) (Dahl et al 2003). In line with those previous studies, our analyses using cultured hippocampal neurons derived from WAVE1 KO mice, revealed no changes in the expression levels of WAVE2 and WAVE3, as compared to controls. For this purpose, the WT, or KO neurons, were cultured, as described in materials and methods, lysed at DIV 14 and the lysates were used for Western blot analysis. (see **Figure 14**). No differences in the protein levels of WAVE2 and WAVE3 were found in hippocampal KO neurons, as compared to littermate controls. In line with previous studies (Dahl et al. 2003) our results show that WAVE1 deficiency has no effect on the WAVE2 or WAVE3 protein levels.

Interestingly, our experiments indicate that co-expression of GFP-gephyrin with either WAVE2 or WAVE3 (kindly provided by Dr. Laura Matchesky, University of Glasgow) in COS-7 cells also leads to a redistribution of GFP-gephyrin into microclusters (see **Figure 13**), similarly to that observed upon WAVE1 expression. Thus, WAVE2 and/or WAVE3 may compensate the loss of WAVE1 in certain neuronal subtypes or brain regions. Accordingly, immunohistochemical analyses of CA1 in the hippocampus of WAVE1 KO mice revealed changes in gephyrin clustering in PV+ interneurons (see **Figure 21**), but not glutamatergic neurons (see **Figure 20**). Here, future studies are required to clarify whether the unchanged gephyrin clustering in glutamatergic cells of the hippocampus and cortex of WAVE1 KO mice is due to compensation by WAVE2 or WAVE3.

4.1.2 β-actin

The efficiency of synaptic transmission depends, among other parameters, on the concentration of the corresponding receptors at the postsynaptic membrane (Patrizio & Specht 2016). The anchoring of the receptors to the subsynaptic cytoskeleton, which is composed of actin, tubulin and intermediate filaments, plays an important role in the efficiency of signal transmission (Kneussel & Loebrich 2007). Previous biochemical and cell biological studies have shown that gephyrin binds to polymerized tubulin with high affinity (Kirsch et al 1991), and that depolymerization of the microtubule network by demecolcin destroys the synaptic localization of gephyrin and the GlyRs in spinal cord cultures (Kirsch & Betz 1995, Kirsch et al 1991). Furthermore, binding of the microtubule motor protein Dlc-1/-2 to gephyrin in the region of amino acids 181-243 was demonstrated (Fuhrmann et al 2002). Deletion of the binding motif in the gephyrin sequence led to a loss of interaction between the two proteins (Fuhrmann et al 2002). The complex formation of gephyrin and Dlc-1/-2 leads to the assumption that Dlc-containing motor protein complexes possibly regulate the transport and subcellular localization of gephyrin (Fuhrmann et al 2002).

On the question of the nature of the interaction, as well as the role of the interaction between gephyrin and the actin cytoskeleton, there are different reports in the literature. On the one hand, it has been previously shown, that incubation of cultured cortical neurons with the alkaloid cytochalasin D, which depolymerizes the actin cytoskeleton, leads to a reduction in the number and size of

postsynaptic gephyrin clusters, whereas the remaining clusters have a significantly higher density (Kirsch & Betz 1995). This is thought to be an antagonistic effect of microfilaments and microtubules on the packing density of gephyrin in the postsynaptic side. Contrary to this study, no influence of F-actin or microtubule structures on gephyrin clustering was detected in hippocampal primary cultures (Allison et al 2000). The different results of the two studies may be due to the different synaptic composition or different differentiation stages of the test systems used (Allison et al 2000, Bausen et al 2006, Kirsch & Betz 1995). Nevertheless, no direct interaction between gephyrin and the actin cytoskeleton has been detected so far.

The identification of β-actin in the unbiased cDNA library screen performed here, whose analysis is based on the redistribution of gephyrin into microclusters, does not indicate a possible direct interaction of β-actin and gephyrin (see WAVE1 and gephyrin interaction **Figure 18**), but underlines the importance of the cytoskeleton in the clustering of gephyrin. This is further supported by the identification of WAVE1 in the same cDNA library screen, a regulator of the actin cytoskeleton.

4.2 The identified candidate-proteins from the 3-4 kb cDNA library screen

4.2.1 The β-subunit of the glycine receptor

The direct and highly-specific interaction between GlyRβ and gephyrin was previously described (Pfeiffer et al 1982). GlyRs are inhibitory receptors and belong to the Cys-loop superfamily, which also includes acetylcholine, serotonin and $GABA_AR$ (Schaefer et al 2018). The binding of glycine to the receptor opens the Cl-selective pore, whereas strychnine acts as an antagonist and thus leads to an inhibition of the channel (Becker et al 1988, Young & Snyder 1973). The functional channel is composed of 5 subunits. A heteropentamer is formed from α (1-4) and β subunits. All subunits have 4 transmembrane domains, whereby the N- and C-terminus are located extracellularly. The α subunits show a high sequence similarity of more than 80%, whereas the β subunit has only a low homology of less than 50% compared to the α subunits (Betz & Laube 2006). Later, it could be shown that a heteropentamer is composed of two α and three β subunits (Grudzinska et al 2005). The α subunit seems to be necessary for the formation of functional channels, since functional homopentamers from β subunits could not be documented (Grudzinska et al 2005). However, it has been shown that the β subunit can be localized in the membrane in a way that is not dependent on the α subunit (Oertel et al 2007). Although a broad expression of the β subunit takes place in the embryonic and adult central nervous system (Malosio et al 1991), the proteins could be detected to a lesser extent using antibodies (Weltzien et al 2012). The detection of GlyRβ was only possible in GlyR positive synapses, so it was hypothesized that in the cells where GlyRβ mRNA but no protein could be detected, the absence of GlyRα leads to a degradation of GlyRβ in ER (Weltzien et al 2012). Dominant in adult GlyR heteropentamers is the α1 subunit, whereas the α2 subunit is expressed almost exclusively in isolated cortical regions (Hoch et al 1989, Langosch et al 1988). In contrast, this subunit is expressed more strongly in the embryonic and perinatal phase of the brain (Hoch et al 1989). In the spinal cord and brain stem of postnatal stages, an accumulation of the α3 subunit can be seen (Malosio et al 1991). Besides the fact that the α4 subunit is present in GlyR in the embryonic sympathetic nervous system, this subunit is largely unexplored (Harvey et al 2000, Laube et al 2002, Malosio et al 1991).

Identifying a protein in this screen, which interaction with gephyrin is already known and very well characterized shows the reliability and functionality of the applied system with the used cDNA library.

4.2.1.1 GlyRβ-induced gephyrin microclusters are localized at the plasma membrane

As described in the previous section, the interaction of gephyrin with GlyRβ is already described in the literature (Pfeiffer et al 1982). Furthermore, previous experiments in HEK cells, in which gephyrin and GlyRβ were cotransfected, indicated that GlyRβ-gephyrin complexes accumulate in intracellular compartments such as the Golgi apparatus or endoplasmic reticulum (Kirsch & Betz 1995). In these experiments, no submembranous microclusters of gephyrin could be detected. This is in contrast to the results shown in this work. In the experimental set-up used here, it was possible to produce a redistribution of GFP-gephyrin into microclusters upon GlyRβ overexpression (see **Figure 8**). Intrigued by this finding, we were highly motivated to further examine the localization of both the GlyRβ-induced GFP-gephyrin microclusters within the cell.

In order to investigate the subcellular localization of GFP-gephyrin microclusters, the cells were simultaneously transfected with IgSF9b, a plasma membrane marker. This brain specific member of the immunoglobulin superfamily member 9 family can bind indirectly to NL2 via interaction with S-SCAM and thus play a role in the regulation of inhibitory synapses (Krueger-Burg et al 2017, Woo et al 2013). The confocal images captured upon co-transfecting Flp-In T-Rex-GFP-gephyrin HEK 293 cells with GlyRβ and IgSF9b, followed by induction of GFP-gephyrin expression, clearly showed that the majority of GlyRβ-induced GFP-gephyrin microclusters are localized at the plasma membrane (see **Figure 9**). A possible reason for the GlyRβ-induced formation of submembranous GFP-gephyrin microclusters observed in our experiments, which is in contrast to the previously published literature, may be the order of expression of GlyRβ and GFP-gephyrin. In previous experiments (Kirsch et al 1995), GlyRβ and GFP-gephyrin were co-transfected and thus expressed simultaneously. In the experimental set-up used here, GlyRβ was first expressed and 24 h later GFP-gephyrin expression was induced by TET treatment. This suggests that the later expression of GFP-gephyrin could lead to the interaction between GlyRβ and gephyrin in a different compartment and thus to a different final localization. To investigate this, an experiment was performed by initiating GFP-gephyrin expression simultaneously with GlyRβ transfection. However, this approach showed that only a few microclusters formed compared to the cells in which GFP-gephyrin expression was initiated 24 h after transfection (data not shown). This result is in line with our assumption that when both proteins are expressed at the same time, they are processed differently, leading to a co-localization of both proteins in intracellular aggregates. Accordingly, posttranslational modifications of GlyRβ upon its single-expression in HEK cells, may be the reason for the submembranous redistribution of inducibly-expressed GFP-gephyrin in cells. For example, GlyRβ has two extracellular glycosylation sites (Oertel et al 2007), which could account for the phenomenon observed here. Additional studies will be required to clarify this point.

In order to investigate this observed phenomenon in more detail, further approaches would have to be pursued, including optimization of expression of different plasma membrane and endomembrane markers, in order to make a more optimal statement regarding the localization. As can be seen in the described results of **Figure 9**, IgSF9b only forms patches in the plasma membrane. Establishing a cell membrane marker that stains the entire membrane evenly and continuously would lead to an increase in quality and a better statement regarding colocalization.

Motivated by our result, that GlyRβ induces formation of submembranous GFP-gephyrin microclusters, we were interested in investigating the subcellular localisation of exogenously expressed GlyRβ in more detail. To this aim, a GlyRβ variant was cloned that has a C-terminal HA-tag. Upon overexpression of GlyRβ-HA, the cells were fixed with PFA as before, but permeabilization was omitted. The C-terminal HA tag is located extracellularly. Thus, it was possible to perform immunolabeling of the HA-tag in order to prove GlyRβ plasma membrane-expression (see **Figure 10**). Cells surface expression of GlyR-β, when expressed alone in COS-7 cells, was also previously reported (Oertel et al 2007). Taken together, our results confirmed that exogenously expressed GlyRβ reaches the plasma membrane in the absence of GlyRα subunits, where it co-localized with GFP-gephyrin microclusters. Thus, our results provide evidence that GlyRβ expressed in the forebrain in the absence of GlyRα subunits may trigger

the formation of a gephyrin network in a subset of inhibitory postsynapses independently of CB. Further experiments are required to clarify this.

4.2.1.2 Generation of a GlyRβ conditional KO mouse line

The results mentioned above motivated us to closer investigate the role of GlyRβ in the development of the inhibitory synapses, and particularly its role in the assembly of the gephyrin postsynaptic scaffold. So far, a GlyRβ KO mouse line has not been described in the literature. However, it has been shown that the recessive mutation spastic (spa)in the β subunit of GlyRs, is associated with a GlyR deficit (Becker et al 1986). In this context, it was previously shown that only the adult form of GlyR is affected by the mutation, which is composed of the α1 and β subunit (Becker et al 1992, Pfeiffer et al 1982). The affected mice do not show any abnormalities at birth, whereas they develop tremors and muscle stiffness from about two weeks onwards. This seems to be the time when the switch from neonatal to adult GlyR takes place. As described above, the postnatal GlyR contains α1 and β subunits, whereas the neonatal GlyR contains a homooligomer of α2 subunits (Becker et al 1988). The described mutation has no effect on the α1 subunit of the postnatal GlyR, whereas the gene for the β subunit has an intronic insertion of an L1 transposable element and leads to the phenotype (Mulhardt et al 1994). This results in a defective mRNA, which is incorrectly spliced and subsequently degraded, leading to a reduction of the GlyR level in the mutant animals (Mulhardt et al 1994). Mutations of the α1 and β subunits have also been found in humans and are associated with hyperekplexia. These results may indicate that not only structural integrity is dependent on the β subunit, but that it may also play a role in inhibitory signaling (Rees et al 2002).

In order to investigate the role of GlyRβ in more detail, we generated a conditional KO mouse line using CRISPR/Cas9. To this aim, two guide RNAs were used to flank exons 8 and 9 with loxP sites (see Figure 11) and thus enable conditional KO of the gene upon mating this line with different Cre-expressing mouse lines. These exons encode half of TMD2, all of TMD3 and part of the intracellular Cys loop of GlyRβ, which we predict to result in the loss of the GlyRβ protein upon Cre-mediated recombination, similarly to a previously described targeting strategy for generating a GlyRα3 KO mouse (Harvey et al 2004b). Successful generation of the +/fl mouse line and later generations with the fl/fl genotype was verified by PCR. In order to confirm Cre-mediated recombination of the "floxed" locus in mice, fl/+ animals were crossed with the EIIα-Cre general deleter line, in which the Cre-recombinase is active at the zygote state of embryonic development (Lakso et al 1996). Again, verification by PCR was successful. Furthermore, +/- EIIα-Cre-negative animals were mated with C57Bl6/J animals, and genotyping of the progeny revealed successful germline transmission. Furthermore, GLRB +/fl, fl/fl and +/- animals are viable and fertile and showed no phenotypic abnormalities. These mice can be used in future studies in order to investigate the functional roles of GlyRβ in different regions of the mouse brain.

4.2.1.3 Generation of GlyRβ-HA KI mouse line (GLRBHA)

For the generation of the GLRBHJA line, two gRNAs were again used to modify the locus of the GlyRβ gene using a HDR fragment to introduce loxP sites into the regions upstream of exon 10 and downstream of the coding sequence and to replace the stop codon with the coding sequence of the

HA-tag and a stop codon. Based on the experiments described above (see 4.2.1.1), the decision was made to introduce a C-terminal HA tag.

An initial PCR-based screen for homologous recombination in mice revealed the absence of the loxP site upstream of exon 10 in the KI allele (see **Figure 12**). In contrast, the presence of the HA tag and the second loxP site in the KI allele was verified by PCR genotyping (see **Figure 12**). In addition, Western blot analyses of brain lysates from homozygous (hom) GLRB-HA mice and their WT littermates using an HA antibody verified the expression of a 58-60 kD protein in samples from GLRB-HA brains but not in those from WT brains (see **Figure 12**). The size of this protein corresponds to a full-length HA-tagged version of the GlyRβ protein (Weltzien et al 2012). Again, homozygous and heterozygous GLRB-HA mice are viable and fertile and show no obvious phenotypic changes. The GLRB-HA line generated in this work will be used in the future to generate a second GLRB-HA KI mouse line with an additional loxP site upstream of exon 10, as was initially planned. This will then allow the intracellular loop between TM3 and TM4, as well as a part of the TM4, of GlyRβ to be specifically deleted in future experiments using Cre-mediated recombination in mice. The intracellular loop between TM3 and TM4 is important for the interaction with gephyrin, but also with other cytoplasmic proteins involved in receptor clustering and trafficking (del Pino et al 2011). Thus, this KI mouse will be a powerful tool for studying the consequences of affecting the interacting of GlyRβ with gephyrin and additional cytoplasmic proteins *in vivo*.

4.2.2 NL2

Previous studies indicated that the cell adhesion protein NL2 is one of the major components involved in the formation and stabilization of inhibitory synapses (Poulopoulos et al 2009, Varoqueaux et al 2006, Varoqueaux et al 2004). Through its interaction with neurexins, which are located at the presynaptic side, NL2 couples pre- and postsynaptic sides both structurally and functionally. Similarly, interaction of NL2 with scaffold proteins and $GABA_A$Rs at the postsynaptic side is essential for the formation of selected inhibitory synapses (Nguyen et al 2016, Poulopoulos et al 2009). Activation of the gephyrin-CB complex is the best-characterized postsynaptic function of NL2. Here, previous studies indicated that gephyrin binds to the cytoplasmic tail of NL2 via a 15-amino-acid stretch. Furthermore NL2 binds to the SH3 domain of CB, thereby functioning as a specific activator of CB and guiding membrane tethering of the inhibitory postsynaptic scaffold (Poulopoulos et al 2009). The resulting NL2-gephyrin-CB complex is sufficient for cell-autonomous clustering of inhibitory neurotransmitter receptors (Poulopoulos et al 2009) Independently of gephyrin, NL2 can interact with specific subunits of $GABA_A$Rs, inducing clustering of these, and in this way influencing GABAergic transmission (Dong et al 2007). For example, it promotes the incorporation of the $GABA_A$R α1 subunit into functional $GABA_A$Rs, thus influencing the kinetics of inhibitory currents (Fu & Vicini 2009). Based on this, NL2 can be assumed to shape inhibitory synaptic function not only by determining $GABA_A$R localization but also by specifying its functional properties.

In vivo studies indicated that the previously described stabilization of synaptic structure by NL2 is initiated as soon as the first synaptic contact is formed (Chubykin et al 2007, Jedlicka et al 2011). Thus, it can be inferred that NL2 maintains synaptic transmission at inhibitory synapses in the cortex, hippocampus, midbrain and retina (Gibson et al 2009b, Hoon et al 2009, Jedlicka et al 2011, Poulopoulos et al 2009, Zhang et al 2015). All studies conducted indicate a role for NL2 as an organizer exclusively at inhibitory synapses. Despite this central and important role of NL2, it appears to perform this function only in specific perisomatic inhibitory synapses (Jedlicka et al 2011, Poulopoulos et al 2009). Thus, NL2 exclusively regulates the function of a subpopulation of inhibitory synapses. A differential expression pattern in cellular compartments is not present here, since NL2 is expressed in the majority of inhibitory

synapses and thus the functional specialization on the subpopulation cannot be explained (Varoqueaux et al 2004).

Thus, in the unbiased cDNA library screen performed in this work, an already known, very well characterized and important interaction partner of gephyrin could be found repeatedly, which again underlines the reliability and significance of the results. Furthermore, this example also shows the necessity of such a screen in order to identify further candidates that take on important roles in the gephyrin-dependent specialization of synapses and can take over the function of e.g. NL2.

4.3 The identified candidate-proteins from the 3-4 kb cDNA library screen

4.3.1 Phogrin

Another interesting candidate protein identified by using the unbiased expression screen is phogrin (synonyms: PTPRN2 or IA-2β). Phogrin is a transmembrane protein that was initially described to be expressed in cells with stimulus-coupled peptide hormone secretion, including pancreatic beta cells, in which it is located to the membrane of insulin-containing dense core vesicles (Wasmeier & Hutton 1996). By sequence, phogrin is a member of the family of receptor-like protein-tyrosine phosphatases, but in contains substitutions in conserved catalytic sequences, and no significant enzymatic activity for phogrin has even been reported (Caromile et al 2010). Instead, phogrin is able to dephosphorylate specific phosphoinositides, including PI(3)P and PI(4,5)P_2 (Caromile et al 2010). Although the function of phogrin in the brain remains poorly understood, phogrin disruptions have been linked to attention deficits (Lionel et al 2011), addiction and mood disorders (Yang et al 2011). Interestingly, a previous study indicated that phogrin is highly expressed in PV+ interneurons throughout different hippocampal regions (Ramirez-Franco et al 2016). These findings are consistent with the presence of phogrin mRNA in the medial ganglionic eminence (Chiang & Flanagan 1996).

4.3.2 HIP1R

Many important cellular functions, such as the continuous uptake of essential nutrients (Jones et al 1984, Pearse 1982), the recycling of synaptic vesicles (Galli & Haucke 2004) and the modulation of signal transduction by controlling the levels of surface receptors (Huang et al 1995, Vieira et al 1996), depend on well-studied clathrin-mediated endocytosis (CME). In 1997, mammalian HIP1 was identified as an interactor of Huntingtin, a protein associated with the genetic neurodegenerative disorder Huntington's disease (Kalchman et al 1997, Wanker et al 1997). The yeast homologue (Sla2p), which functions as a regulator of membrane cytoskeleton assembly, was previously described (Holtzman et al 1993). HIP1R, the third member of the protein family, was identified some time later based on structural homology (Engqvist-Goldstein et al 1999, Seki et al 1998). All members of this protein family is an N-terminally localized ANTH (AP180N-terminal homology) domain, a central coiled-coil domain and a talin-like domain at the C-terminus (Kalchman et al 1997, Seki et al 1998, Wanker et al 1997)(see Figure 24).

Figure 24 Domains of HIP1R;
ANTH: AP180 N-terminal homology domain, coiled-coil: central coiled-coil domain; USH: upstream helix domain; PRD: proline rich domain; Talin like: THATCH domain

The ANTH domain of HIP1R was previously described to preferentially bind to PI(3,4)P_2 and PI(3,5)P_2 (Hyun et al 2004). The actin-binding talin-like domain, also called the I/LWEQ module or THATCH domain (Brett et al 2006), is a structural feature of proteins that function as links between the actin cytoskeleton and cellular compartments. Furthermore, it has been shown that this domain is able to bind F-actin (Brett et al 2006, McCann & Craig 1997). Through an intrasterial mechanism, the upstream helix (SH) domain inhibits actin binding (Senetar et al 2004). A distinctive feature of HIP1R, compared to the other members of the protein family, is the proline-rich region that enables the binding of the SH3 domain of cortactin (Le Clainche et al 2007). This interaction indicates a possible actin-modifying potential of HIP1R (Le Clainche et al 2007). Numerous mutations of HIP1R that lead to disruption of actin binding or organization have been described in the literature (Brett et al 2006, McCann & Craig 1997). Furthermore, an altered endocytosis has been observed through siRNA-mediated knock down of HIP1R, resulting in abnormal actin organization in the cytoskeleton (Engqvist-Goldstein et al 2004).

Repeatedly, a regulator of the actin cytoskeleton was found in the unbiased cDNA library screen performed here. Again, a possible direct interaction between HIP1R and gephyrin has not been described in the literature. Additional studies will be required to clarify whether HIP1R is involved in gephyrin-dependent formation of inhibitory synapses.

4.3.3 NSF

NSF belongs to the AAA1 (ATPases associated with various cellular activities) family and is one of the first members identified (Malhotra et al 1988). NSF has been described in the literature as playing a key role in intracellular membrane fusion events (Malhotra et al 1988, Wilson et al 1989). The AAA1 superfamily comprises a large number of members that exhibit broad functional diversity (Hanson & Whiteheart 2005). The enzymes can interact with various substrates through ATP hydrolysis cycles and thus participate in numerous cellular processes such as membrane fusion, protein disaggregation/refolding, proteolysis, DNA replication, transcription and DNA recombination (Sauer & Baker 2011, Ulbrich et al 2009, Xu et al 2009, Zhu et al 2008). An NSF monomer that assembles into homohexamers has two ATPase domains, as well as an N-terminal domain [(Hanson et al 1997); (Fleming et al 1998, Hanson et al 1997, Lenzen et al 1998); see **Figure 25**]. The ATPase domains undergo conformational changes during ATP binding and ATP hydrolysis (Hanson et al 1997).

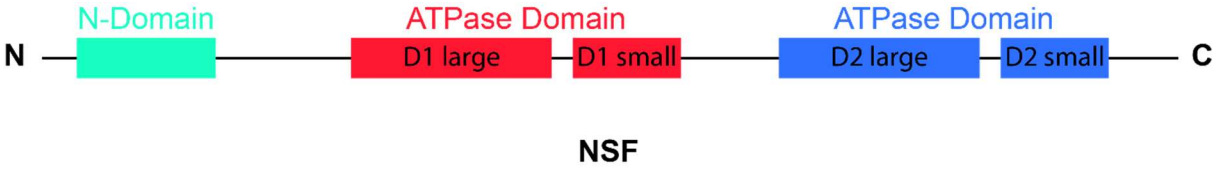

Figure 25 Domains of monomeric NSF
Each ATPase Domain have a large and small domain (D)

There are reports in the literature associating decreased NSF production with epilepsy (Matveeva et al 2007). Furthermore, NFS has been described to be involved in the dynamic control of $GABA_AR$ expression at the cell surface via binding to $GABA_AR$-associated protein (Moss & Smart 2001).

A direct interaction of NFS with scaffold proteins is not described in the literature. Due to its involvement in numerous intracellular transport processes, it could also be involved in necessary transport processes during gephyrin clustering. Despite fewer described connections between inhibitory postsynapses and NFS, the protein, which is controversially discussed in the literature, represents an interesting candidate for screening. All previously described and discussed candidates of the unbiased cDNA library screen were either already known and well characterised interaction partners of gephyrin or showed possible links to inhibitory neurotransmission in the literature.

5 Summary

In the work presented here, a set of full-length size-selected and unamplified cDNA expression libraries [30.000 CFU in total; size-fractionated into 2-3, 3-4, and 4-5 kb pools of 10.000 CFU each] was screened for proteins that may function in gephyrin-dependent formation of inhibitory synapses similarly to CB or NL2. The assay we used is based on the previously described observation that in nonneuronal cells, coexpression of GFP-gephyrin together with CB_{SH3-} alone or with CB_{SH3+} in the presence of NL2 leads to a redistribution of gephyrin into submembranous microclusters (Kins et al 2000, Poulopoulos et al 2009). In our assay, this phenotypic change was adopted by using Flp-In T-Rex-GFP-gephyrin HEK 293 cells inducibly expressing GFP-gephyrin (Papadopoulos et al 2017). Using this strategy, we were able to identify 7 clones from the cDNA library that induce redistribution (see **Table 9**). As a proof-of-principle for our screening assay, we were able to isolate previously known gephyrin-interacting proteins, such as GlyRβ and NL2 (Pfeiffer et al 1982, Poulopoulos et al 2009), thereby demonstrating the physiological relevance of the regulatory proteins identified by our approach. Furthermore, we identified novel candidate-proteins with potential roles in the formation of inhibitory synapses. These proteins are involved in the regulation of actin dynamics (WASF1/WAVE1, β-actin, HIP1R), phosphoinositide metabolism (PTPRN2, HIP1R) and transfer of membrane vesicles (HIP1R, NSF). We initially focused our studies in examining whether two of the candidate proteins, WAVE1 and GlyRβ, are relevant for the formation of inhibitory synapses in the mouse forebrain.

First, we aimed to investigate the importance of WAVE1 for the formation and stability of GABAergic synapses. Our *in vitro* binding assays (see **Figure 18**) confirmed the interaction of the WRP with WAVE1, as previously described (Soderling et al 2002), but did not show a direct binding of WAVE1 to gephyrin (see **Figure 18**). In contrast, we indicated a specific interaction between the SH3-domain of CB and WAVE1 (see **Figure 16**), as untagged WAVE1 was found to consistently bind to the GST-tagged versions of the SH3-domain of CB (GST-SH3) and full-length, SH3-domain containing, CB (GST-CB_{SH3+}), but not to GST alone or to CB lacking the SH3-domain (GST-CB_{SH3-}). In order to use an untagged version of WAVE1 in the *in vitro* binding assay, GST-WAVE1 was cut with thrombin, resulting in fragmentation of WAVE1, which was also observed in the pulldown with GST-SH3, whereas the pulldown with GST-CB resulted mainly in a pulldown of the full-length WAVE1 (see **Figure 16**). This result, combined with a subsequent mass spectrometric analysis (see **Figure 17**) indicated that WAVE1 may have an additional, N-terminal, binding site for the full-length SH3 domain-containing CB.

In addition to biochemical studies on possible interaction partners of WAVE1, this work investigated the effect of loss of WAVE1 on gephyrin clustering in the cerebellum, as well as hippocampus using immunohistochemical experiments in brain slices derived from 5-week-old WAVE1 KO mice. Our immunohistochemical analyses using WAVE1 KO mice (Soderling et al 2003) and their WT or +/- littermates, revealed no differences in the clustering of gephyrin in glutamatergic neurons, but a significant increase in the densities of dendritic gephyrin puncta in PV+ interneurons of the CA1 area of the hippocampus in brains of WAVE1 KO mice, as compared to controls (see **Figure 21**). This increase of gephyrin puncta in PV+ interneurons was accompanied by a decrease in the mean gephyrin puncta size (see **Figure 22**), as well as by a decrease in the percentages of gephyrin puncta apposed to the presynaptic marker VIAAT (see **Figure 22**), in slices derived from WAVE1 KOs, as compared to controls.
The second candidate of the screen, which we examined more closely, was GlyRβ. In contrast to previous publications (Kirsch & Betz 1995) in our unbiased expression screen, the GlyR-β-induced formation of submembranous gephyrin microclusters was robust and consistent. In addition, we were able to demonstrate a localization of GlyRβ in the plasma membrane (see **Figure 10**).

In order to study the expression pattern and the roles of the GlyRβ protein in selected regions and neuronal subtypes of the mouse forebrain, we generated two new mouse lines by using the CRISPR-

Cas9 technology and corresponding HDR fragments (see **Figure 11** and **Figure 12**). The first line (see **Figure 11**; GLRB-CO) is a conditional KO line, carrying two loxP-sites in the intronic regions upstream of exons 8 and downstream of exon 9, respectively. Exons 8 and 9 encode half of the TMD2, the whole TMD3 and a part of the intracellular loop of GlyRβ, which we predict to result in the loss of the GlyRβ protein upon Cre-mediated recombination in mice. Mouse genotyping was carried out by PCR indicating the successful generation (see **Figure 11**).

The HDR fragment for the second mouse line was designed to introduce loxP-sites in the regions upstream of exon 10 and downstream of the coding sequence, and to replace the Stop codon with the coding sequence of the HA-tag and a Stop codon. Initial PCR-based screening for homologous recombination in mice indicated the absence of the loxP-site upstream of exon 10 in the KI allele (see **Figure 12**). In contrast, the presence of the HA-tag and the second loxP-site in the KI allele was verified by PCR genotyping (see **Figure 12**). Furthermore, Western blot analysis of brain lysates derived from hom GLRB-HA mice and their WT-littermates using an HA-antibody verified the expression of a 58-60 kD protein in samples derived from GLRB-HA brains, but not in those from WT brains (see **Figure 12**). The size of this protein corresponds to a HA-tagged version of the full-length GlyRβ protein (Weltzien et al 2012).

Finally, a comprehensive and unbiased screen of a cDNA library was successfully performed in this work, which identified both known and novel regulatory proteins involved in the gephyrin-dependent formation of inhibitory synapses. In the case of WAVE1, this work was able to indicate an important role of WAVE1 in the clustering of gephyrin at inhibitory synapses of PV+ interneurons. Our data provide evidence that all candidates identified in our screen have potentially important roles in the formation of gephyrin-dependent inhibitory synapses.

6 Acknowledgement

I am very grateful for the support I have received over the years from colleagues, mentors, friends and family.

I would especially like to thank Theofilos Papadopoulos. He was there for me every day with advice and support in the lab, not only to help advance the project, but also to promote my personal development as a person and scientist. I am very grateful to have had a supervisor during this time who puts his heart and soul into science.

I would also like to thank Prof. Dr. Nils Brose, the first member of my thesis committee for their critical feedback on my work, their encouragement and mentoring. I am grateful for the advice from Prof. Dr. Blanche Schwappach and Dr. Camin Dean during my thesis committee meetings. I would like to thank Jennifer Weiss, who carried out a master thesis under my supervision. Her enthusiasm and determination for our project made the time really enjoyable.

In general, I wish to thank all my colleagues in the Department of Molecular Neurobiology who warmly welcomed me into the group and provided a warm and above average working atmosphere. In particular, I would like to thank Kerstin, Birgit, Astrid, Sabine, Manu, and Sally, who provided a positive distraction and always cheerful conversations during the midday breaks. I would also like to thank the AGCT-Lab, especially Fritz Benseler and Christiane Harenberg for their constant support and huge help in generating the new mouse lines.

I am grateful to the GGNB for the numerous opportunities for further training. Moreover, I enjoyed very much the possibility of interdisciplinary networking of numerous students and the resulting acquaintances and friendships.

After numerous and sometimes long lab days, my friends Yannik, Stefan, Felix, Suse and Caro, who I found here, were always able to ground me and provide some distraction. The entire badminton team also helped me to generate energy and also to get to know my girlfriend Imke, who has provided me with indispensable support over the past few years and has thus become an important and central element in my life.

Not least, I would like to thank my parents Bärbel and Horst Wagner for always supporting me in my life so far. Without you I would not be where I am now. Thank you for all that you have made possible for me!

7 Abbreviations

AAA1	ATPases associated with various cellular activities
AAV	Adeno associated virus
Abl	Ableson tyrosine kinase
AChE	Acetylcholinesterase
ADP	Adenosine Di-Phosphate
Amp	Ampicilline
ANTH	AP180N-terminal homology
ATP	Adenosine Tri-Phosphate
$Carb^{+}$	Carbenicillin containing
CASK	Calcium/calmodulin-dependent serine protein kinase
CB	Collybistin
CB_{SH3+}	CB variants containing the N-terminal SH3 domain
CB_{SH3-}	Splice variant of CB lacking the SH3 domain
CFU	Colony forming units
CNS	Central nervous system
COS-7	African green monkey kidney fibroblast-like cell line
DAPI	4',6-diamidino-2-phenylindole
DGC	Dystrophin-associated glycoprotein complex
DH	Dbl homology
DIV	Days *in vitro*
Dlc-1/-2	Dynein-1/-2
DMEM	Dulbecco's Modified Eagle's medium
DNA	Deoxyribonucleic acid
DTT	Dithiothreitol
ECL	Enhanced chemiluminescence
EDTA	Ethylendiamtetracetic acid
E-I balance	Excitation-inhibition balance
Ena/VASP	Enabled vasodilator stimulated phosphoprotein
E18	Embryonic day 18

EVH1	Ena/VASP homologous domain 1
Fl	Floxed
FCS	Fetal Calf Serum
GABA	Gamma-aminobutyric acid (4-aminobutanoic acid)
$GABA_AR$	Gamma-aminobutyric acid receptor type A
$GABA_BR$	Gamma-aminobutyric acid receptor type B
$GABA_CR$	Gamma-aminobutyric acid receptor type C
GABA-T	GABA-α-oxoglutarate transaminase
GABARAP	Gamma-aminobutyric acid receptor adopter protein
GAD	Glutamic acid decarboxylase
GAP	GTPase activating protein
GBD	GTPase binding domain
GEF	Guanine nucleotide exchange factor
GFP	Green fluorescence protein
GLRBHA	GlyRβ-HA KI mouse line
GlyR	Glycine receptor
$GlyR_β$	Beta subunit of the Glycine receptor
GST	Glutathione-S-transferase
HBSS	Hank's Balanced Salt Solution
HEK	Human embryonic kidney cells
HIP1R	Huntingtin interacting protein 1 related
hPEM2	Human posterior end mark 2
Hsc70	Heat-shock protein 70
ICC	Immunocytochemistry
IgSF9	Members of immunoglobulin superfamily 9
IgSF9b	Members of immunoglobulin superfamily 9 b
IHC	Immunohistochemistry
IPSC	Inhibitory postsynaptic currents
KI	Knock in
KO	Knockout
LB	Lysogeny broth

LGIC	Ligand-gated ion channel
MDGA	MAM domain-containing GPI anchor proteins
MEGAP	Mental disorder-associated GAP
Mena/Vasp	Mammalian enabled /vasodilator stimulated phosphoprotein
MINT	Munc18-interacting protein
Moco	Molybdenum cofactors
mIPSC	Miniature inhibitory postsynaptic currents
NaCl	Sodium chloride
NEB	New England Biolabs
NL1-4	Neuroligin 1-4
NMDA	N-methyl-D-aspartate
NSF	N-ethylmaleimide sensitive factor
PBS	Phosphate buffered saline
PCR	Polymerase chain reaction
PDZ	PSD95/disk-large/zona-occludens-1 domains
PEM-2	Posterior end mark 2
PFA	Paraformaldehyde
PH	Pleckstrin homology
PIP_3	Phosphatidylinositol-3,4,5-trisphosphate
PI(3)P	Phosphatidylinositol-3-phosphate
PI(3,4)P	Phosphatidylinositol-3,4-bisphosphate
PI(3,5)P	Phosphatidylinositol-3,5-bisphosphate
PI(4,5)P	Phosphatidylinositol-4,5-bisphosphate
P/S	Penicilline/Streptomycin
PSD	Postsynaptic density
PTP	Protein tyrosine phosphatase
PTPRN2	Protein tyrosine phosphatase receptor type N2
P0	Postnatal day 0
P11	Postnatal day 11
SDS	Sodium dodecyl sulfate
SG	Stratum ganglionare

SHD	Scar homology domain
SH3	Src homology 3
SM	Stratum moleculare
SO	Stratum Oriens
SP	Stratum Pyramidale
SR	Stratum Radiatum
SSA	Glutamate
SSADH	Succinic semialdehyde dehydrogenase
S-SCAM	Synaptic scaffolding molecule
TEMED	Tetramethyethylethylendiamine
TMD	Transmembrane domain
VDCC	Voltage-dependent calcium channels
VIAAT	Vesicular inhibitory amino acid transporter
WASP	Wiskott-Aldrich syndrome protein
WB	Western blot
WHD	WAVE homology domain
WT	Wild type

8 List of figures

9 List of tables

10 References

Allen NJ, Barres BA. 2009. Neuroscience: Glia - more than just brain glue. *Nature* 457: 675-7

Allison DW, Chervin AS, Gelfand VI, Craig AM. 2000. Postsynaptic scaffolds of excitatory and inhibitory synapses in hippocampal neurons: maintenance of core components independent of actin filaments and microtubules. *J Neurosci* 20: 4545-54

Allison DW, Gelfand VI, Spector I, Craig AM. 1998. Role of actin in anchoring postsynaptic receptors in cultured hippocampal neurons: differential attachment of NMDA versus AMPA receptors. *J Neurosci* 18: 2423-36

Araki Y, Lin DT, Huganir RL. 2010. Plasma membrane insertion of the AMPA receptor GluA2 subunit is regulated by NSF binding and Q/R editing of the ion pore. *Proc Natl Acad Sci U S A* 107: 11080-5

Babaev O, Cruces-Solis H, Piletti Chatain C, Hammer M, Wenger S, et al. 2018. IgSF9b regulates anxiety behaviors through effects on centromedial amygdala inhibitory synapses. *Nat Commun* 9: 5400

Bartos M, Vida I, Jonas P. 2007. Synaptic mechanisms of synchronized gamma oscillations in inhibitory interneuron networks. *Nat Rev Neurosci* 8: 45-56

Baudouin SJ, Gaudias J, Gerharz S, Hatstatt L, Zhou K, et al. 2012. Shared synaptic pathophysiology in syndromic and nonsyndromic rodent models of autism. *Science* 338: 128-32

Bausen M, Fuhrmann JC, Betz H, O'Sullivan G A. 2006. The state of the actin cytoskeleton determines its association with gephyrin: role of ena/VASP family members. *Mol Cell Neurosci* 31: 376-86

Bayes A, van de Lagemaat LN, Collins MO, Croning MD, Whittle IR, et al. 2011. Characterization of the proteome, diseases and evolution of the human postsynaptic density. *Nat Neurosci* 14: 19-21

Bear JE, Rawls JF, Saxe CL, 3rd. 1998. SCAR, a WASP-related protein, isolated as a suppressor of receptor defects in late Dictyostelium development. *J Cell Biol* 142: 1325-35

Becker CM, Hermans-Borgmeyer I, Schmitt B, Betz H. 1986. The glycine receptor deficiency of the mutant mouse spastic: evidence for normal glycine receptor structure and localization. *J Neurosci* 6: 1358-64

Becker CM, Hoch W, Betz H. 1988. Glycine receptor heterogeneity in rat spinal cord during postnatal development. *EMBO J* 7: 3717-26

Becker CM, Schmieden V, Tarroni P, Strasser U, Betz H. 1992. Isoform-selective deficit of glycine receptors in the mouse mutant spastic. *Neuron* 8: 283-9

Betz H, Laube B. 2006. Glycine receptors: recent insights into their structural organization and functional diversity. *J Neurochem* 97: 1600-10

Bird CM, Burgess N. 2008. The hippocampus and memory: insights from spatial processing. *Nat Rev Neurosci* 9: 182-94

Bown AW, Shelp BJ. 1997. The Metabolism and Functions of [gamma]-Aminobutyric Acid. *Plant Physiol* 115: 1-5

Boyken J, Gronborg M, Riedel D, Urlaub H, Jahn R, Chua JJ. 2013. Molecular profiling of synaptic vesicle docking sites reveals novel proteins but few differences between glutamatergic and GABAergic synapses. *Neuron* 78: 285-97

Bradford MM. 1976. A rapid and sensitive method for the quantitation of microgram quantities of protein utilizing the principle of protein-dye binding. *Anal Biochem* 72: 248-54

Brenman JE, Topinka JR, Cooper EC, McGee AW, Rosen J, et al. 1998. Localization of postsynaptic density-93 to dendritic microtubules and interaction with microtubule-associated protein 1A. *J Neurosci* 18: 8805-13

Brett TJ, Legendre-Guillemin V, McPherson PS, Fremont DH. 2006. Structural definition of the F-actin-binding THATCH domain from HIP1R. *Nat Struct Mol Biol* 13: 121-30

Bucan M, Abrahams BS, Wang K, Glessner JT, Herman EI, et al. 2009. Genome-wide analyses of exonic copy number variants in a family-based study point to novel autism susceptibility genes. *PLoS Genet* 5: e1000536

Budreck EC, Scheiffele P. 2007. Neuroligin-3 is a neuronal adhesion protein at GABAergic and glutamatergic synapses. *Eur J Neurosci* 26: 1738-48

Burgalossi A, Jung S, Man KN, Nair R, Jockusch WJ, et al. 2012. Analysis of neurotransmitter release mechanisms by photolysis of caged Ca(2)(+) in an autaptic neuron culture system. *Nat Protoc* 7: 1351-65

Burt DR, Kamatchi GL. 1991. GABAA receptor subtypes: from pharmacology to molecular biology. *FASEB J* 5: 2916-23

Cao F, Liu JJ, Zhou S, Cortez MA, Snead OC, et al. 2020. Neuroligin 2 regulates absence seizures and behavioral arrests through GABAergic transmission within the thalamocortical circuitry. *Nat Commun* 11: 3744

Carlin RK, Grab DJ, Cohen RS, Siekevitz P. 1980. Isolation and characterization of postsynaptic densities from various brain regions: enrichment of different types of postsynaptic densities. *J Cell Biol* 86: 831-45

Caromile LA, Oganesian A, Coats SA, Seifert RA, Bowen-Pope DF. 2010. The neurosecretory vesicle protein phogrin functions as a phosphatidylinositol phosphatase to regulate insulin secretion. *J Biol Chem* 285: 10487-96

Caston J, Vasseur F, Stelz T, Chianale C, Delhaye-Bouchaud N, Mariani J. 1995. Differential roles of cerebellar cortex and deep cerebellar nuclei in the learning of the equilibrium behavior: studies in intact and cerebellectomized lurcher mutant mice. *Brain Res Dev Brain Res* 86: 311-6

Cellot G, Cherubini E. 2013. Functional role of ambient GABA in refining neuronal circuits early in postnatal development. *Front Neural Circuits* 7: 136

Chiang MK, Flanagan JG. 1996. PTP-NP, a new member of the receptor protein tyrosine phosphatase family, implicated in development of nervous system and pancreatic endocrine cells. *Development* 122: 2239-50

Chiou TT, Bonhomme B, Jin H, Miralles CP, Xiao H, et al. 2011. Differential regulation of the postsynaptic clustering of gamma-aminobutyric acid type A (GABAA) receptors by collybistin isoforms. *J Biol Chem* 286: 22456-68

Chubykin AA, Atasoy D, Etherton MR, Brose N, Kavalali ET, et al. 2007. Activity-dependent validation of excitatory versus inhibitory synapses by neuroligin-1 versus neuroligin-2. *Neuron* 54: 919-31

Cohen RS, Chung SK, Pfaff DW. 1985. Immunocytochemical localization of actin in dendritic spines of the cerebral cortex using colloidal gold as a probe. *Cell Mol Neurobiol* 5: 271-84

Colonnier M. 1968. Synaptic patterns on different cell types in the different laminae of the cat visual cortex. An electron microscope study. *Brain Res* 9: 268-87

Dahl JP, Wang-Dunlop J, Gonzales C, Goad ME, Mark RJ, Kwak SP. 2003. Characterization of the WAVE1 knock-out mouse: implications for CNS development. *J Neurosci* 23: 3343-52

Davis GA, Bloom FE. 1973. Isolation of synaptic junctional complexes from rat brain. *Brain Res* 62: 135-53

DeFeudis FV. 1983. Psychoactive agents and GABA-receptors. *Pharmacol Res Commun* 15: 29-39

del Pino I, Paarmann I, Karas M, Kilimann MW, Betz H. 2011. The trafficking proteins Vacuolar Protein Sorting 35 and Neurobeachin interact with the glycine receptor beta-subunit. *Biochem Biophys Res Commun* 412: 435-40

Doetsch F. 2003. The glial identity of neural stem cells. *Nat Neurosci* 6: 1127-34

Dong N, Qi J, Chen G. 2007. Molecular reconstitution of functional GABAergic synapses with expression of neuroligin-2 and GABAA receptors. *Mol Cell Neurosci* 35: 14-23

Dumoulin A, Triller A, Dieudonne S. 2001. IPSC kinetics at identified GABAergic and mixed GABAergic and glycinergic synapses onto cerebellar Golgi cells. *J Neurosci* 21: 6045-57

Eden S, Rohatgi R, Podtelejnikov AV, Mann M, Kirschner MW. 2002. Mechanism of regulation of WAVE1-induced actin nucleation by Rac1 and Nck. *Nature* 418: 790-3

Ehlers MD, Fung ET, O'Brien RJ, Huganir RL. 1998. Splice variant-specific interaction of the NMDA receptor subunit NR1 with neuronal intermediate filaments. *J Neurosci* 18: 720-30

Emes RD, Grant SG. 2012. Evolution of synapse complexity and diversity. *Annu Rev Neurosci* 35: 111-31

Endris V, Wogatzky B, Leimer U, Bartsch D, Zatyka M, et al. 2002. The novel Rho-GTPase activating gene MEGAP/ srGAP3 has a putative role in severe mental retardation. *Proc Natl Acad Sci U S A* 99: 11754-9

Engqvist-Goldstein AE, Kessels MM, Chopra VS, Hayden MR, Drubin DG. 1999. An actin-binding protein of the Sla2/Huntingtin interacting protein 1 family is a novel component of clathrin-coated pits and vesicles. *J Cell Biol* 147: 1503-18

Engqvist-Goldstein AE, Zhang CX, Carreno S, Barroso C, Heuser JE, Drubin DG. 2004. RNAi-mediated Hip1R silencing results in stable association between the endocytic machinery and the actin assembly machinery. *Mol Biol Cell* 15: 1666-79

Essrich C, Lorez M, Benson JA, Fritschy JM, Luscher B. 1998. Postsynaptic clustering of major GABAA receptor subtypes requires the gamma 2 subunit and gephyrin. *Nat Neurosci* 1: 563-71

Feng G, Tintrup H, Kirsch J, Nichol MC, Kuhse J, et al. 1998. Dual requirement for gephyrin in glycine receptor clustering and molybdoenzyme activity. *Science* 282: 1321-4

Fifkova E. 1985. A possible mechanism of morphometric changes in dendritic spines induced by stimulation. *Cell Mol Neurobiol* 5: 47-63

Fiszer S, Robertis ED. 1967. Action of triton X-100 on ultrastructure and membrane-bound- enzymes of isolated nerve endings from rat brain. *Brain Res* 5: 31-44

Fleming KG, Hohl TM, Yu RC, Muller SA, Wolpensinger B, et al. 1998. A revised model for the oligomeric state of the N-ethylmaleimide-sensitive fusion protein, NSF. *J Biol Chem* 273: 15675-81

Forstera B, Belaidi AA, Juttner R, Bernert C, Tsokos M, et al. 2010. Irregular RNA splicing curtails postsynaptic gephyrin in the cornu ammonis of patients with epilepsy. *Brain* 133: 3778-94

Fritschy JM, Mohler H. 1995. GABAA-receptor heterogeneity in the adult rat brain: differential regional and cellular distribution of seven major subunits. *J Comp Neurol* 359: 154-94

Fu Z, Vicini S. 2009. Neuroligin-2 accelerates GABAergic synapse maturation in cerebellar granule cells. *Mol Cell Neurosci* 42: 45-55

Fuhrmann JC, Kins S, Rostaing P, El Far O, Kirsch J, et al. 2002. Gephyrin interacts with Dynein light chains 1 and 2, components of motor protein complexes. *J Neurosci* 22: 5393-402

Fujita M, Sato K, Sato M, Inoue T, Kozuka T, Tohyama M. 1991. Regional distribution of the cells expressing glycine receptor beta subunit mRNA in the rat brain. *Brain Res* 560: 23-37

Fukaya M, Kamata A, Hara Y, Tamaki H, Katsumata O, et al. 2011. SynArfGEF is a guanine nucleotide exchange factor for Arf6 and localizes preferentially at post-synaptic specializations of inhibitory synapses. *J Neurochem* 116: 1122-37

Furshpan EJ, Potter DD. 1959. Transmission at the giant motor synapses of the crayfish. *J Physiol* 145: 289-325

Furst J, Sutton RB, Chen J, Brunger AT, Grigorieff N. 2003. Electron cryomicroscopy structure of N-ethyl maleimide sensitive factor at 11 A resolution. *EMBO J* 22: 4365-74

Galli T, Haucke V. 2004. Cycling of synaptic vesicles: how far? How fast! *Sci STKE* 2004: re19

Gertler FB, Niebuhr K, Reinhard M, Wehland J, Soriano P. 1996. Mena, a relative of VASP and Drosophila Enabled, is implicated in the control of microfilament dynamics. *Cell* 87: 227-39

Gibson DG, Young L, Chuang RY, Venter JC, Hutchison CA, 3rd, Smith HO. 2009a. Enzymatic assembly of DNA molecules up to several hundred kilobases. *Nat Methods* 6: 343-5

Gibson JR, Huber KM, Sudhof TC. 2009b. Neuroligin-2 deletion selectively decreases inhibitory synaptic transmission originating from fast-spiking but not from somatostatin-positive interneurons. *J Neurosci* 29: 13883-97

Giesemann T, Schwarz G, Nawrotzki R, Berhorster K, Rothkegel M, et al. 2003. Complex formation between the postsynaptic scaffolding protein gephyrin, profilin, and Mena: a possible link to the microfilament system. *J Neurosci* 23: 8330-9

Gokce O, Sudhof TC. 2013. Membrane-tethered monomeric neurexin LNS-domain triggers synapse formation. *J Neurosci* 33: 14617-28

Goodenough DA, Paul DL. 2009. Gap junctions. *Cold Spring Harb Perspect Biol* 1: a002576

Graf ER, Zhang X, Jin SX, Linhoff MW, Craig AM. 2004. Neurexins induce differentiation of GABA and glutamate postsynaptic specializations via neuroligins. *Cell* 119: 1013-26

Grant SG. 2013. SnapShot: Organizational principles of the postsynaptic proteome. *Neuron* 80: 534 e1

Gray EG. 1959. Electron microscopy of synaptic contacts on dendrite spines of the cerebral cortex. *Nature* 183: 1592-3

Grudzinska J, Schemm R, Haeger S, Nicke A, Schmalzing G, et al. 2005. The beta subunit determines the ligand binding properties of synaptic glycine receptors. *Neuron* 45: 727-39

Gulyas AI, Megias M, Emri Z, Freund TF. 1999. Total number and ratio of excitatory and inhibitory synapses converging onto single interneurons of different types in the CA1 area of the rat hippocampus. *J Neurosci* 19: 10082-97

Gunther U, Benson J, Benke D, Fritschy JM, Reyes G, et al. 1995. Benzodiazepine-insensitive mice generated by targeted disruption of the gamma 2 subunit gene of gamma-aminobutyric acid type A receptors. *Proc Natl Acad Sci U S A* 92: 7749-53

Hanson PI, Roth R, Morisaki H, Jahn R, Heuser JE. 1997. Structure and conformational changes in NSF and its membrane receptor complexes visualized by quick-freeze/deep-etch electron microscopy. *Cell* 90: 523-35

Hanson PI, Whiteheart SW. 2005. AAA+ proteins: have engine, will work. *Nat Rev Mol Cell Biol* 6: 519-29

Harborth J, Elbashir SM, Bechert K, Tuschl T, Weber K. 2001. Identification of essential genes in cultured mammalian cells using small interfering RNAs. *J Cell Sci* 114: 4557-65

Harris KM, Kater SB. 1994. Dendritic spines: cellular specializations imparting both stability and flexibility to synaptic function. *Annu Rev Neurosci* 17: 341-71

Harvey K, Duguid IC, Alldred MJ, Beatty SE, Ward H, et al. 2004a. The GDP-GTP exchange factor collybistin: an essential determinant of neuronal gephyrin clustering. *J Neurosci* 24: 5816-26

Harvey RJ, Depner UB, Wassle H, Ahmadi S, Heindl C, et al. 2004b. GlyR alpha3: an essential target for spinal PGE2-mediated inflammatory pain sensitization. *Science* 304: 884-7

Harvey RJ, Schmieden V, Von Holst A, Laube B, Rohrer H, Betz H. 2000. Glycine receptors containing the alpha4 subunit in the embryonic sympathetic nervous system, spinal cord and male genital ridge. *Eur J Neurosci* 12: 994-1001

Hines RM, Wu L, Hines DJ, Steenland H, Mansour S, et al. 2008. Synaptic imbalance, stereotypies, and impaired social interactions in mice with altered neuroligin 2 expression. *J Neurosci* 28: 6055-67

Hirao K, Hata Y, Ide N, Takeuchi M, Irie M, et al. 1998. A novel multiple PDZ domain-containing molecule interacting with N-methyl-D-aspartate receptors and neuronal cell adhesion proteins. *J Biol Chem* 273: 21105-10

Hoch W, Betz H, Becker CM. 1989. Primary cultures of mouse spinal cord express the neonatal isoform of the inhibitory glycine receptor. *Neuron* 3: 339-48

Holtzman DA, Yang S, Drubin DG. 1993. Synthetic-lethal interactions identify two novel genes, SLA1 and SLA2, that control membrane cytoskeleton assembly in Saccharomyces cerevisiae. *J Cell Biol* 122: 635-44

Homanics GE, DeLorey TM, Firestone LL, Quinlan JJ, Handforth A, et al. 1997. Mice devoid of gamma-aminobutyrate type A receptor beta3 subunit have epilepsy, cleft palate, and hypersensitive behavior. *Proc Natl Acad Sci U S A* 94: 4143-8

Hoon M, Bauer G, Fritschy JM, Moser T, Falkenburger BH, Varoqueaux F. 2009. Neuroligin 2 controls the maturation of GABAergic synapses and information processing in the retina. *J Neurosci* 29: 8039-50

Hoon M, Soykan T, Falkenburger B, Hammer M, Patrizi A, et al. 2011. Neuroligin-4 is localized to glycinergic postsynapses and regulates inhibition in the retina. *Proc Natl Acad Sci U S A* 108: 3053-8

Huang Z, Chen Y, Nissenson RA. 1995. The cytoplasmic tail of the G-protein-coupled receptor for parathyroid hormone and parathyroid hormone-related protein contains positive and negative signals for endocytosis. *J Biol Chem* 270: 151-6

Huttelmaier S, Mayboroda O, Harbeck B, Jarchau T, Jockusch BM, Rudiger M. 1998. The interaction of the cell-contact proteins VASP and vinculin is regulated by phosphatidylinositol-4,5-bisphosphate. *Curr Biol* 8: 479-88

Hyun TS, Rao DS, Saint-Dic D, Michael LE, Kumar PD, et al. 2004. HIP1 and HIP1r stabilize receptor tyrosine kinases and bind 3-phosphoinositides via epsin N-terminal homology domains. *J Biol Chem* 279: 14294-306

Jacob TC, Moss SJ, Jurd R. 2008. GABA(A) receptor trafficking and its role in the dynamic modulation of neuronal inhibition. *Nat Rev Neurosci* 9: 331-43

Jahn O, Hesse D, Reinelt M, Kratzin HD. 2006. Technical innovations for the automated identification of gel-separated proteins by MALDI-TOF mass spectrometry. *Anal Bioanal Chem* 386: 92-103

Jarrard LE. 1993. On the role of the hippocampus in learning and memory in the rat. *Behav Neural Biol* 60: 9-26

Jedlicka P, Hoon M, Papadopoulos T, Vlachos A, Winkels R, et al. 2011. Increased dentate gyrus excitability in neuroligin-2-deficient mice in vivo. *Cereb Cortex* 21: 357-67

Jinek M, Chylinski K, Fonfara I, Hauer M, Doudna JA, Charpentier E. 2012. A programmable dual-RNA-guided DNA endonuclease in adaptive bacterial immunity. *Science* 337: 816-21

Jonas P, Bischofberger J, Sandkuhler J. 1998. Corelease of two fast neurotransmitters at a central synapse. *Science* 281: 419-24

Jones AL, Hradek GT, Hornick C, Renaud G, Windler EE, Havel RJ. 1984. Uptake and processing of remnants of chylomicrons and very low density lipoproteins by rat liver. *J Lipid Res* 25: 1151-8

Kalchman MA, Koide HB, McCutcheon K, Graham RK, Nichol K, et al. 1997. HIP1, a human homologue of S. cerevisiae Sla2p, interacts with membrane-associated huntingtin in the brain. *Nat Genet* 16: 44-53

Kalscheuer VM, Musante L, Fang C, Hoffmann K, Fuchs C, et al. 2009. A balanced chromosomal translocation disrupting ARHGEF9 is associated with epilepsy, anxiety, aggression, and mental retardation. *Hum Mutat* 30: 61-8

Kandel ER, Squire LR. 2000. Neuroscience: breaking down scientific barriers to the study of brain and mind. *Science* 290: 1113-20

Kandel ER, Schartz J, Jessell T, Siegelbaum S 2012. Principles of Neural Science; ISBN: 9780071390118

Karlsson R, Graae L, Lekman M, Wang D, Favis R, et al. 2012. MAGI1 copy number variation in bipolar affective disorder and schizophrenia. *Biol Psychiatry* 71: 922-30

Khaitlina SY. 2001. Functional specificity of actin isoforms. *Int Rev Cytol* 202: 35-98

Kilisch M, Mayer S, Mitkovski M, Roehse H, Hentrich J, et al. 2020. A GTPase-induced switch in phospholipid affinity of collybistin contributes to synaptic gephyrin clustering. *J Cell Sci* 133

Kim EY, Schrader N, Smolinsky B, Bedet C, Vannier C, et al. 2006. Deciphering the structural framework of glycine receptor anchoring by gephyrin. *EMBO J* 25: 1385-95

Kins S, Betz H, Kirsch J. 2000. Collybistin, a newly identified brain-specific GEF, induces submembrane clustering of gephyrin. *Nat Neurosci* 3: 22-9

Kirsch J, Betz H. 1995. The postsynaptic localization of the glycine receptor-associated protein gephyrin is regulated by the cytoskeleton. *J Neurosci* 15: 4148-56

Kirsch J, Kuhse J, Betz H. 1995. Targeting of glycine receptor subunits to gephyrin-rich domains in transfected human embryonic kidney cells. *Mol Cell Neurosci* 6: 450-61

Kirsch J, Langosch D, Prior P, Littauer UZ, Schmitt B, Betz H. 1991. The 93-kDa glycine receptor-associated protein binds to tubulin. *J Biol Chem* 266: 22242-5

Kneussel M, Brandstatter JH, Laube B, Stahl S, Muller U, Betz H. 1999. Loss of postsynaptic GABA(A) receptor clustering in gephyrin-deficient mice. *J Neurosci* 19: 9289-97

Kneussel M, Engelkamp D, Betz H. 2001. Distribution of transcripts for the brain-specific GDP/GTP exchange factor collybistin in the developing mouse brain. *Eur J Neurosci* 13: 487-92

Kneussel M, Loebrich S. 2007. Trafficking and synaptic anchoring of ionotropic inhibitory neurotransmitter receptors. *Biol Cell* 99: 297-309

Knuesel I, Mastrocola M, Zuellig RA, Bornhauser B, Schaub MC, Fritschy JM. 1999. Short communication: altered synaptic clustering of GABAA receptors in mice lacking dystrophin (mdx mice). *Eur J Neurosci* 11: 4457-62

Kosaka T, Katsumaru H, Hama K, Wu JY, Heizmann CW. 1987. GABAergic neurons containing the Ca2+-binding protein parvalbumin in the rat hippocampus and dentate gyrus. *Brain Res* 419: 119-30

Kowalczyk S, Winkelmann A, Smolinsky B, Forstera B, Neundorf I, et al. 2013. Direct binding of GABAA receptor beta2 and beta3 subunits to gephyrin. *Eur J Neurosci* 37: 544-54

Krause M, Dent EW, Bear JE, Loureiro JJ, Gertler FB. 2003. Ena/VASP proteins: regulators of the actin cytoskeleton and cell migration. *Annu Rev Cell Dev Biol* 19: 541-64

Krnjevic K, Schwartz S. 1966. Is gamma-aminobutyric acid an inhibitory transmitter? *Nature* 211: 1372-4

Krueger-Burg D, Papadopoulos T, Brose N. 2017. Organizers of inhibitory synapses come of age. *Curr Opin Neurobiol* 45: 66-77

Krueger DD, Tuffy LP, Papadopoulos T, Brose N. 2012. The role of neurexins and neuroligins in the formation, maturation, and function of vertebrate synapses. *Curr Opin Neurobiol* 22: 412-22

Kuhse J, Betz H, Kirsch J. 1995. The inhibitory glycine receptor: architecture, synaptic localization and molecular pathology of a postsynaptic ion-channel complex. *Curr Opin Neurobiol* 5: 318-23

Kuzirian MS, Paradis S. 2011. Emerging themes in GABAergic synapse development. *Prog Neurobiol* 95: 68-87

Laemmli UK. 1970. Cleavage of structural proteins during the assembly of the head of bacteriophage T4. *Nature* 227: 680-5

Lakso M, Pichel JG, Gorman JR, Sauer B, Okamoto Y, et al. 1996. Efficient in vivo manipulation of mouse genomic sequences at the zygote stage. *Proc Natl Acad Sci U S A* 93: 5860-5

Lalonde R. 1987a. Motor abnormalities in staggerer mutant mice. *Exp Brain Res* 68: 417-20

Lalonde R. 1987b. Motor abnormalities in weaver mutant mice. *Exp Brain Res* 65: 479-81

Lalonde R. 1994. Motor learning in lurcher mutant mice. *Brain Res* 639: 351-3

Lambrechts A, van Damme J, Goethals M, Vandekerckhove J, Ampe C. 1995. Purification and characterization of bovine profilin II. Actin, poly(L-proline) and inositolphospholipid binding. *Eur J Biochem* 230: 281-6

Landis DM, Reese TS. 1983. Cytoplasmic organization in cerebellar dendritic spines. *J Cell Biol* 97: 1169-78

Langosch D, Hoch W, Betz H. 1992. The 93 kDa protein gephyrin and tubulin associated with the inhibitory glycine receptor are phosphorylated by an endogenous protein kinase. *FEBS Lett* 298: 113-7

Langosch D, Thomas L, Betz H. 1988. Conserved quaternary structure of ligand-gated ion channels: the postsynaptic glycine receptor is a pentamer. *Proc Natl Acad Sci U S A* 85: 7394-8

Laube B, Maksay G, Schemm R, Betz H. 2002. Modulation of glycine receptor function: a novel approach for therapeutic intervention at inhibitory synapses? *Trends Pharmacol Sci* 23: 519-27

Laumonnier F, Bonnet-Brilhault F, Gomot M, Blanc R, David A, et al. 2004. X-linked mental retardation and autism are associated with a mutation in the NLGN4 gene, a member of the neuroligin family. *Am J Hum Genet* 74: 552-7

Le Clainche C, Pauly BS, Zhang CX, Engqvist-Goldstein AE, Cunningham K, Drubin DG. 2007. A Hip1R-cortactin complex negatively regulates actin assembly associated with endocytosis. *EMBO J* 26: 1199-210

Le PU, Nguyen TN, Drolet-Savoie P, Leclerc N, Nabi IR. 1998. Increased beta-actin expression in an invasive moloney sarcoma virus-transformed MDCK cell variant concentrates to the tips of multiple pseudopodia. *Cancer Res* 58: 1631-5

Lee K, Kim Y, Lee SJ, Qiang Y, Lee D, et al. 2013. MDGAs interact selectively with neuroligin-2 but not other neuroligins to regulate inhibitory synapse development. *Proc Natl Acad Sci U S A* 110: 336-41

Lenzen CU, Steinmann D, Whiteheart SW, Weis WI. 1998. Crystal structure of the hexamerization domain of N-ethylmaleimide-sensitive fusion protein. *Cell* 94: 525-36

Levi S, Grady RM, Henry MD, Campbell KP, Sanes JR, Craig AM. 2002. Dystroglycan is selectively associated with inhibitory GABAergic synapses but is dispensable for their differentiation. *J Neurosci* 22: 4274-85

Levi S, Logan SM, Tovar KR, Craig AM. 2004. Gephyrin is critical for glycine receptor clustering but not for the formation of functional GABAergic synapses in hippocampal neurons. *J Neurosci* 24: 207-17

Li J, Han W, Pelkey KA, Duan J, Mao X, et al. 2017. Molecular Dissection of Neuroligin 2 and Slitrk3 Reveals an Essential Framework for GABAergic Synapse Development. *Neuron* 96: 808-26 e8

Li J, Liu J, Feng G, Li T, Zhao Q, et al. 2011. The MDGA1 gene confers risk to schizophrenia and bipolar disorder. *Schizophr Res* 125: 194-200

Linhoff MW, Lauren J, Cassidy RM, Dobie FA, Takahashi H, et al. 2009. An unbiased expression screen for synaptogenic proteins identifies the LRRTM protein family as synaptic organizers. *Neuron* 61: 734-49

Lionel AC, Crosbie J, Barbosa N, Goodale T, Thiruvahindrapuram B, et al. 2011. Rare copy number variation discovery and cross-disorder comparisons identify risk genes for ADHD. *Sci Transl Med* 3: 95ra75

Lionel AC, Vaags AK, Sato D, Gazzellone MJ, Mitchell EB, et al. 2013. Rare exonic deletions implicate the synaptic organizer Gephyrin (GPHN) in risk for autism, schizophrenia and seizures. *Hum Mol Genet* 22: 2055-66

Lobo IA, Harris RA. 2008. GABA(A) receptors and alcohol. *Pharmacol Biochem Behav* 90: 90-4

Long P, May MM, James VM, Granno S, Johnson JP, et al. 2015. Missense Mutation R338W in ARHGEF9 in a Family with X-linked Intellectual Disability with Variable Macrocephaly and Macro-Orchidism. *Front Mol Neurosci* 8: 83

Luddens H, Wisden W. 1991. Function and pharmacology of multiple GABAA receptor subunits. *Trends Pharmacol Sci* 12: 49-51

Luscher B, Fuchs T, Kilpatrick CL. 2011. GABAA receptor trafficking-mediated plasticity of inhibitory synapses. *Neuron* 70: 385-409

Lynch JW. 2004. Molecular structure and function of the glycine receptor chloride channel. *Physiol Rev* 84: 1051-95

Machado P, Rostaing P, Guigonis JM, Renner M, Dumoulin A, et al. 2011. Heat shock cognate protein 70 regulates gephyrin clustering. *J Neurosci* 31: 3-14

Machesky LM, Mullins RD, Higgs HN, Kaiser DA, Blanchoin L, et al. 1999. Scar, a WASp-related protein, activates nucleation of actin filaments by the Arp2/3 complex. *Proc Natl Acad Sci U S A* 96: 3739-44

Malhotra V, Orci L, Glick BS, Block MR, Rothman JE. 1988. Role of an N-ethylmaleimide-sensitive transport component in promoting fusion of transport vesicles with cisternae of the Golgi stack. *Cell* 54: 221-7

Malosio ML, Marqueze-Pouey B, Kuhse J, Betz H. 1991. Widespread expression of glycine receptor subunit mRNAs in the adult and developing rat brain. *EMBO J* 10: 2401-9

Mammoto A, Sasaki T, Asakura T, Hotta I, Imamura H, et al. 1998. Interactions of drebrin and gephyrin with profilin. *Biochem Biophys Res Commun* 243: 86-9

Maric HM, Mukherjee J, Tretter V, Moss SJ, Schindelin H. 2011. Gephyrin-mediated gamma-aminobutyric acid type A and glycine receptor clustering relies on a common binding site. *J Biol Chem* 286: 42105-14

Marshall CR, Young EJ, Pani AM, Freckmann ML, Lacassie Y, et al. 2008. Infantile spasms is associated with deletion of the MAGI2 gene on chromosome 7q11.23-q21.11. *Am J Hum Genet* 83: 106-11

Martin DL, Rimvall K. 1993. Regulation of gamma-aminobutyric acid synthesis in the brain. *J Neurochem* 60: 395-407

Matveeva EA, Vanaman TC, Whiteheart SW, Slevin JT. 2007. Asymmetric accumulation of hippocampal 7S SNARE complexes occurs regardless of kindling paradigm. *Epilepsy Res* 73: 266-74

Mayer S, Kumar R, Jaiswal M, Soykan T, Ahmadian MR, et al. 2013. Collybistin activation by GTP-TC10 enhances postsynaptic gephyrin clustering and hippocampal GABAergic neurotransmission. *Proc Natl Acad Sci U S A* 110: 20795-800

McCann RO, Craig SW. 1997. The I/LWEQ module: a conserved sequence that signifies F-actin binding in functionally diverse proteins from yeast to mammals. *Proc Natl Acad Sci U S A* 94: 5679-84

Meyer G, Kirsch J, Betz H, Langosch D. 1995a. Identification of a gephyrin binding motif on the glycine receptor beta subunit. *Neuron* 15: 563-72

Meyer M, Granderath K, Andreesen JR. 1995b. Purification and characterization of protein PB of betaine reductase and its relationship to the corresponding proteins glycine reductase and sarcosine reductase from Eubacterium acidaminophilum. *Eur J Biochem* 234: 184-91

Mihic SJ, Ye Q, Wick MJ, Koltchine VV, Krasowski MD, et al. 1997. Sites of alcohol and volatile anaesthetic action on GABA(A) and glycine receptors. *Nature* 389: 385-9

Miki H, Suetsugu S, Takenawa T. 1998. WAVE, a novel WASP-family protein involved in actin reorganization induced by Rac. *EMBO J* 17: 6932-41

Miki H, Takenawa T. 1998. Direct binding of the verprolin-homology domain in N-WASP to actin is essential for cytoskeletal reorganization. *Biochem Biophys Res Commun* 243: 73-8

Mishra A, Traut MH, Becker L, Klopstock T, Stein V, Klein R. 2014. Genetic evidence for the adhesion protein IgSF9/Dasm1 to regulate inhibitory synapse development independent of its intracellular domain. *J Neurosci* 34: 4187-99

Missler M. 2003. Synaptic cell adhesion goes functional. *Trends Neurosci* 26: 176-8

Missler M, Sudhof TC, Biederer T. 2012. Synaptic cell adhesion. *Cold Spring Harb Perspect Biol* 4: a005694

Moss SJ, Smart TG. 2001. Constructing inhibitory synapses. *Nat Rev Neurosci* 2: 240-50

Mulhardt C, Fischer M, Gass P, Simon-Chazottes D, Guenet JL, et al. 1994. The spastic mouse: aberrant splicing of glycine receptor beta subunit mRNA caused by intronic insertion of L1 element. *Neuron* 13: 1003-15

Nakagawa H, Miki H, Ito M, Ohashi K, Takenawa T, Miyamoto S. 2001. N-WASP, WAVE and Mena play different roles in the organization of actin cytoskeleton in lamellipodia. *J Cell Sci* 114: 1555-65

Nawrotzki R, Islinger M, Vogel I, Volkl A, Kirsch J. 2012. Expression and subcellular distribution of gephyrin in non-neuronal tissues and cells. *Histochem Cell Biol* 137: 471-82

Nguyen QA, Horn ME, Nicoll RA. 2016. Distinct roles for extracellular and intracellular domains in neuroligin function at inhibitory synapses. *Elife* 5

Niebuhr K, Ebel F, Frank R, Reinhard M, Domann E, et al. 1997. A novel proline-rich motif present in ActA of Listeria monocytogenes and cytoskeletal proteins is the ligand for the EVH1 domain, a protein module present in the Ena/VASP family. *EMBO J* 16: 5433-44

Niethammer M, Valtschanoff JG, Kapoor TM, Allison DW, Weinberg RJ, et al. 1998. CRIPT, a novel postsynaptic protein that binds to the third PDZ domain of PSD-95/SAP90. *Neuron* 20: 693-707

Noctor SC, Martinez-Cerdeno V, Kriegstein AR. 2007. Contribution of intermediate progenitor cells to cortical histogenesis. *Arch Neurol* 64: 639-42

Nomura T, Fukuda T, Aika Y, Heizmann CW, Emson PC, et al. 1997. Laminar distribution of non-principal neurons in the rat hippocampus, with special reference to their compositional difference among layers. *Brain Res* 764: 197-204

Nozumi M, Nakagawa H, Miki H, Takenawa T, Miyamoto S. 2003. Differential localization of WAVE isoforms in filopodia and lamellipodia of the neuronal growth cone. *J Cell Sci* 116: 239-46

Nyiri G, Freund TF, Somogyi P. 2001. Input-dependent synaptic targeting of alpha(2)-subunit-containing GABA(A) receptors in synapses of hippocampal pyramidal cells of the rat. *Eur J Neurosci* 13: 428-42

Oertel J, Villmann C, Kettenmann H, Kirchhoff F, Becker CM. 2007. A novel glycine receptor beta subunit splice variant predicts an unorthodox transmembrane topology. Assembly into heteromeric receptor complexes. *J Biol Chem* 282: 2798-807

Oh S, Rubin JB, Bennett MV, Verselis VK, Bargiello TA. 1999. Molecular determinants of electrical rectification of single channel conductance in gap junctions formed by connexins 26 and 32. *J Gen Physiol* 114: 339-64

Owens DF, Kriegstein AR. 2002. Is there more to GABA than synaptic inhibition? *Nat Rev Neurosci* 3: 715-27

Palacios-Prado N, Huetteroth W, Pereda AE. 2014. Hemichannel composition and electrical synaptic transmission: molecular diversity and its implications for electrical rectification. *Front Cell Neurosci* 8: 324

Papadopoulos T, Eulenburg V, Reddy-Alla S, Mansuy IM, Li Y, Betz H. 2008. Collybistin is required for both the formation and maintenance of GABAergic postsynapses in the hippocampus. *Mol Cell Neurosci* 39: 161-9

Papadopoulos T, Korte M, Eulenburg V, Kubota H, Retiounskaia M, et al. 2007. Impaired GABAergic transmission and altered hippocampal synaptic plasticity in collybistin-deficient mice. *EMBO J* 26: 3888-99

Papadopoulos T, Rhee HJ, Subramanian D, Paraskevopoulou F, Mueller R, et al. 2017. Endosomal Phosphatidylinositol 3-Phosphate Promotes Gephyrin Clustering and GABAergic Neurotransmission at Inhibitory Postsynapses. *J Biol Chem* 292: 1160-77

Papadopoulos T, Schemm R, Grubmuller H, Brose N. 2015. Lipid binding defects and perturbed synaptogenic activity of a Collybistin R290H mutant that causes epilepsy and intellectual disability. *J Biol Chem* 290: 8256-70

Papadopoulos T, Soykan T. 2011. The role of collybistin in gephyrin clustering at inhibitory synapses: facts and open questions. *Front Cell Neurosci* 5: 11

Patrizi A, Viltono L, Frola E, Harvey K, Harvey RJ, Sassoe-Pognetto M. 2012. Selective localization of collybistin at a subset of inhibitory synapses in brain circuits. *J Comp Neurol* 520: 130-41

Patrizio A, Specht CG. 2016. Counting numbers of synaptic proteins: absolute quantification and single molecule imaging techniques. *Neurophotonics* 3: 041805

Pearse BM. 1982. Coated vesicles from human placenta carry ferritin, transferrin, and immunoglobulin G. *Proc Natl Acad Sci U S A* 79: 451-5

Peckham M, Miller G, Wells C, Zicha D, Dunn GA. 2001. Specific changes to the mechanism of cell locomotion induced by overexpression of beta-actin. *J Cell Sci* 114: 1367-77

Pennisi E. 2013. The CRISPR craze. *Science* 341: 833-6

Pfeiffer F, Graham D, Betz H. 1982. Purification by affinity chromatography of the glycine receptor of rat spinal cord. *J Biol Chem* 257: 9389-93

Poulopoulos A, Aramuni G, Meyer G, Soykan T, Hoon M, et al. 2009. Neuroligin 2 Drives Postsynaptic Assembly at Perisomatic Inhibitory Synapses through Gephyrin and Collybistin. *Neuron* 63: 628-42

Prasad A, Merico D, Thiruvahindrapuram B, Wei J, Lionel AC, et al. 2012. A discovery resource of rare copy number variations in individuals with autism spectrum disorder. *G3 (Bethesda)* 2: 1665-85

Ramamoorthi K, Lin Y. 2011. The contribution of GABAergic dysfunction to neurodevelopmental disorders. *Trends Mol Med* 17: 452-62

Ramirez-Franco JJ, Munoz-Cuevas FJ, Lujan R, Jurado S. 2016. Excitatory and Inhibitory Neurons in the Hippocampus Exhibit Molecularly Distinct Large Dense Core Vesicles. *Front Cell Neurosci* 10: 202

Reddy-Alla S, Schmitt B, Birkenfeld J, Eulenburg V, Dutertre S, et al. 2010. PH-domain-driven targeting of collybistin but not Cdc42 activation is required for synaptic gephyrin clustering. *Eur J Neurosci* 31: 1173-84

Rees MI, Harvey K, Ward H, White JH, Evans L, et al. 2003. Isoform heterogeneity of the human gephyrin gene (GPHN), binding domains to the glycine receptor, and mutation analysis in hyperekplexia. *J Biol Chem* 278: 24688-96

Rees MI, Lewis TM, Kwok JB, Mortier GR, Govaert P, et al. 2002. Hyperekplexia associated with compound heterozygote mutations in the beta-subunit of the human inhibitory glycine receptor (GLRB). *Hum Mol Genet* 11: 853-60

Reid T, Bathoorn A, Ahmadian MR, Collard JG. 1999. Identification and characterization of hPEM-2, a guanine nucleotide exchange factor specific for Cdc42. *J Biol Chem* 274: 33587-93

Reinhard M, Giehl K, Abel K, Haffner C, Jarchau T, et al. 1995. The proline-rich focal adhesion and microfilament protein VASP is a ligand for profilins. *EMBO J* 14: 1583-9

Saiepour L, Fuchs C, Patrizi A, Sassoe-Pognetto M, Harvey RJ, Harvey K. 2010. Complex role of collybistin and gephyrin in GABAA receptor clustering. *J Biol Chem* 285: 29623-31

Saiyed T, Paarmann I, Schmitt B, Haeger S, Sola M, et al. 2007. Molecular basis of gephyrin clustering at inhibitory synapses: role of G- and E-domain interactions. *J Biol Chem* 282: 5625-32

Sander B, Tria G, Shkumatov AV, Kim EY, Grossmann JG, et al. 2013. Structural characterization of gephyrin by AFM and SAXS reveals a mixture of compact and extended states. *Acta Crystallogr D Biol Crystallogr* 69: 2050-60

Satou Y, Satoh N. 1999. Developmental gene activities in ascidian embryos. *Curr Opin Genet Dev* 9: 542-7

Sauer RT, Baker TA. 2011. AAA+ proteases: ATP-fueled machines of protein destruction. *Annu Rev Biochem* 80: 587-612

Schaefer N, Roemer V, Janzen D, Villmann C. 2018. Impaired Glycine Receptor Trafficking in Neurological Diseases. *Front Mol Neurosci* 11: 291

Scheiffele P, Fan J, Choih J, Fetter R, Serafini T. 2000. Neuroligin expressed in nonneuronal cells triggers presynaptic development in contacting axons. *Cell* 101: 657-69

Schrader N, Kim EY, Winking J, Paulukat J, Schindelin H, Schwarz G. 2004. Biochemical characterization of the high affinity binding between the glycine receptor and gephyrin. *J Biol Chem* 279: 18733-41

Seki N, Muramatsu M, Sugano S, Suzuki Y, Nakagawara A, et al. 1998. Cloning, expression analysis, and chromosomal localization of HIP1R, an isolog of huntingtin interacting protein (HIP1). *J Hum Genet* 43: 268-71

Senetar MA, Foster SJ, McCann RO. 2004. Intrasteric inhibition mediates the interaction of the I/LWEQ module proteins Talin1, Talin2, Hip1, and Hip12 with actin. *Biochemistry* 43: 15418-28

Shelp BJ, Bown AW, McLean MD. 1999. Metabolism and functions of gamma-aminobutyric acid. *Trends Plant Sci* 4: 446-52

Shen K, Teruel MN, Subramanian K, Meyer T. 1998. CaMKIIbeta functions as an F-actin targeting module that localizes CaMKIIalpha/beta heterooligomers to dendritic spines. *Neuron* 21: 593-606

Shyn SI, Shi J, Kraft JB, Potash JB, Knowles JA, et al. 2011. Novel loci for major depression identified by genome-wide association study of Sequenced Treatment Alternatives to Relieve Depression and meta-analysis of three studies. *Mol Psychiatry* 16: 202-15

Soderling SH, Binns KL, Wayman GA, Davee SM, Ong SH, et al. 2002. The WRP component of the WAVE-1 complex attenuates Rac-mediated signalling. *Nature cell biology* 4: 970-5

Soderling SH, Guire ES, Kaech S, White J, Zhang F, et al. 2007. A WAVE-1 and WRP signaling complex regulates spine density, synaptic plasticity, and memory. *J Neurosci* 27: 355-65

Soderling SH, Langeberg LK, Soderling JA, Davee SM, Simerly R, et al. 2003. Loss of WAVE-1 causes sensorimotor retardation and reduced learning and memory in mice. *Proc Natl Acad Sci U S A* 100: 1723-8

Soderling SH, Scott JD. 2006. WAVE signalling: from biochemistry to biology. *Biochem Soc Trans* 34: 73-6

Sola M, Bavro VN, Timmins J, Franz T, Ricard-Blum S, et al. 2004. Structural basis of dynamic glycine receptor clustering by gephyrin. *EMBO J* 23: 2510-9

Song JY, Ichtchenko K, Sudhof TC, Brose N. 1999. Neuroligin 1 is a postsynaptic cell-adhesion molecule of excitatory synapses. *Proc Natl Acad Sci U S A* 96: 1100-5

Sossey-Alaoui K, Head K, Nowak N, Cowell JK. 2003. Genomic organization and expression profile of the human and mouse WAVE gene family. *Mamm Genome* 14: 314-22

Soykan T, Schneeberger D, Tria G, Buechner C, Bader N, et al. 2014. A conformational switch in collybistin determines the differentiation of inhibitory postsynapses. *EMBO J* 33: 2113-33

Specht CG, Izeddin I, Rodriguez PC, El Beheiry M, Rostaing P, et al. 2013. Quantitative nanoscopy of inhibitory synapses: counting gephyrin molecules and receptor binding sites. *Neuron* 79: 308-21

Stovold CF, Millard TH, Machesky LM. 2005. Inclusion of Scar/WAVE3 in a similar complex to Scar/WAVE1 and 2. *BMC Cell Biol* 6: 11

Sudhof TC. 2008. Neuroligins and neurexins link synaptic function to cognitive disease. *Nature* 455: 903-11

Sugita S, Saito F, Tang J, Satz J, Campbell K, Sudhof TC. 2001. A stoichiometric complex of neurexins and dystroglycan in brain. *J Cell Biol* 154: 435-45

Sumita K, Sato Y, Iida J, Kawata A, Hamano M, et al. 2007. Synaptic scaffolding molecule (S-SCAM) membrane-associated guanylate kinase with inverted organization (MAGI)-2 is associated with cell adhesion molecules at inhibitory synapses in rat hippocampal neurons. *J Neurochem* 100: 154-66

Sun C, Cheng MC, Qin R, Liao DL, Chen TT, et al. 2011. Identification and functional characterization of rare mutations of the neuroligin-2 gene (NLGN2) associated with schizophrenia. *Hum Mol Genet* 20: 3042-51

Takahashi H, Craig AM. 2013. Protein tyrosine phosphatases PTPdelta, PTPsigma, and LAR: presynaptic hubs for synapse organization. *Trends Neurosci* 36: 522-34

Takahashi H, Katayama K, Sohya K, Miyamoto H, Prasad T, et al. 2012. Selective control of inhibitory synapse development by Slitrk3-PTPdelta trans-synaptic interaction. *Nat Neurosci* 15: 389-98, S1-2

Taniguchi H, Gollan L, Scholl FG, Mahadomrongkul V, Dobler E, et al. 2007. Silencing of neuroligin function by postsynaptic neurexins. *J Neurosci* 27: 2815-24

Todd AJ, Sullivan AC. 1990. Light microscope study of the coexistence of GABA-like and glycine-like immunoreactivities in the spinal cord of the rat. *J Comp Neurol* 296: 496-505

Towbin H, Staehelin T, Gordon J. 1979. Electrophoretic transfer of proteins from polyacrylamide gels to nitrocellulose sheets: procedure and some applications. *Proc Natl Acad Sci U S A* 76: 4350-4

Tretter V, Jacob TC, Mukherjee J, Fritschy JM, Pangalos MN, Moss SJ. 2008. The clustering of GABA(A) receptor subtypes at inhibitory synapses is facilitated via the direct binding of receptor alpha 2 subunits to gephyrin. *J Neurosci* 28: 1356-65

Tretter V, Kerschner B, Milenkovic I, Ramsden SL, Ramerstorfer J, et al. 2011. Molecular basis of the gamma-aminobutyric acid A receptor alpha3 subunit interaction with the clustering protein gephyrin. *J Biol Chem* 286: 37702-11

Tyagarajan SK, Fritschy JM. 2014. Gephyrin: a master regulator of neuronal function? *Nat Rev Neurosci* 15: 141-56

Tyagarajan SK, Ghosh H, Harvey K, Fritschy JM. 2011. Collybistin splice variants differentially interact with gephyrin and Cdc42 to regulate gephyrin clustering at GABAergic synapses. *J Cell Sci* 124: 2786-96

Ulbrich C, Diepholz M, Bassler J, Kressler D, Pertschy B, et al. 2009. Mechanochemical removal of ribosome biogenesis factors from nascent 60S ribosomal subunits. *Cell* 138: 911-22

Ullian EM, Sapperstein SK, Christopherson KS, Barres BA. 2001. Control of synapse number by glia. *Science* 291: 657-61

Vandekerckhove J, Weber K. 1978. At least six different actins are expressed in a higher mammal: an analysis based on the amino acid sequence of the amino-terminal tryptic peptide. *J Mol Biol* 126: 783-802

Varoqueaux F, Aramuni G, Rawson RL, Mohrmann R, Missler M, et al. 2006. Neuroligins determine synapse maturation and function. *Neuron* 51: 741-54

Varoqueaux F, Jamain S, Brose N. 2004. Neuroligin 2 is exclusively localized to inhibitory synapses. *Eur J Cell Biol* 83: 449-56

Vieira AV, Lamaze C, Schmid SL. 1996. Control of EGF receptor signaling by clathrin-mediated endocytosis. *Science* 274: 2086-9

Wang H, Bedford FK, Brandon NJ, Moss SJ, Olsen RW. 1999. GABA(A)-receptor-associated protein links GABA(A) receptors and the cytoskeleton. *Nature* 397: 69-72

Wanker EE, Rovira C, Scherzinger E, Hasenbank R, Walter S, et al. 1997. HIP-I: a huntingtin interacting protein isolated by the yeast two-hybrid system. *Hum Mol Genet* 6: 487-95

Wasmeier C, Hutton JC. 1996. Molecular cloning of phogrin, a protein-tyrosine phosphatase homologue localized to insulin secretory granule membranes. *J Biol Chem* 271: 18161-70

Weltzien F, Puller C, O'Sullivan GA, Paarmann I, Betz H. 2012. Distribution of the glycine receptor beta-subunit in the mouse CNS as revealed by a novel monoclonal antibody. *The Journal of comparative neurology* 520: 3962-81

Westphal RS, Soderling SH, Alto NM, Langeberg LK, Scott JD. 2000. Scar/WAVE-1, a Wiskott-Aldrich syndrome protein, assembles an actin-associated multi-kinase scaffold. *EMBO J* 19: 4589-600

Wilson DW, Wilcox CA, Flynn GC, Chen E, Kuang WJ, et al. 1989. A fusion protein required for vesicle-mediated transport in both mammalian cells and yeast. *Nature* 339: 355-9

Witke W, Podtelejnikov AV, Di Nardo A, Sutherland JD, Gurniak CB, et al. 1998. In mouse brain profilin I and profilin II associate with regulators of the endocytic pathway and actin assembly. *EMBO J* 17: 967-76

Wojcik SM, Katsurabayashi S, Guillemin I, Friauf E, Rosenmund C, et al. 2006. A shared vesicular carrier allows synaptic corelease of GABA and glycine. *Neuron* 50: 575-87

Woo J, Kwon SK, Nam J, Choi S, Takahashi H, et al. 2013. The adhesion protein IgSF9b is coupled to neuroligin 2 via S-SCAM to promote inhibitory synapse development. *J Cell Biol* 201: 929-44

Xu Q, Rife CL, Carlton D, Miller MD, Krishna SS, et al. 2009. Crystal structure of a novel archaeal AAA+ ATPase SSO1545 from Sulfolobus solfataricus. *Proteins* 74: 1041-9

Yang BZ, Han S, Kranzler HR, Farrer LA, Gelernter J. 2011. A genomewide linkage scan of cocaine dependence and major depressive episode in two populations. *Neuropsychopharmacology* 36: 2422-30

Yang Q, Peng L, Wu Y, Li Y, Wang L, et al. 2018. Endocytic Adaptor Protein HIP1R Controls Intracellular Trafficking of Epidermal Growth Factor Receptor in Neuronal Dendritic Development. *Front Mol Neurosci* 11: 447

Yim YS, Kwon Y, Nam J, Yoon HI, Lee K, et al. 2013. Slitrks control excitatory and inhibitory synapse formation with LAR receptor protein tyrosine phosphatases. *Proc Natl Acad Sci U S A* 110: 4057-62

Young AB, Snyder SH. 1973. Strychnine binding associated with glycine receptors of the central nervous system. *Proc Natl Acad Sci U S A* 70: 2832-6

Zhang B, Chen LY, Liu X, Maxeiner S, Lee SJ, et al. 2015. Neuroligins Sculpt Cerebellar Purkinje-Cell Circuits by Differential Control of Distinct Classes of Synapses. *Neuron* 87: 781-96

Zhu L, Wrabl JO, Hayashi AP, Rose LS, Thomas PJ. 2008. The torsin-family AAA+ protein OOC-5 contains a critical disulfide adjacent to Sensor-II that couples redox state to nucleotide binding. *Mol Biol Cell* 19: 3599-612

11 Publications

2021

Wagner S, Lee C, Rojas L, Specht CG, Rhee J, Brose N, Papadopoulos T,
The α3 subunit of $GABA_A$ receptors promotes formation of inhibitory synapses in the absence of collybistin, Journal of Biological Chemistry (2021), doi: https://doi.org/10.1016/j.jbc.2021.100709.